Untangling neuronal diversity:

a quantitative electrophysiological and morphological characterization of VIP expressing interneurons

Dissertation

for the award of the degree

"Doctor rerum naturalium"

Faculty of Biology

of the Georg-August University Göttingen

within the doctoral program Sensory and Motor Neuroscience

of the Georg-August University School of Science (GAUSS)

submitted by

Alvar Prönneke

from Engelskirchen

Göttingen 2016

Thesis Committee

PROF. DR. JOCHEN F. STAIGER Institute of Neuroanatomy, University Medical Center, Göttingen

CAMIN DEAN, PHD Euopean Neuroscience Institute, Göttingen

PROF. DR. SWEN HÜLSMANN Experimental Neuroanesthesiology, University Medical Center, Göttingen

Members of the Examination Board

First Referee:
PROF. DR. JOCHEN F. STAIGER Institute of Neuroanatomy, University Medical Center, Göttingen

Second Referee:
PROF. DR. SWEN HÜLSMANN Experimental Neuroanesthesiology, University Medical Center, Göttingen

Further members of the Examination Board

CAMIN DEAN, PHD Euopean Neuroscience Institute, Göttingen

PROF. DR. RALF HEINRICH Cellular Neurobiology, Schwann-Schleiden Research Center, Göttingen

PROF. DR. HANSJÖRG SCHERBERGER German Primate Center, Göttingen

PROF. DR. TOBIAS MOSER Institute for Auditory Neuroscience & InnerEar Lab, University Medical Center, Göttingen

Date of the oral examination: 12.10.2016

I, Alvar Prönneke, hereby certify that the present doctoral thesis has been written independently with no other sources than cited. All results presented here were the outcome of my own workings unless stated otherwise.

....

Göttingen, 01.09.2016

Table of Contents

Table of Figures

List of Abbreviations

5HT	Serotonin
$5HT_{2a}R$	Serotonin receptor type 2a
$5HT_{2c}R$	Serotonin receptor type 2c
$5HT_2R$	Serotonin receptor type 2
$5HT_{3a}R$	Serotonin receptor type 3a
ACh	Acetylcholine
AD1	Cluster 1 of the adaptation analysis
AD2	Cluster 2 of the adaptation analysis
AD3	Cluster 3 of the adaptation analysis
AHP	Afterhyperpolarization
ANOVA	Analysis of variance
AP	Action potential
AP1	Cluster 1 of the action potential waveform analysis
AP2	Cluster 2 of the action potential waveform analysis
AP3	Cluster 3 of the action potential waveform analysis
AP4	Cluster 4 of the action potential waveform analysis
AP5	(2*R*)-amino-5-phosphonovaleric acid
BS	Bursting
CA	Continuous adapting
Chat	Cholinergic acetyltransferase
DF1	Cluster 1 of the dynamic frequency range analysis
DF2	Cluster 2 of the dynamic frequency range analysis
DF3	Cluster 3 of the dynamic frequency range analysis
DF4	Cluster 4 of the dynamic frequency range analysis
DFR	Dynamic frequency range
fAHP	Fast afterhyperpolarization component
GABA	Gamma-aminobutyric acid

Gpc3	Gene encoding Glypican-3
I_D	Delayed K$^+$ current
IS	Irregular spiking
mAHP	Slower afterhyperpolarizing component
non-α7	Nicotinic cholinergic receptors without the α7 subunit
Mybpc1	Gene encoding Myosin binding protein C
NA	Noradrenalin
NBQX	2,3-dihydroxy-6-nitro-7-sulfamoyl-benzo[f]quinoxaline-2,3-dione
PA1	Cluster 1 of the passive properties analysis
PA2	Cluster 2 of the passive properties analysis
PA3	Cluster 3 of the passive properties analysis
Parm1	Gene encoding Prostate Androgen-regulated Mucin-like Protein1
PV	Parvalbumin
RMP	Resting membrane potential
Sncg	Gene encoding gamma-Synuclein
SOM	Somatostatin
VIP	Vasoactive intestinal polypeptide
VPm	Ventral posteriomedial nucleus

1 Introduction

The mammalian neocortex integrates and contextualizes sensory information to modulate behavior. The basis for this information processing is an intricate network of neurons that are highly diverse. Sensory information entering the neocortex is processed primarily by glutamatergic excitatory neurons which are organized in a laminated manner. Their somata are located in different densities throughout the depth of the neocortex, an organizational principle that results in anatomically identifiable layers. Even though different cortical areas process different information, these are organized in a similar manner. This consistency in cytoarchitecture hints towards a certain uniformity in cortical circuitry. Thus, it is likely that circuit motifs deciphered in a specific cortical area will be found throughout the whole neocortex. Circuit motifs can only be described to their full extent if all elements are known. Since any cortical circuitry is based on neurons, a thorough characterization of these core elements is crucial for the comprehension of cortical information processing.

1.1 Neurons of the neocortex

Cortical information processing is based on a staggering diversity of neurons. Most of the cortical neurons are excitatory. Their output is shaped and controlled by a smaller inhibitory subpopulation comprising ~15% of all cortical neurons (Meyer et al. 2011). These neurons are inhibitory interneurons because they release gamma-aminobutyric acid (GABA) as their primary neurotransmitter and are locally restricted to the cortex. Despite their low frequency of occurrence, inhibitory interneurons are key elements in learning and memory, rhythmic cortical activity, feedforward and feedback inhibition, integration of information from other cortical areas and neuromodulation (Porter et al. 1999; Ferezou et al. 2002; Silberberg and Markram 2007; Buzsaki and Wang 2012; Donato et al. 2013; Lee et al. 2013; Pi et al. 2013; Fu et al. 2014; Chen et al. 2015). Inhibitory interneurons display a broad spectrum of diversity in their morphology, electrophysiology, and molecular profile which proved to be very challenging for past classification attempts. The current consensus is to differentiate between subgroups of inhibitory interneurons by the expression of certain proteins. Since this classification results in non-overlapping subgroups, it serves the purpose of studying one specific subgroup of interneurons in an isolated manner well. The three molecularly distinct subpopulations of inhibitory interneurons are: parvalbumin (PV), somatostatin (SOM),

and serotonin receptor 3a (5HT$_{3a}$R) -expressing interneurons. Approximately 40% of 5HT$_{3a}$R interneurons also express vasoactive intestinal polypeptide (VIP; Rudy et al. 2011).

1.2 The disinhibitory circuit motif mediated by VIP neurons

Apart from inhibiting excitatory neurons by directly targeting them, some inhibitory interneurons also synapse onto other inhibitory interneurons. Consequentially, excitatory neurons are disinhibited (Freund et al. 1983; Somogyi et al. 1983). Recently, the disinhibitory circuit motif was deciphered on the basis of the aforementioned molecularly distinguished inhibitory interneurons. These studies showed that VIP neurons are the key elements in disinhibition mediated by top-down inputs. The preferred targets of VIP neurons are several other types of inhibitory interneurons. Most of these interneurons are SOM and, to a lesser extent, PV neurons which inhibit excitatory neurons (Staiger et al. 2004; David et al. 2007; Pfeffer et al. 2013). By inhibiting PV and SOM neurons, VIP neurons are capable of releasing excitatory neurons from inhibition. The disinhibitory circuit motif involving the VIP to SOM connectivity has been identified in the visual (Fu et al. 2014; Zhang et al. 2014), the auditory (Pi et al. 2013), and the barrel cortex (Lee et al. 2013). In the visual cortex, activation of VIP neurons by ACh increases the gain of excitation during locomotion (Fu et al. 2014). In the auditory cortex, VIP neurons are most active during the reinforcement period of learning a behavioral task. Also here, activity of VIP neurons increases cortical activity (Pi et al. 2013). In the barrel cortex, VIP neurons are directly innervated by the motor cortex during active whisking (Gentet et al. 2012; Lee et al. 2013). Thus, VIP neurons disinhibit excitatory neurons in various cortical areas by integrating neuromodulatory and cross-cortical input. However, these are not the only sources of input to VIP neurons because they are also reciprocally connected to local excitatory neurons (Porter et al. 1998; Caputi et al. 2009). Further sources of input include the thalamus (Staiger et al. 1996; Fu et al. 2014) and other cortical areas (Lee et al. 2013; Zhang et al. 2014). Additionally, they are not only depolarized by the neuromodulator acetylcholine (ACh) via non-α7 nicotinic receptors (Porter et al. 1999) but also by serotonin via 5HT$_{3a}$R (Ferezou et al. 2002). Further roles of cortical VIP neurons include neurovascular coupling (Cauli et al. 2004) and regulation of neuronal energy metabolism (Magistretti et al. 1998).

Figure 1 Distribution of VIP neurons in the barrel cortex of mice

A Projection view of an image stack visualizing the native fluorescence in a 300 µm thick coronal section through the barrel cortex of a VIPcre/tdTomato mouse. **B** Bar graphs depicting the population analysis of the density of VIP neurons (x-axis) in a layer-dependent (light red in cells/mm³ cortex; 12 animals, 150 sections) and layer-independent manner (dark red in cells/0.05 mm³; 12 animals, 150 sections). The density in each layer is significantly different from all others (one way ANOVA, H = 983.520, p < 0.001, post-hoc Tukey analysis), except for layers Va and b. For the layer-independent analysis, somata were counted in 20 bins of 50 µm ranging from the pial surface (0 µm) to the white matter border (1000 µm; y-axis; dark red bar graph). Location of layer borders was determined by identifying layers in DAPI stainings of 150 sections from 12 animals. Layer thickness was measured perpendicular to the pial surface. The resulting mean is shown as dashed lines in **A** and **B** (Roman numerals depict layers; error bars = SD; scale bar = 150 µm; *adapted from Prönneke et al. 2015*).

1.3 Properties of VIP neurons

All of the above functions of VIP neurons are based on a variety of intrinsic properties: during development, VIP neurons migrate from the caudal ganglionic eminence to

enter the cortex between E12.5 and 18.5 (Miyoshi et al. 2010). Approximately 2200 VIP neurons are distributed throughout 1 mm³ barrel cortex in a distinct fashion. 60% are located in layer II/III whereas 40% are found in all other layers. The highest density of somata of VIP neurons is 150 µm away from the pial surface in upper layer II/III (Figure 1). In total, 13% of all inhibitory interneurons in the barrel cortex are VIP neurons. However, almost a third of all inhibitory interneurons in layer II/III express VIP (Lee et al. 2010; Rudy et al. 2011; Taniguchi et al. 2011; Prönneke et al. 2015). One of the earliest descriptions of the morphology of VIP neurons described them as being bipolar. This term refers to two primary dendrites stemming from opposing poles of the soma (Morrison et al. 1984). In later studies, more somatodendritic configurations of VIP neurons were identified including tufted, modified bipolar (tripolar) and multipolar (Bayraktar et al. 2000). Axons of VIP neurons are oriented perpendicular to the pial surface and project towards the white matter (Porter et al. 1998; Bayraktar et al. 2000; Karagiannis et al. 2009). However, a thorough description of morphological features of VIP neurons is still missing. Of all inhibitory interneuron populations, VIP neurons are probably the most heterogeneous in their electrophysiological properties. They have a high input resistance in comparison to other interneurons which might be the source for their strong excitability (Porter et al. 1998; Lee et al. 2010). Additionally VIP neurons display a vast variety of firing patterns. Continuous firing with adaptation (CA), irregular spiking (IS), and bursting (BS) firing patterns were described previously (Porter et al. 1998; Karagiannis et al. 2009). Most of the VIP neurons have CA firing patterns and none are fast spiking (Karagiannis et al. 2009).

1.4 Classification of VIP neurons

The spectrum of functions in which VIP neurons participate as well as their heterogeneity in morphological and electrophysiological properties suggests that the population of VIP neurons is very non-homogeneous. This observation is also reflected in classifications which included VIP neurons. Here, VIP neurons were either differentiated by electrophysiological parameters (Karagiannis et al. 2009) or their molecular profile (Zeisel et al. 2015; Tasic et al. 2016). In the work of Karagiannis et al. (2009) VIP neurons in rats were separated into two groups: adapting and bursting VIP neurons. These terms refer to firing patterns which were either CA or burst firing. However, no obvious differences in morphology were observed. The most recent molecular distinction of VIP neurons (Tasic et al. 2016) was based on the evaluation of the mRNA expression in

all cells in the visual cortex. Among these, VIP neurons were separated into 5 different subgroups which were labeled according to their distinct co-expression of genes: *Vip Gpc3*, *Vip Chat*, *Vip Parm1*, *Vip Mybpc1*, and *Vip Sncg*. These genes are of partially obscure nature. *Gpc3* encodes for the proteoglycan Glypican-3*, Parm1* for Prostate Androgen-regulated Mucin-like Protein 1, *Mybpc1* for Myosin binding protein C, and *Sncg* for gamma-Synuclein. The function and involvement in neuronal activity of these proteins is not well understood. Only *Chat*, the gene for choline acetyltransferase, can be assigned a specific function. The presence of ChAT means that a subgroup of VIP neurons might also release ACh, a finding that is in line with previous reports (Gonchar et al. 2007; von Engelhardt et al. 2007). Tasic et al. (2016) also found tendencies for a differential distribution of the 5 VIP neuron classes. *Vip Parm1*, *Vip Mybpc1*, and *Vip Sncg* were predominantly found in the upper layers I-IV of the visual cortex, and *Vip Gpc3* in lower layers V and VI. *Vip Chat* neurons did not show a location preference. Thus, VIP neurons in the upper layers of the neocortex seem to show a greater molecular diversity than those in deeper areas.

1.5 Aim of this study

A molecular distinction of neurons is certainly a powerful tool to target specific neuronal subgroups and study them in a selective manner. However, especially VIP neurons show a great heterogeneity beyond their molecular profile. This heterogeneity suggests that these inhibitory interneurons might form subgroups in their electrophysiological and morphological profile. To identify these possible subgroups, VIP neurons were targeted in acute thalamocortical slices of the barrel cortex in mice and recorded by whole-cell patch clamp. Their electrophysiological profile was determined and neurons with a sufficient staining were reconstructed to analyze their morphology. By using analytical methods designed to detect patterns in a dataset, the heterogeneity of VIP neurons was broken down into quantifiable details. In this manner, not only were the basic properties described thoroughly but also subgroups were identified in electrophysiological and morphological properties. Furthermore, novel features of VIP neurons were discovered which expand their spectrum of functions.

2 Materials and Methods

2.1 Animals

Homozygous *Vip-ires-cre* (VIP[tm1(cre)Zjh],The Jackson Laboratory, Bar Harbor, USA) mice were crossed with homozygous *Ai9* mice (Madisen et al. 2010; floxed tdTomato mice: B6.Cg-*Gt(ROSA)26Sor*[tm9(CAG-tdTomato)Hze]/J, floxed YFP mice: B6.Cg-*Gt(ROSA)26Sor*[tm3(CAG-EYFP)Hze]/J, The Jackson Laboratory, Bar Harbor, USA). Offspring (21-36 days old) which was heterozygous for VIPcre/tdTomato or VIPcre/YFP from the breeding facility of the University Medical Center Göttingen (Göttingen, Germany) was used in this study. These mice are highly sensitive and specific for the population of VIP expressing interneurons (Taniguchi et al. 2011; Prönneke et al. 2015). All experimental procedures were performed in accordance with German laws on animal research (TierSchG und TierSchVersV 2013).

2.2 In vitro electrophysiology

VIPcre/tdTomato mice were deeply anesthetized with isoflurane and decapitated. Thalamocortical slices (300 µm; Porter et al. 2001) containing the primary somatosensory (barrel) cortex were cut using a vibratome (Leica VT1200S, Wetzlar, Germany). The cold (4°C) cutting solution contained (in mM): 75 sucrose, 87 NaCl, 2.5 KCL, 0.5 $CaCl_2$, 7.0 $MgCl_2$, 26 $NaHCO_3$, 1.25 NaH_2PO_4 and 10 glucose, continuously equilibrated with 95% O_2 and 5% CO_2, pH 7.4. Slices were incubated for 0.5-1h at 34°C prior to recording in extracellular solution (ACSF) of the following composition (in mM): 125 NaCl, 2.5 KCL, 2 $CaCl_2$, 1 $MgCl_2$, 26 $NaHCO_3$, 1.25 NaH_2PO_4 and 25 glucose, pH 7.4 when equilibrated with 95% O_2 and 5% CO_2. Slices were transferred to a fixed-stage recording chamber in an upright microscope (Axio Examiner, Zeiss, Germany) and continuously perfused at a rate of 2 ml/min with ACSF. All experiments were performed at 32°C. The barrel field was visualized at low magnification (2.5x) under bright-field illumination. Target neurons were identified by tdTomato or YFP fluorescence using a 40x water immersion objective (40x/0.75W, Olympus, Germany). For whole-cell patch-clamp recordings, filamented borosilicate glass capillaries (Science Products, Hofheim, Germany) of 5-8 MΩ resistances were filled with (in mM): 135 K-gluconate, 5 KCL, 10 HEPES, 0.5 EGTA, 4 Mg-ATP, 0.3 Na-GTP, 10 phosphocreatin phosphate and 0.3-0.5% biocytin. Membrane potentials were not corrected for a liquid junction potential of

~16 mV. Membrane potentials were recorded using a SEC05L amplifier (npi electronics, Tamm, Germany) in discontinuous current-clamp mode with a switching frequency of 50 kHz, filtered at 3 kHz, and digitized at 10-25 kHz using a CED Power1401 (CED Limited, Cambridge, England). Access resistance was monitored and compensated if changes appeared. Recordings during which the access resistance could not be compensated were discarded. Data was collected, stored and analyzed with Signal 5 software (CED Limited, Cambridge, England). Passive and active properties of a neuron were determined immediately after reaching whole-cell configuration by applying one second long hyperpolarizing or depolarizing rectangular current pulses of varying strength at resting membrane potential.

2.3 Pharmacological experiments

Neurons were exposed to pharmacological agents either by bath application or short and local pressure application. Bath application of neuromodulators was monitored by recording in current clamp mode. To control for changes in input resistance, every 6 seconds a hyperpolarizing stimulus of -10 pA lasting 200 ms was applied. Bath applied neuromodulators were: nor-adrenalin (NA, 40 µM; Sigma, Deisenhofen, Germany), serotonin (5HT, 5 µM; Tocris, Wiesbaden, Germany), and acetylcholine (ACh, 40 µM; Sigma, Deisenhofen, Germany). Bath applied receptor antagonists were: 2,3-dihydroxy-6-nitro-7-sulfamoyl-benzo[f]quinoxaline-2,3-dione (NBQX, AMPA receptor antagonist, 10 µM; Biotrend, Zürich, Switzerland), (2R)-amino-5-phosphonovaleric acid (AP5, NMDA receptor antagonist, 50 µM; Tocris, Wiesbaden, Germany), tropisetron (5HT3aR antagonist, 10 nM; Biotrend, Zürich, Switzerland), cinanserin (5HT2a and 5HT2c receptor antagonist, 400 µM; Tocris, Wiesbaden, Germany), and mecamylamine (non-a7 nicotinic ACh receptor antagonist, 100 µM; Biotrend, Zürich, Switzerland). Pressure application of the neuromodulators 5HT (200 µM) and ACh (100 µM) was performed by placing a micropipette at a distance of 15-20 µm to the soma of the recorded neuron and applying short pressure pulses of 7 psi using a pressure application system (Toohey Spritzer, Toohey Company, Fairfield, NJ). Short and local pressure experiments were recorded in voltage clamp. Membrane potential of neurons was clamped to -65 mV.

2.4 Staining of biocytin filled cells

Staining of biocytin-filled cells has previously been described in detail (Staiger et al. 2004; 2014). In brief, after recording slices were fixed in 4% formaldehyde (in PB) at 4°C for 12 to 20 hours. To stop fixation, the tissue was rinsed extensively with PB including an intermediate step with 1% H_2O_2 (in PB) to block endogenous peroxidase activity. Next, slices were incubated in a cryoprotectant (25% saccharose, 10% glycerol in 0.01 M PB) for 1h. They were freeze–thawed three times over liquid nitrogen. After three rinses in PB, the slices were incubated overnight with Avidin-Biotin Complex (ABC; 1:200; Vector, Burlingame, CA) at 4°C. Afterward, 1 mg/ml 3,3'diaminobenzidine (DAB; Sigma, Deisenhofen, Germany) was preincubated for 10 min and the peroxidase was revealed by starting the reaction with 0.01% H_2O_2. The reaction was stopped by rinsing with PB. To intensify the reaction product, sections were incubated in 1.4% silver nitrate at 56°C for 30 min, followed by 0.2% gold chloride at RT for 10 min, and fixed with 5% sodium thiosulfate for 5 min. The barrel field was visualized by cytochrome oxidase histochemistry.

2.5 Reconstruction of biocytin-filled neurons

Neurons with consistently intense staining of neurites and no obvious truncation of processes were reconstructed using live digital images acquired by a digital camera (CX9000, MBF Bioscience, Colchester, VT) mounted on a microscope (Eclipse 80i, Nikon, Ratingen, Germany) with a 63x oil-immersion objective (NA = 1.4) and connected to a computer running Neurolucida (MBF Bioscience, Colchester, VT). Dendritic processes were distinguished from axonal structures by their diameter, fine structure, and branching pattern (see Figure 2 for details).

2.6 Analysis of electrophysiological data

Basic characterization. Electrophysiological data was analyzed using custom written scripts for Signal 5 (courtesy of Dr. Martin Möck). Most of the passive properties were analyzed using averages of ten responses to a hyperpolarizing current pulse of 10 pA. The membrane time constant was determined by fitting an exponential to the averaged membrane potential response ($f(x) = Ae^{-x/\tau}+B$; A = maximum amplitude, B = membrane
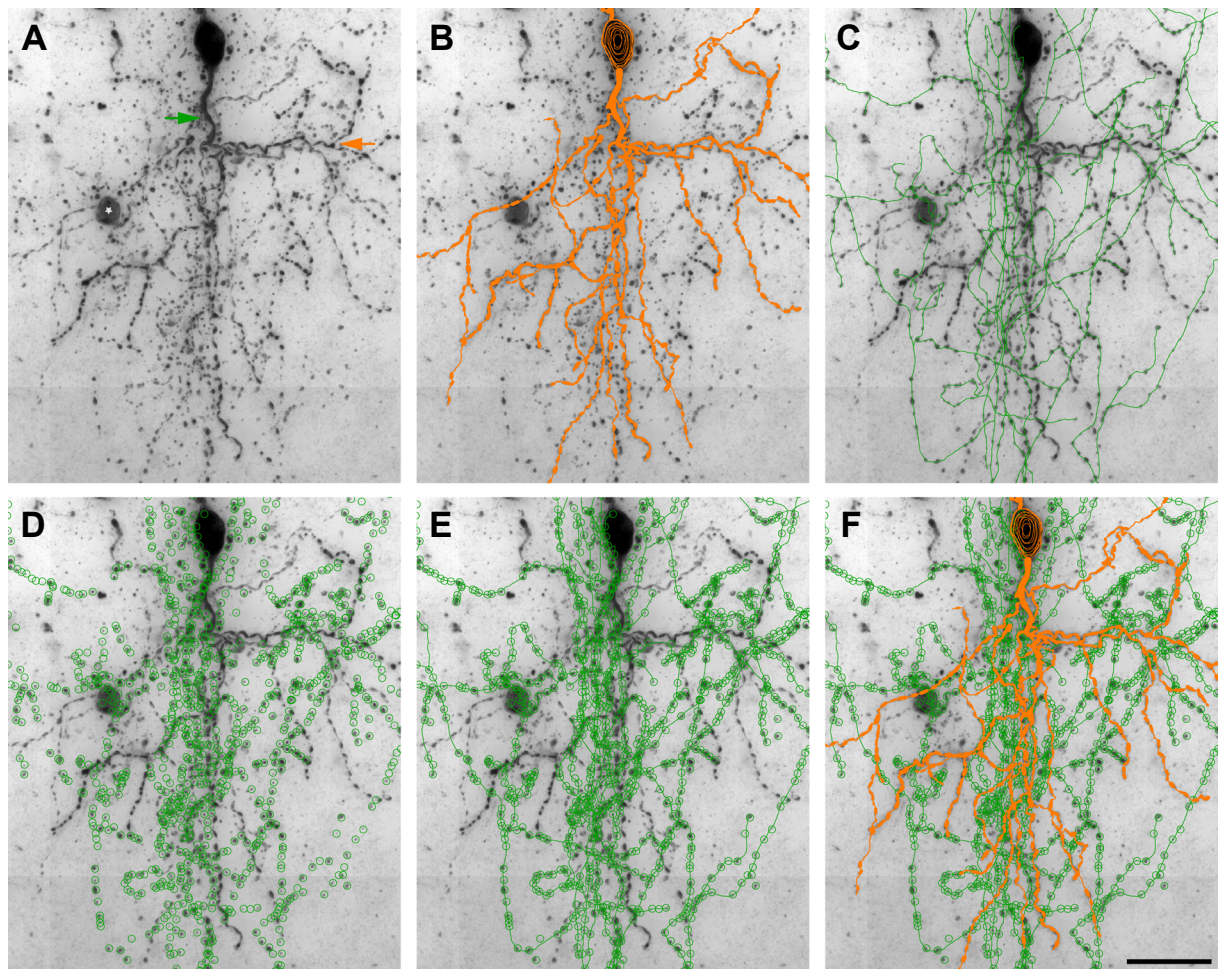
Figure 2 Distinction of dendrite from axon in a biocytin-filled VIP neuron

(A) depicts a minimum intensity projection of a magnified area of a 300 µm thick slice containing the labeled neuron shown in Fig. 4 Ac. The soma is identified by its shape, size, and intense staining. We use certain criteria to distinguish dendrites from axon in VIP neurons. (i) Size: dendrites (B; reconstructed soma and dendrites in orange) usually have a larger diameter than axonal processes (C and E; reconstructed axon in green). (ii) Fine structure: Dendritic branches contain several swellings which are large, ellipsoid, and oriented along the path direction. Axonal boutons appear smaller and more roundish (compare B and axonal boutons in D marked by green open circles). (iii) Branching pattern: branching angles of dendrites are always obtuse (orange arrow in A), whereas the axon sometimes branches in a perpendicular but often in a sharp manner (C). (iv) Continuity: the axon has one origin (green arrow in A) from which any connected process is traced to the next branching point and/or end. After identification of this origin using criteria i-iii, neuronal structures can be subdivided into dendrites and axon and reconstructed fully (F; asterisk in A marks an unspecific labeling; scale bar = 25 µm; *adapted from Prönneke et al. 2015*).

potential at maximum amplitude of response; $R^2 > 0.9$). Input resistance was determined according to Ohm's law using the maximum amplitude of the membrane potential response and the amplitude of the injected current. The sag index is an indicator of slow inward rectification. It was calculated by comparing the input resistance at the maximum amplitude to that at steady state (averaged membrane potential toward the end of the stimulus). Differences are given as percentages. Fast inward rectification (rectification index, RI) was measured by comparing the maximal membrane potential changes as responses to current pulses of 10 pA to those to 100 pA. Linearity (response

to 10 pA is 10% of that to 100 pA) suggests that the deflection depends exclusively on passive membrane properties. An increase in the percentage indicates involvement of fast inward rectification. For clarity, 10 was subtracted from the resulting values, thus no fast inward rectification is set to 0. Firing threshold, time to peak, half width, amplitude (measured from firing threshold to peak) of action potentials were analyzed at action potentials evoked at rheobase. The amplitude of afterhyperpolarizations (AHP) was determined by measuring the difference in voltage from firing threshold to maximum deflection of the repolarization. The time to peak of AHP was measured from the time point the repolarization of the action potential crossed the firing threshold to the maximum amplitude of the AHP.

Quantification of firing rate adaptation and current dependency. Firing patterns were quantified based on responses to depolarizing current steps of 10 pA. Neurons were stimulated from just above threshold (minimal stimulation strength) until fluctuations of AP amplitudes became visible (maximal stimulation strength). Recorded traces were subdivided into 100 ms long bins from onset to end of stimulus. Since all current stimulations lasted for 1 s, 10 bins per trace were defined. Firing adaptation was described numerically by dividing the average number of APs during the last 100 ms by the average number of APs during the first 100 ms. The resulting value was subtracted from 1. Thus, strong adaptation was described by large values and weak by low. This variable is referred to as firing rate adaptation (10:1). Another variable describing early firing rate adaptation was calculated in the same manner except that the average number of APs during the first and second 100 ms was compared. This variable is referred to as firing rate adaptation (2:1). Additionally, the number of APs during the first 100 ms in responses to minimal stimulation strength was divided by the number of spikes during maximal. The resulting value was subtracted from 1. This variable described the current dependency of firing patterns with large values describing a strong and low values a weak current dependency. It is referred to as current dependency (min:max). Current dependency was also determined for half-maximal stimulation strength in the same manner except by comparing minimal to half-maximal stimulation strength. This variable is referred to as current dependency (min:half).

Analysis of the dynamic frequency range. The frequency spectrum of APs was analyzed in a cumulative manner. For this, all instantaneous frequencies (the reciprocal of inter spike intervals) were pooled for each neuron and binned in 10 Hz from 10 Hz to 390 Hz. To make data comparable between neurons, these numbers are given as percent in a

cumulative manner. Based on this, the dynamic frequency range (DFR) was defined as 5% to 95% of all instantaneous frequencies found in corresponding frequency bins. Also, the first frequency bin in which more than 50% of all frequencies are found is given in the results.

Analysis of pharmacological experiments. Membrane potential changes induced by neuromodulators were analyzed using a custom written script for Signal 5 (courtesy of Dr. Martin Möck). The membrane potential was measured at the beginning and at the end of the recording at 10 time points each. Determined values were averaged and described the membrane potential before and during neuromodulation. The same measurements were repeated for recordings during the washout of the neuromodulators to determine the repolarization after neuromodulation.

2.7 Analysis of morphological data

Properties of reconstructed neurons were quantified with Neurolucida Explorer (MBF Bioscience, Colchester, VT). Data was not corrected for tissue shrinkage. However, from several measurements, the shrinkage was determined to be around 10–15 % in the x-/y-axes and 40–60 % in the z axis. The horizontal spread of dendritic and axonal fibers was determined by measuring the maximum distance of structures parallel to the pial surface, whereas the vertical spread was measured perpendicular to the pial surface. Density profiles of dendrites and axonal boutons were determined by subdividing each reconstruction into 10 µm wide bins. These were aligned either vertically or horizontally to the pial surface. Dendritic length and number of axonal boutons were determined for each bin. To superimpose multiple reconstructions and show the distribution of neuronal processes as a population average, reconstructed neurons were registered into one file using defined layer borders as a reference (average of layers identified in DAPI stainings of 150 sections through the barrel cortex), somata aligned at the same horizontal level, and all fibers plotted as one binary image. This was filtered using a Gaussian filter with a comparable radial sigma (20 at 300 dpi) for all structures and a color look-up-table ranging from cold (blue and green for white to light gray) to warm colors (yellow and red for dark gray to black) was applied to the resulting grayscale image. This was then merged with the original black and white image and resulted in heat-maps visualizing areas of highest density of axonal and dendritic trees.

2.8 Unsupervised clustering

6 individual classifications for electrophysiological and morphological properties were performed. Individual parameters used are given in the results and were always normalized to the maximum value. Unsupervised clustering was based on Ward's method (Ward 1963) using the squared euclidean distance as a discriminator. Neurons with the smallest difference in variability of the euclidean distance of tested parameters were identified as nearest neighbors. Clusters were agglomerated by identifying nearest neighbors. Hierarchical levels were determined by linking nearest neighbors which were combined two-by-two into objects of higher hierarchic order. All hierarchical levels were determined by repeating this linkage procedure. Definition of final clusters depended on the individual analyses which are described in the results. Ward's clustering was performed using R (algorithm used: ward.d2; R Foundation for Statistical Computing, Vienna, Austria). Resulting dendrograms and heat maps of values were also plotted using R.

2.9 Statistical tests

For statistical comparisons, data was tested for normality (Shapiro-Wilk test) and equal variance. If both passed, a one-way student *t*-test was used. If one or both failed, a Mann-Whitney rank sum test was used. For any multiple group comparison one way analysis of variance (ANOVA) was used. When significant differences were found and normality or equal variance tests passed, a *post-hoc* Holm-Sidak method as an all pairwise multiple comparison procedure was applied. If normality or equal variance tests failed, ANOVA was based on ranks with *post-hoc* Tukey or Dunn's method as an all pairwise multiple comparison procedure. All statistical tests were performed with SigmaPlot (Version 13.0, Systat Software, Inc., Erkrath, Germany). Values are given as mean±SD if not indicated otherwise.

3 Results

To understand the heterogeneity in the population of VIP neurons and identify possible subgroups, VIP neurons were recorded in whole cell patch clamp mode and subsequently analyzed. Firstly, their electrophysiological profile was determined by describing their basic parameters. Firing patterns were used as a basis to identify features which separated VIP neurons into electrophysiological types. Because firing patterns were previously described in a qualitative manner only, an analytical strategy was developed to translate properties of firing patterns into meaningful and quantifiable variables. These variables were used in unsupervised cluster analyses and, in conjunction with spike waveform properties and subthreshold or passive properties, described the full electrophysiological spectrum of VIP neurons. 5 major subtypes were identified based on the frequency of occurrence of certain combinations of electrophysiological properties. Following this, the distribution of these 5 types throughout the barrel cortex was elucidated (chapter 3.1).

Secondly, one of these electrophysiological types, bursting VIP neurons, was investigated further. These neurons switched their firing pattern to tonic when their membrane potential was depolarized. This depolarization was induced experimentally by a constant current injection. However, as was shown previously, neuromodulators depolarize VIP neurons. Thus, the effects of noradrenalin, acetylcholine, and serotonin in VIP neurons and some of the receptors mediating this depolarization were identified. Furthermore, whether or not these neuromodulators were capable of mediating the switch of firing patterns in bursting VIP neurons was tested (chapter 3.2).

Thirdly, the morphology of VIP neurons was quantitavely analyzed based on their reconstructed morphology. After a description of common features, unsupervised clustering was used to identify possible subgroups and clarify differences between VIP neurons from layer II/III to those found in deeper layers. The morphology of VIP neurons from layer II/III was investigated further to determine their preferred domains of input and output. Lastly, the correlation between morphological and electrophysiological types was examined (chapter 3.3).

3.1 Electrophysiological Characterization of VIP Neurons

3.1.1 Basic electrophysiological properties of VIP neurons

Electrophysiological properties of 303 VIP neurons were characterized. Parameters included resting membrane potential (RMP; -66.5±4 mV; mean±SD), input resistance (313.9±130.5 MΩ), time constant (16.6±5.9 ms), slow rectification (sag; 10.2±5.6%), fast rectification (RI; 4.1±3.7%), capacitance (49.6±14 pF), rheobase (66.8±35.3 pA), latency of APs (110±83.3 ms), AP firing threshold (-35.5±3 mV), AP time to peak (0.43±0.13 ms), AP amplitude (67.9±8.1 mV), AP slope (217.4±56.1 V/s), and AP width (0.55±0.18 ms). Afterhyperpolarizations (AHP) were diverse in timing and composition. Faster (fAHP: 0.72±0.31 ms, peak at -49.6±3.7 mV) or slower peaking AHPs (mAHP: 28.9±15.4 ms, peak at -49.6±2.9 mV) occurred sequentially or individually.

3.1.2 Firing patterns

In terms of circuit function, the more meaningful electrophysiological property of neurons is their firing patterns because the spectrum of AP frequencies and changes of these frequencies during longer stimulations shape their output within a network. In the past, several attempts have been made to define certain properties of firing patterns. These properties were then used to describe the firing behavior of cortical interneurons. One of the most recent descriptions of firing patterns is the Petilla nomenclature (Ascoli et al. 2008). This defined a variety of firing patterns distinguished by firing rate adaptation, continuity of firing, and frequency. Following this definition, VIP neurons could be categorized as continuous non-adapting, continuous adapting, continuous irregular spiking, burst non-adapting, burst adapting, and burst irregular spiking. Fast spiking,

Figure 3 Quantification of firing patterns ▶

The quantification of firing patterns was based on counting APs in 100 ms wide bins. Recordings from 4 individual VIP neurons are shown here (**A**-**D**). Three responses to 1s long depolarizing current stimuli are plotted sequentially from top to bottom for each neuron. Top traces are responses to just above threshold stimulation (min), middle traces are responses to half-maximal stimulation (half). Bottom traces are responses to strongest current stimuli (max). 4 ratios were determined which describe firing rate adaptation and current dependency of firing patterns. A ratio between the average number of APs between the first and last 100 ms of all stimuli described firing rate adaptation for the duration of current stimulations (10:1, dark blue arrows, bins indicated by dashed grey rectangles and numbers inside). 0 equated that the same average number of APs was counted in the last and the first 100 ms which means no firing rate adaptation. 1 equated that no APs were determined during the last 100 ms which is the strongest form of firing rate adaptation (see **D** for an example). A second ratio between the average number of APs during the first and second 100 ms described early firing rate adaptation (2:1, light blue arrows). Current dependency was described by a ratio calculated between the number of APs fired as responses during the first 100 ms to minimal and maximal stimulation strength (min:max, dark red arrows) and minimal to half maximal stimulation strength (min:half, light red arows). Together, these 4 variables described firing patterns of VIP neurons in a numerical manner. Neurons in (**A**) and (**B**) were classified as continuously adapting (CA) using a qualitative description, the neuron in **C** as irregular spiking (IS), the neuron in (**D**) as bursting (BS). Note that the two CA neurons in **A** and **B** showed similar current dependency variables. However, firing rate adaptation of the second neuron in **B** was much stronger. Firing rate adaptation was strongest for the IS and bursting neuron (**C** and **D**). The bursting neuron in **D** was the least dependent on stimulation strength.
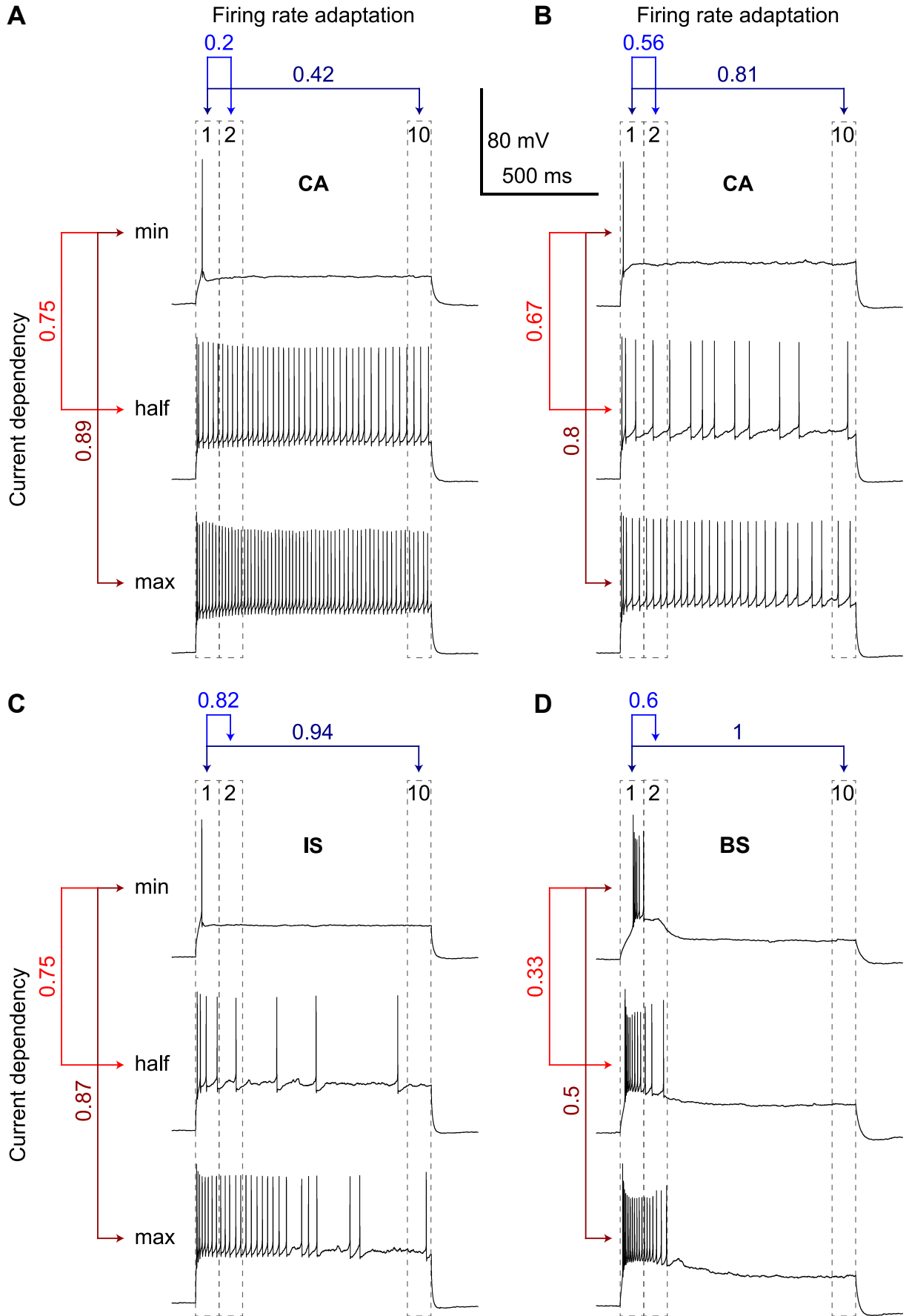
intrinsic burst firing (also defined as regular bursting) and accelerating firing patterns were never observed.

This identification of firing patterns was based on the evaluation of a single AP train. The pattern of APs was then compared to representative traces for each firing pattern defined in the Petilla nomenclature. By this method, firing patterns of VIP neurons were identified in an observer-dependent and qualitative manner. However, selecting an individual AP train was difficult if it was supposed to represent the whole firing behavior of a VIP neuron. When stimulated with incremental current steps, some VIP neurons changed their firing pattern from one type to another. Also, distinguishing between pre-defined types of firing patterns by comparing a single AP train to a representative depiction was in some cases impossible. Additionally, this definition of firing patterns was not informative about the current dependency or the precise spectrum of AP frequencies of firing patterns.

To circumvent these problems, an analytical method was developed that described firing patterns in an unsupervised manner. The basis of this novel approach was to determine meaningful variables that represented firing rate adaptation (decrease in frequency within one train of APs) over multiple current stimuli of different strength. For this analysis, all responses to 1 s lasting current stimuli were subdivided into ten 100 ms lasting bins and the number of APs counted in each (Figure 3; see Materials and Methods for details). From this, a ratio was calculated between the average number of APs during 900-1000 ms (10th bin) and 0-100 ms (1st bin). Resulting values were subtracted from 1. This variable described firing rate adaptation for the complete duration of the stimulus (10:1). A second ratio was calculated between the average number of APs during 100-200 ms (2nd bin) and 0-100 ms (1st bin) and resulting values subtracted from 1. This variable described firing rate adaptation during the first 200 ms (2:1). Furthermore, the dependency of firing patterns on strength of current was analyzed. For this, the ratio of the number of APs during the first 100 ms between minimal and maximal stimulation strength was determined (min:max) and subtracted from 1. The same variable was calculated for half-maximal stimulation strength (min:half). Another property of firing patterns was the frequency of APs. Because the analysis of adaptation was relative it did not describe how fast VIP neurons could fire APs. To access this information, all recorded instantaneous frequencies (the reciprocal of the inter spike interval) were pooled for each neuron. Instantaneous frequencies were binned in 10 Hz intervals and plotted in a cumulative manner. This described

the dynamic frequency range (DFR) of VIP neurons (i.e. 5-95% of all instantaneous frequencies).

As a population, firing patterns of VIP neurons showed a strong firing rate adaptation during current stimulation of 0.75±0.23 (10:1). It was strong because a ratio of 0 would describe that neurons fired the exact same number of APs in the last 100 ms of the stimulus as in the first. In contrast, a ratio of 1 means that no APs were fired during the last 100 ms. Firing rate adaptation within the first 200 ms was weaker with 0.44±0.21 (2:1). Firing patterns of VIP neurons were strongly dependent on stimulation strength (0.83±0.11; min:max). This dependency was strong because a ratio of 0 would describe that neurons fired the exact same number of spikes when stimulated strongly as when stimulated just above rheobase. Current dependency was also strong in the ratio between minimal and half-maximal stimulation strength (0.73±0.15; min:half)). In which frequencies could VIP neurons elicit APs? The average DFR of the VIP neuron population spanned from 10 Hz (5.5±6.3%) to 190 Hz (94.6±12.2%) with a half maximum at 50 Hz (54.3±26.5%).

The aforementioned diversity of firing patterns manifested in large standard deviations of the variables describing firing rate adaptation and DFR. How could the diversity in firing patterns be described in more detail? First, an analysis had to be chosen which fulfilled certain requirements. It had to be based on the determined variables and sort them in an unsupervised manner. Also, it should group neurons with similar firing patterns to identify similarities and differences in firing behavior and make them comparable. Cluster analysis fulfills these requirements. For this dataset, Ward's clustering algorithm was chosen (see Materials and Methods for details). First, firing rate adaptation was analyzed using this unsupervised hierarchical clustering (Chapter 3.1.3, Figure 4). In a separate second clustering the DFR was analyzed (Chapter 3.1.4, Figure 5). Together, these two cluster analyses identified and described firing patterns of VIP neurons. These firing patterns were formed by APs. The waveform of APs could predict certain firing patterns which is why differences in AP waveform were identified in a third cluster analysis (Chapter 3.1.5, Figure 6). Subthreshold or passive properties were analyzed in a fourth cluster analysis (Chapter 3.1.6, Figure 7). This separation into four different electrophysiological realms solved the problem of weights in cluster analyses: if all parameters would have been analyzed in one clustering, those described by a smaller amount of variables would have been weighted lower than those represented by a large number of variables. Thus, adaptation, DFR, AP
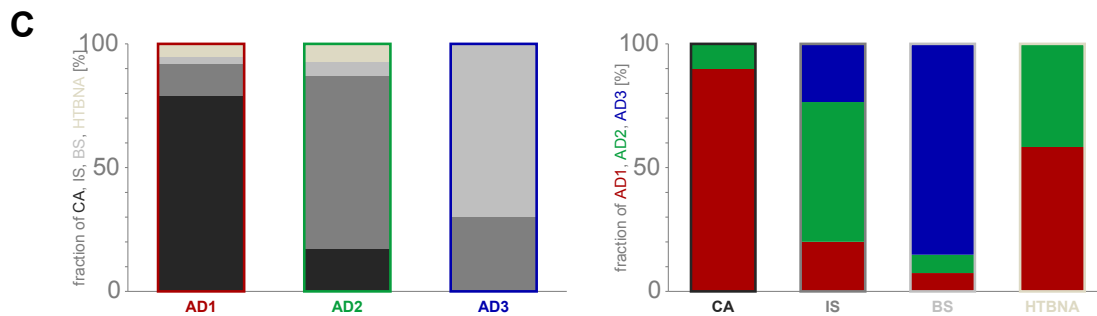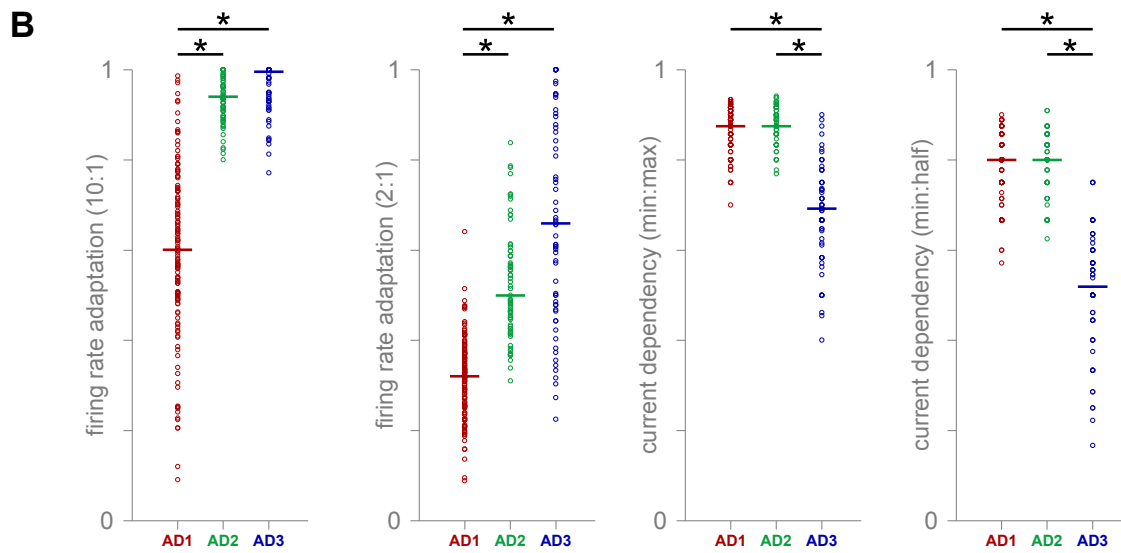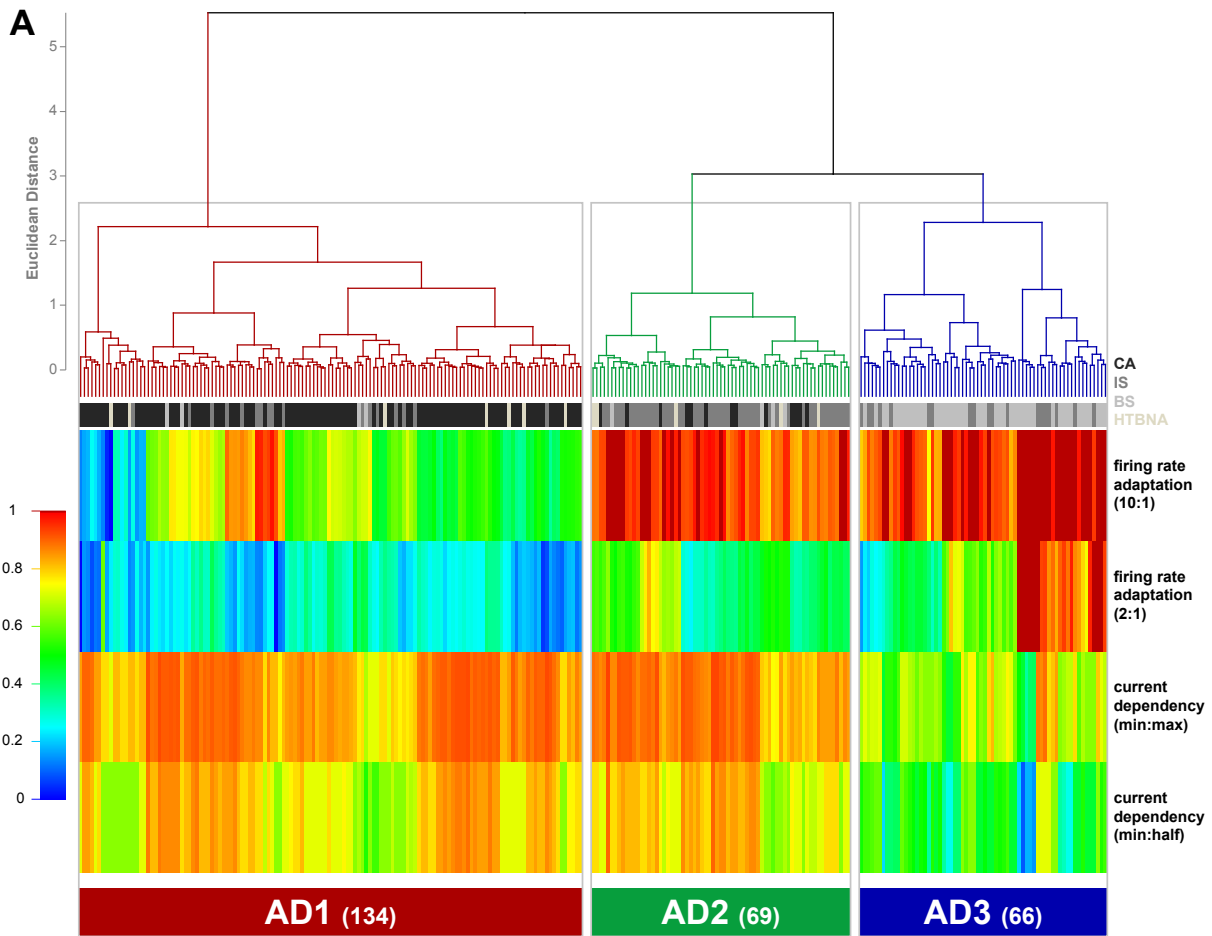
◄**Figure 4** Cluster analysis of the firing rate adaptation of VIP neurons

Firing rate adaptation and current dependency of firing patterns of VIP neurons consisted of three major types: AD1, AD2, and AD3 (**A** and **B**). These matched a qualitative description to a great extent (**C**). Results of the cluster analysis of 269 VIP neurons were plotted as a dendrogram (**A**, top). Leaves of the dendrogram represent individual neurons. Horizontal bars connecting individual neurons are the average euclidean distance between neurons based on 4 variables (time dependent adaptation 10:1 and 2:1, current dependency min:max and min:half). Branches of the three major clusters were colored individually (AD1 in dark red, AD2 in dark green, and AD3 in dark blue). The bar directly beneath the dendrogram visualizes the identity of neurons according to a qualitative classification (CA in black, IS in grey, BS in light grey, and HTBNA in yellowish grey). Individual variables were visualized using a heatmap ranging from cold colors (low values) to warm colors (high values, bottom, color key middle left). Thus, each column described the values for firing rate adaptation for an individual neuron. Neurons found in AD1 had low values for time dependent adaptation (first two rows (10:1 and 2:1) in cold colors) and high values for current dependency (last two rows (min:max and min:half) in warm colors). Neurons found in AD2 had high values for time dependent adaptation (warm colors) and also high values for current dependency (warm colors). Neurons found in AD3 had high values for time dependent adaptation (warm colors) but low values for current dependency (cold colors). These differences were significant, as shown in **B**. 4 graphs were plotted showing the distribution of the variables throughout the 3 clusters (AD1, AD2, and AD3). Data points are shown as open circles with their median as a horizontal bar. Significant differences between certain clusters are indicated as black bars with an asterisk. (**C**) A bar graph visualizing the fraction of CA, IS, B, and HTBNA neurons throughout AD1, AD2, and AD3 are shown on the left. The bar graph on the right visualizes the fraction of AD1, AD2, and AD3 neurons in CA, IS, B, and HTBNA neurons.

waveform, and passive properties of VIP neurons were analyzed independently of each other. Major electrophysiological types were identified by frequency of occurrence of certain combinations of these four electrophysiological realms (Chapters 3.1.7 and 3.1.8, Figures 8 to 12). This analyzing strategy was employed for 269 VIP neurons from layer II/III of the barrel cortex. Results were used as a reference to understand similarities and differences to VIP neurons from layers IV-VI (Chapter 3.1.10, Figure 15).

3.1.3 Firing rate adaptation of VIP neurons

In this first analysis, the firing rate adaptation of VIP neurons was described by identifying similarly behaving neurons in an unsupervised manner. Unsupervised clustering of firing rate adaptation was based on the 4 variables mentioned above. 2 ratios described time dependency (10:1 and 2:1), and 2 ratios current dependency (min:max and min:half). Firing rate adaptation and current dependency of VIP neurons was described best with 3 major clusters (Figure 4 A and B):

AD1: 134 of 269 VIP neurons (50%) had firing rate adaptations with, in relation to the other clusters, a weak time (10:1 = 0.6±0.19; 2:1 = 0.32±0.09) but strong current dependency (min:max = 0.87±0.05; min:half = 0.78±0.08; Figure 4 in red).

AD2: 69 VIP neurons (26%) had firing rate adaptations with a strong

time (10:1 = 0.94±0.05; 2:1 = 0.52±0.12) and strong current dependency (min:max = 0.88±0.04; min:half = 0.79±0.07; Figure 4 in green).

AD3: 66 VIP neurons (24%) had firing rate adaptations with a strong time (10:1 = 0.96±0.06; 2:1 = 0.68±0.23) but weak current dependency (min:max = 0.68±0.11; min:half = 0.51±0.13; Figure 4 in blue).

Differences in time dependent adaptation were significant when comparing AD1 to AD2, and AD1 to AD3 (one way ANOVA, 10:1: H = 182.762, 2:1: H = 152.657, $p <$ 0.001, *post-hoc* Dunn's method). Current dependent adaptation was significantly different when comparing AD3 to AD2, and AD3 to AD1 (one way ANOVA, min:max: H = 122.573, min:half: H = 133.028, $p < 0.001$, *post-hoc* Dunn's method).

These results were compared to a qualitative description of firing patterns. This was done to understand the composition of clusters in greater detail. For this comparison, firing patterns of VIP neurons were identified in an observer-dependent manner based on the Petilla nomenclature. 4 types of firing patterns were differentiated by this qualitative approach. Firing patterns with continuous firing of APs during current stimulation and acommodating firing rate adaptation were defined as continuously adapting (CA; for single neuron examples see Figure 3 A and B and Figure 3.10 A and B). Firing patterns with a high frequency doublet of APs during strong current stimulations without obvious adaptation were defined as high-threshold bursting non-adapting (HTBNA). Neurons that fired a high frequency burst of APs at rheobase were classified as bursting (BS; for single neuron examples see Figure 3 D, Figure 12 E, and Figure 18 A). Any firing behavior that showed neither of the aforementioned parameters was defined as irregular spiking (IS; for single neuron examples see Figure 3 C and Figure 12 C and D). 118 of 269 VIP neurons (44%) were classified as CA, 12 (4%) as HTBNA, 55 (20%) as B, and 84 (31%) as IS.

113 of 118 (90%) CA VIP neurons were objectively clustered into AD1, 48 of 84 (57%) IS VIP neurons into AD2, 47 of 55 (85%) of B VIP neurons into AD3, and 7 of 12 (58%) HTBNA VIP neurons into AD1. The distribution of these qualitatively defined neurons throughout the clusters showed clear preferences. AD1 consisted of 79% CA, 13% IS, 5% HTBNA, and 3% B VIP neurons. AD2 consisted of 70% IS, 17% CA, 7% HTBNA, and 6% B VIP neurons. AD3 consisted of 71% B and 29% IS but neither CA nor HTBNA VIP neurons. Because of the scarcity of HTBNA neurons these were re-classified as CA for later analyses. In summary, 50% of the neurons had firing patterns

which adapted slightly and were dependent on stimulus strength (AD1). The other 50% did not fire APs continuously which was reflected in their high adaptation rates. These were further differentiated by high (AD2) and low current dependency (AD3). This description was based on a quantification of firing patterns and unsupervised clustering. It distinguished firing patterns of VIP neurons in a very similar manner to qualitative descriptions as a comparison of these two strategies revealed (Figure 4 C).

3.1.4 Dynamic frequency range of VIP neurons

Unsupervised clustering of the dynamic frequency range of VIP neurons was based on 39 variables. They described the relative amount of instantaneous AP frequencies found from 10 to 390 Hz (in bins of 10 Hz) in a cumulative manner. VIP neurons showed 4 distinct DFRs, best described by the 4 following major clusters (Figure 5 A and B):

DF1: 101 of 269 VIP neurons (37%) had, in relation to the other clusters, a narrow DFR (median >5% and <95%) from 10 Hz (7.8±5.9%) to 90 Hz (94.9±4.7%) with 50% of all instantaneous AP frequencies at 40 Hz. This DFR was visualized as a rectangle in Figure 5 B (dark yellow).

DF2: 98 VIP neurons (36%) had an intermediate DFR from 20 Hz (9±6.7%) to 120 Hz (94±4.5%) with 50% of all instantaneous AP frequencies at 60 Hz. This DFR was visualized as a rectangle in Figure 5 B (steel blue).

DF3: 10 VIP neurons (4%) had the broadest DFR from 60 Hz (9.4±5.3%) to 330 Hz (89.4±10.5%) with 50% of all instantaneous AP frequencies at 230 Hz. This DFR was visualized as a rectangle in Figure 5 B (red).

DF4: 60 VIP neurons (22%) had a broad DFR from 20 Hz (9.4±7.7%) to 220 Hz (92.8±6.5%) with 50% of all instantaneous AP frequencies at 90 Hz. This DFR was visualized as a rectangle in Figure 5 B (brown).

The cumulative fraction of instantaneous AP frequencies was significantly different between all clusters except DF3 and DF4 in frequency bins 40 to 200 Hz. DF3 differed from all other clusters in frequency bins 230 to 350 Hz (Figure 5 C; one way ANOVA, $p < 0.05$, *post-hoc* Dunn's method).

How were the VIP neurons distinguished by firing rate adaptation distributed throughout the DFR clusters? DF1 consisted of 65 neurons from AD1 (64%), 28 from AD2 (28%),

◄**Figure 5** Cluster analysis of the dynamic frequency range of VIP neurons

VIP neurons showed 4 distinct dynamic frequency ranges (DFR): narrow (DF1), intermediate (DF2), very broad (DF3), and broad (DF4). Results of the cluster analysis of 269 VIP neurons were plotted as a dendrogram (**A**; top). Leaves of the dendrogram represent individual neurons. Horizontal bars connecting individual neurons are the average euclidean distance between neurons based on 39 variables. These were the cumulative fraction of instantaneous frequencies of all APs during different current stimulations in 10 Hz bins (10-390 Hz). Branches of the three major clusters were colored individually (DF1 in dark yellow, DF2 in steel blue, DF3 in light red, and DF4 in brown). The bar directly beneath the dendrogram visualizes the identity of neurons according to their firing rate adaptation type (AD1 dark red, AD2 in dark green, AD3 in dark blue, and bursting in light blue). Individual variables were visualized using a heatmap ranging from cold colors (low values) to warm colors (high values, bottom, color key middle left). Each column described the range of frequencies of an individual neuron. Neurons with a narrow DFR reached 100% of all frequencies already in relatively low frequency bins. Thus, their columns comprised a low amount of low variables (cold colors) and a high amount of high values (red). In contrast, neurons with a broad DFR had a high amount of cold and few red colors. Individual dynamic frequency ranges formed by neurons of the 4 clusters were plotted in **B** as the cumulative fraction of instantaneous frequencies versus the binned instantaneous frequency from 10 to 350 Hz. Data points for each neuron are shown as well as the median for each bin. Rectangles depict the DFR for each cluster which was defined as a median of the population >5% and <95%. The frequency bin in which 50% was crossed is indicated by a dashed line. DF1 neurons had a narrow DFR of 10 to 90 Hz with 50% at 40 Hz. DF2 neurons had an intermediate DFR of 20 to 120 Hz with 50% at 60 Hz. DF3 neurons had a very broad DFR of 60 to 330 Hz with 50% at 230 Hz. DF4 neurons had a broad DFR of 20 to 220 Hz with 50% at 90 Hz (colors as in A). These were distinct from each other as visualized in **C**. Here, DFRs of all clusters were plotted in one graph for a direct comparison (colors according to **A** and **B**). All clusters were significantly different from each other in frequency bins 40 to 200 Hz except for DF3 versus DF4 (black asterisks). DF3 and DF4 significantly differed in bins 230 to 350 Hz (red asterisks).

and 8 from AD3 (8%). The greatest fraction of neurons with a narrow DFR was from AD1. DF2 consisted of 67 neurons from AD1 (68%), 20 from AD2 (20%), and 11 from AD3 (11%). Also the greatest fraction of neurons with a narrow DFR was from AD1. DF3 consisted of 10 neurons from AD3 (100%), and none from AD1 or 2. All of the neurons with a very broad DFR were from AD3. DF4 consisted of 2 neurons from AD1 (3%), 21 from AD2 (35%), and 37 from AD3 (62%). The greatest fraction of neurons with a broad DFR was from AD3 (Figure 9 B). In summary, VIP neurons showed a broad spectrum of frequencies. These could be described best by distinguishing 4 major DFR. In conjunction with firing rate adaptation both, narrow (DF1) and intermediate DFR (DF2) were shown mainly by neurons with a slight firing rate adaptation and strong current dependency. In contrast, broad (DF4) and very broad (DF3) DFR were shown mainly by neurons with a strong firing rate adaptation but low current dependency.

3.1.5 AP waveform of VIP neurons

The cluster analysis of AP waveform of VIP neurons was based on 7 variables. These described amplitude, width, and slope of APs as well as the peak and time to peak of fAHP and mAHP. APs of VIP neurons could be described as 3 distinct types separated into the clusters (Figure 6):
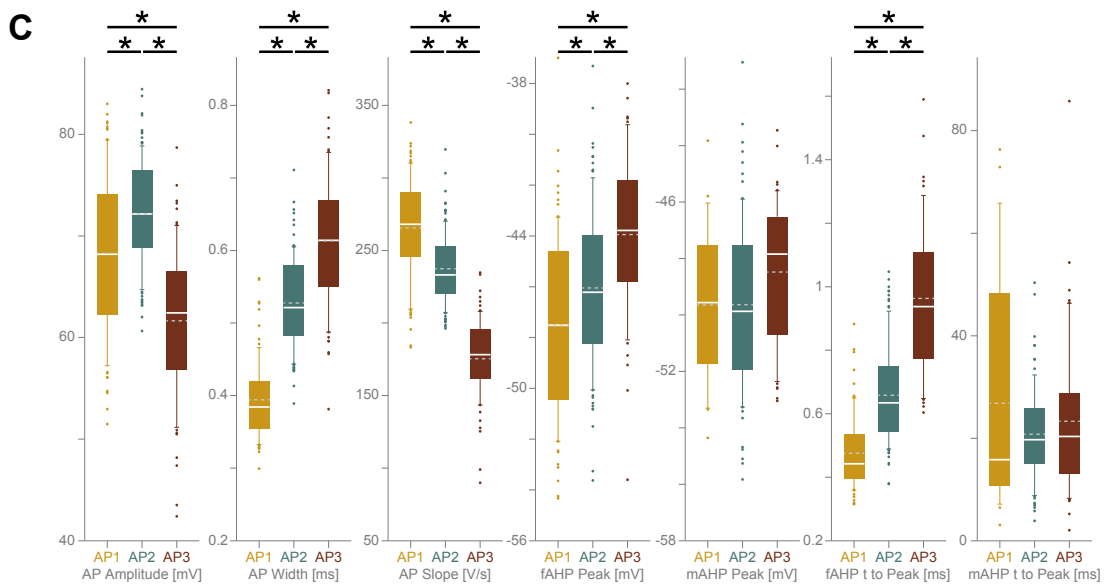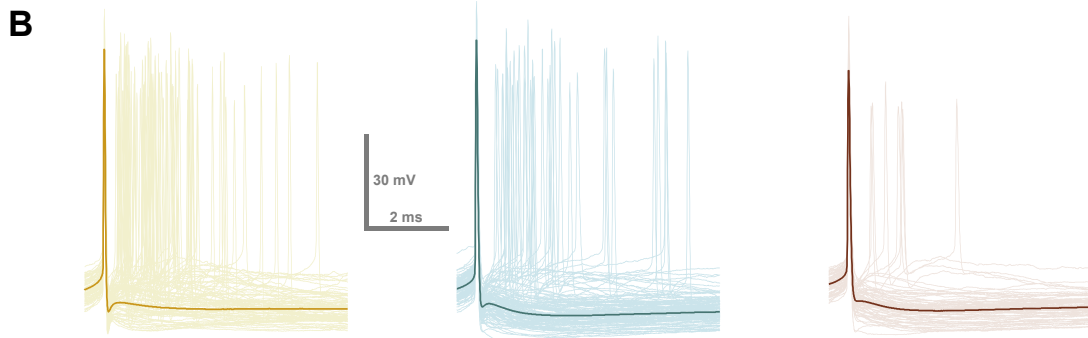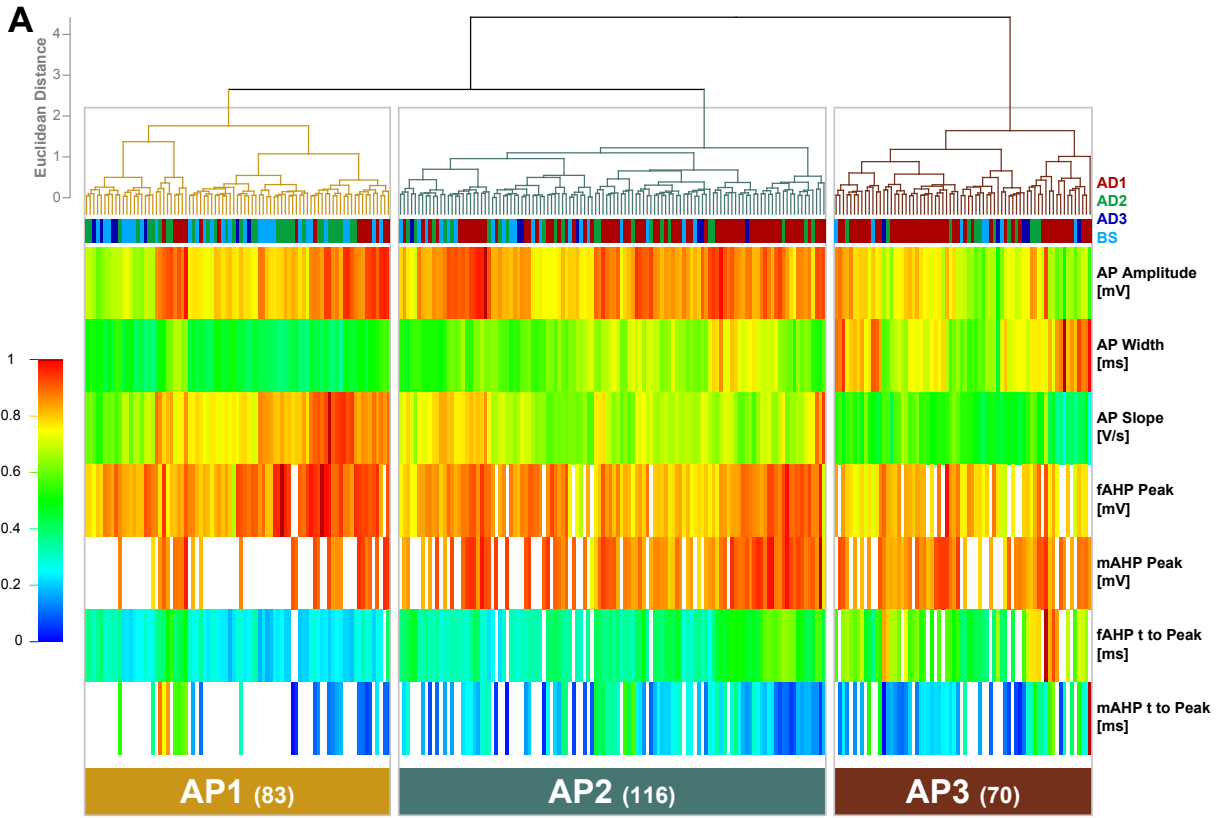
◄**Figure 6** Cluster analysis of the AP waveform of VIP neurons

VIP neurons fired 3 major types of APs: AP1, AP2, and AP3. Results of the cluster analysis of 269 VIP neurons were plotted as a dendrogram (**A**; top). Leaves of the dendrogram represent individual neurons. Horizontal bars connecting individual neurons are the average euclidean distance between neurons based on 7 variables. These were amplitude, width and slope of APs, as well as peak and time to peak of fAHP and mAHP. Branches of the three major clusters were colored individually (AP1 in dark yellow, AP2 in steel blue, and AP3 in brown). The bar directly beneath the dendrogram visualizes the identity of neurons according to their firing rate adaptation type (AD1 dark red, AD2 in dark green, AD3 in dark blue, and bursting in light blue). Individual normalized variables were visualized using a heatmap ranging from cold colors (low values) to warm colors (high values, color key middle left). Each column described the values for the AP waveform of each neuron in relation to all other neurons. In **B** APs from clusters AP1, AP2, and AP3 were overlaid separately (faint traces) and their average plotted (thick line, colors as in **A**). AP waveforms of AP1, AP2 and AP3 were distinct because variables describing those were significantly different between all clusters except for their mAHPs. This was visualized as box plots in **C** (median in white, average as dashed grey lines; black bars and asterisks indicate significant differences).

AP1: 83 of 269 VIP neurons (31%) had the narrowest APs (width of 0.39±0.05 ms) of intermediate amplitude (68.3±8 mV) with the steepest incline (slope of 265.5±45 V/s), the most negative fAHP peak (-47.5±3.6 mV) and the fastest fAHPs (time to peak of 0.47±0.12 ms; Figure 6 in dark yellow).

AP2: 116 VIP neurons (43%) had intermediatly wide APs (width of 0.53±0.06 ms) of highest amplitude (72.2±5.2 mV) with an intermediate steep incline (slope of 237.5±24 V/s), an intermediate fAHP peak (-46±3.1 mV) and intermediatly fast fAHPs (time to peak of 0.66±0.15 ms; Figure 6 in steel blue).

AP3: 70 VIP neurons (26%) had the broadest APs (width of 0.61±0.09 ms) of lowest amplitude (61.6±7.4 mV) with the flattest incline (slope of 175.4±27.4 V/s), the most positive fAHP peak (-43.9±3.1 mV) and the slowest fAHPs (time to peak of 0.96±0.23 ms; Figure 6 in brown).

All of the variables above were significantly different between clusters (one way ANOVA, $p < 0.05$, *post-hoc* Dunn's method). However, no differences were found in the peak (AP1 -49.6±2.5 mV, AP2 -49.6±3 mV, AP3 -48.5±2.5 mV) and time to peak of mAHPs (AP1 26.8±22.3 ms, AP2 20.8±9.3 ms, and AP3 23.3±15 ms).

The composition of clusters was analyzed under the aspect of firing rate adaptation and DFR to understand to which degree AP waveform correlated with firing patterns. AP1 consisted of 16 neurons from AD1 (19%), 33 from AD2 (40%), and 34 from AD3 (41%). Thus, AP1 was preferred by neurons from AD2 and 3. AP2 consisted of 71 neurons from AD1 (61%), 23 from AD2 (20%), and 22 from AD3 (19%). Thus, AP2 was preferred by neurons from AD1. AP3 consisted of 47 neurons from AD1 (67%), 13 from AD2 (19%), and 10 from AD3 (14%). Thus, AP3 was also preferred by neurons
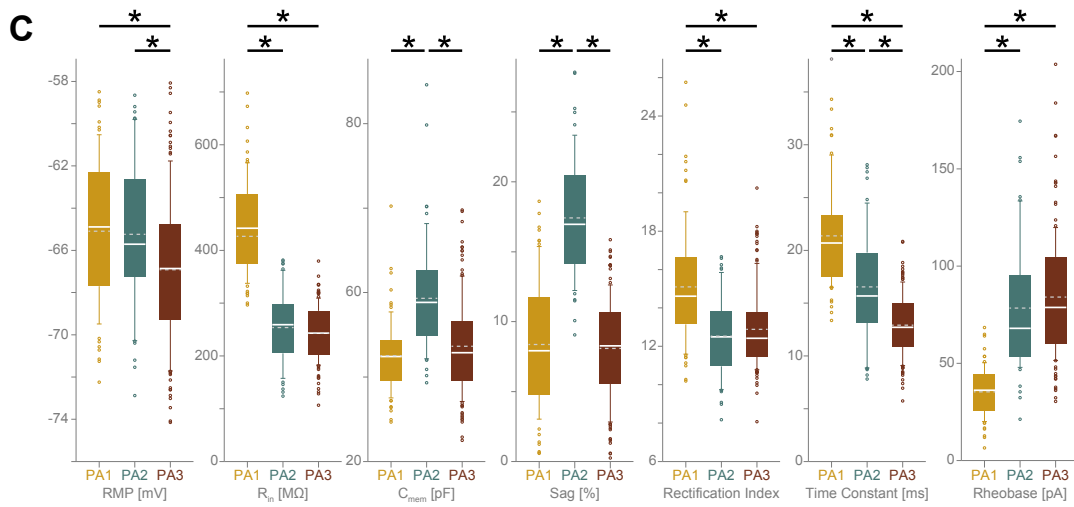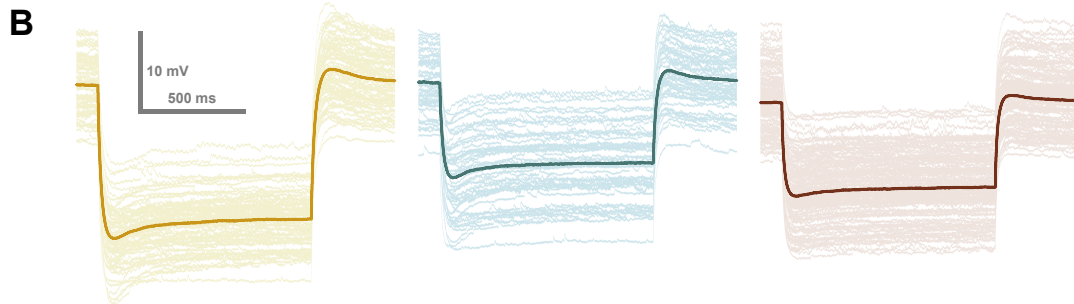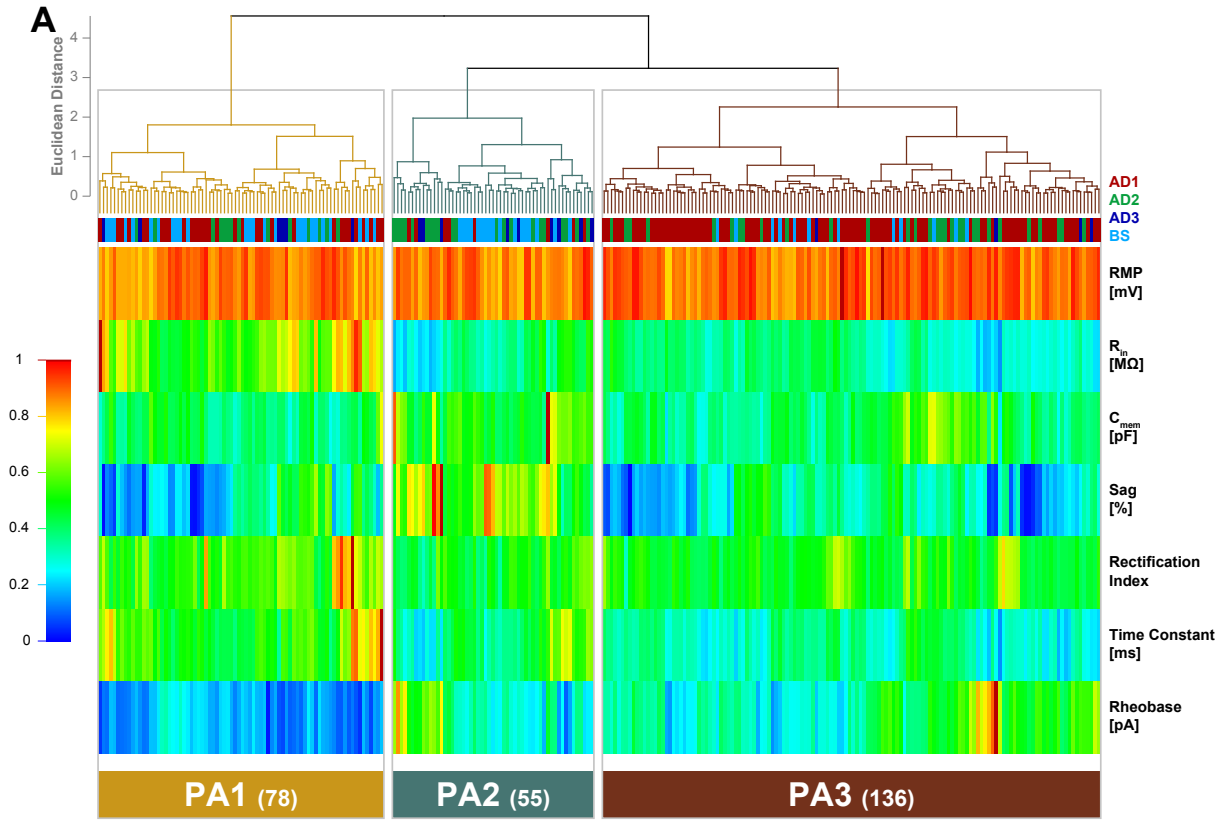
◄Figure 7 Cluster analysis of passive properties of VIP neurons

3 major types of passive or subthreshold properties of VIP neurons were identified: PA1, PA2, and PA3. Result of the cluster analysis of 269 VIP neurons were plotted as a dendrogram (**A**; top). Leaves of the dendrogram represent individual neurons. Horizontal bars connecting individual neurons are the average euclidean distance between neurons based on 7 variables. These were RMP, input resistance (Rin), capacitance (Cmem), slow (sag) and fast rectification (RI), time constant and rheobase. Branches of the three major clusters were colored individually (PA1 in dark yellow, PA2 in steel blue, and PA3 in brown). The bar directly beneath the dendrogram visualizes the identity of neurons according to their firing rate adaptation type (AD1 dark red, AD2 in dark green, AD3 in dark blue, and bursting in light blue). Individual normalized variables were visualized using a heatmap ranging from cold colors (low values) to warm colors (high values, color key middle left). Each column described the values for passive properties of each neuron in relation to all other neurons. In **B** hyperpolarizing responses to a current injection of -50 pA from clusters PA1, PA2, and PA3 were overlaid separately (faint traces) and their average plotted (thick line, colors as in **A**). Passive properties of PA1, PA2, and PA3 were distinct because variables describing those were significantly different between all clusters. This was visualized as box plots in **C** (median in white, average as dashed grey lines; black bars and asterisks indicate significant differences).

from AD1. In terms of DFR, AP1 consisted of 7 neurons from DF1 (8%), 27 from DF2 (32%), 10 from DF3 (12%), and 29 from DF4 (47%). Thus, AP1 was preferred by neurons from DF4. AP2 consisted of 54 neurons from DF1 (47%), 49 from DF2 (42%), and 13 from DF4 (11%) but none from DF3. Thus, AP2 was preferred by neurons from DF1 and 2. AP3 consisted of 40 neurons from DF1 (57%), 22 from DF2 (31%), and 8 from DF4 (11%) but none from DF3. Thus, AP3 was preferred by neurons from DF1 (Figure 9 C). In summary, the three types of APs identified by unsupervised clustering did not dictate properties of firing pattern to a great extent. However, some tendencies became apparent. Most of the VIP neurons with narrow APs and fast fAHPs (AP1) were strongly adapting with an either weak or strong current dependency. Additionally, their DFR was broad. Most of the VIP neurons with APs of highest amplitude (AP2) or lowest amplitude with slow fAHPs (AP3) displayed slight firing rate adaptation with a strong current dependency and an either narrow or intermediate DFR.

3.1.6 Passive properties of VIP neurons

The cluster analysis of passive properties of VIP neurons was based on 7 variables. These described resting membrane potential, input resistance, capacitance, sag, slow rectification, time constant, and rheobase. Passive properties of VIP neurons could be described best as 3 major clusters (Figure 7):

PA1: 78 of 269 VIP neurons (29%) had the highest input resistance (442±91 MΩ), strongest RI (5.1±3), slowest time constant (21.3±5 ms), and lowest rheobase (35.3±12.6 pA; Figure 7 in dark yellow).

PA2: 55 VIP neurons (20%) had the highest capacitance (58.6±13.4 pF), largest sag (17.4±4.2%), and intermediate time constant (16.5±5.2 ms; Figure 7 in steel blue).

PA3: 136 VIP neurons (51%) had the most hyperpolarized RMP (-66.9±3.5 mV), and the fastest time constant (12.9±2.9 ms; Figure 7 in brown).

RMP was significantly different between PA3 (-66.9±3.5 mV) and PA1 (-65.1±3.4 mV), and PA3 and PA2 (-65.2±3.6 mV) but not between PA1 and PA2 (one way ANOVA, H = 153.8, *p* < 0.05, *post-hoc* Holm-Sidak method). Input resistance was significantly different between PA1 (442±91 MΩ) and PA2 (254±70 MΩ), and PA1 and PA3 (243±52 MΩ) but not between PA2 and PA3 (one way ANOVA, H = 153.8, *p* < 0.05, *post-hoc* Dunn's method). Capacitance was significantly different between PA2 (58.6±13.4 pF) and PA1 (45±8.6 pF), and PA2 and PA3 (47.3±11.2 pF) but not between PA1 and PA3 (one way ANOVA, H = 44.4, *p* < 0.05, *post-hoc* Dunn's method). Sag was significantly different between PA2 (17.4±4.2%) and PA1 (8.4±4.5%), and PA2 and PA3 (8.1±3.5%) but not between PA1 and PA3 (one way ANOVA, H = 105.9, *p* < 0.05, *post-hoc* Dunn's method). RI was significantly different between PA1 (5.1±3) and PA2 (2.5±2), and PA1 and PA3 (2.9±2.1) but not between PA2 and PA3 (one way ANOVA, H = 42.5, *p* < 0.05, *post-hoc* Dunn's method). Time constant was significantly different between all clusters (one way ANOVA, *p* < 0.05, H = 126.3, *post-hoc* Dunn's method). Rheobase was significantly different between PA1 (35.3±12.6 pA) and PA2 (78.4.3±4.6 pA), and PA1 and PA3 (84±31.4 pA) but not between PA2 and PA3 (one way ANOVA, H = 135.2, *p* < 0.05, *post-hoc* Dunn's method).

PA1 consisted of 34 neurons from AD1 (44%), 16 from AD2 (20%), and 28 from AD3 (36%). Thus, PA1 was preferred by neurons from AD1. PA2 consisted of 9 neurons from AD1 (16%), 23 from AD2 (42%), and 23 from AD3 (42%). Thus PA2 was preferred by neurons from AD2 and AD3. PA3 consisted of 91 neurons from AD1 (67%), 30 from AD2 (22%), and 15 from AD3 (11%). Thus, PA3 was preferred by neurons from AD1. In terms of DFR, PA1 consisted of 15 neurons from DF1 (19%), 31 from DF2 (40%), 2 from DF3 (3%), and 30 from DF4 (38%). Thus, PA1 was preferred by neurons from DF2 and DF4. PA2 consisted of 19 neurons from DF1 (34%), 13 from DF2 (24%), 5 from DF3 (9%), and 18 from DF4 (24%). Thus, PA2 was preferred by neurons from DF1, DF2, and DF4. PA3 consisted of 67 neurons from DF1 (49%), 54 from DF2 (40%), 3 from DF3 (2%), and 12 from DF4 (9%). Thus, PA3 was preferred by neurons from DF1 and DF2. In terms of AP waveform, PA1 consisted of 22 neurons from AP1 (28%), 30 from AP2 (38%), and 26 from AP3 (33%). Thus, PA1 did not show preferences for a specific

AP waveform. PA2 consisted of 28 neurons from AP1 (51%), 14 from AP2 (25%), and 13 from AP3 (24%). Thus, PA2 was preferred by neurons from AP1. PA3 consisted of 33 neurons from AP1 (24%), 72 from AP2 (53%), and 31 from AP3 (23%). Thus, PA3 was preferred by neurons from AP2 (Figure 9 D). In summary, most of the neurons with high input resistance, low rheobase, strong RI, and slow time constant (PA1) were slightly adapting, had an intermediate or broad DFR, and APs with any waveform. In contrast, most of the neurons with high capacitance and large sag (PA2) were strongly adapting with an either weak or strong current dependency and any DFR. Additionally, their APs were preferentially narrow with fast fAHPs. Most of the neurons with a fast time constant and a hyperpolarized RMP (PA3) were slightly adapting, had a narrow or intermediate DFR, and APs of high amplitude.

3.1.7 Electrophysiological heterogeneity of VIP neurons

In the previous chapters four electrophysiological realms of VIP neurons were analyzed independently. Even though this strategy provided a very detailed description of each of these properties, their results had to be combined to understand the full spectrum of electrophysiological properties of VIP neurons. This combination was based on the classification of individual VIP neurons throughout the 4 cluster analyses. For example, a VIP neuron with weak firing rate adaptation, a narrow DFR, APs of high amplitude and a more hyperpolarized RMP was classified as AD1, DF1, AP2, and PA3. These combinations were determined for all VIP neurons and pooled to identify the similarity between neurons. Next, a perspective had to be chosen from which the dataset could be evaluated. As mentioned before, firing patterns are global parameters that are decisive for neuronal communication. Thus, firing rate adaptation and DFR were used as a starting point to combine the results of the 4 cluster analyses. Firing rate adaptation subdivided into 3 major clusters, DFR into 4, AP waveform into 3, and passive properties into 3. By multiplying the number of clusters, a hypothetical number of 108 combinations was determined (Figure 8 A). If VIP neurons separate into all 108 combinations, they would be perfectly heterogeneous. In contrast, if only 3 combinations appeared, VIP neurons would be perfectly stereotypical in their electrophysiological properties.

VIP neurons separated into 61 combinations which is 58% of 108 possibilities. However, this heterogeneity was structured (Figure 8 B): 123 neurons were found in 8
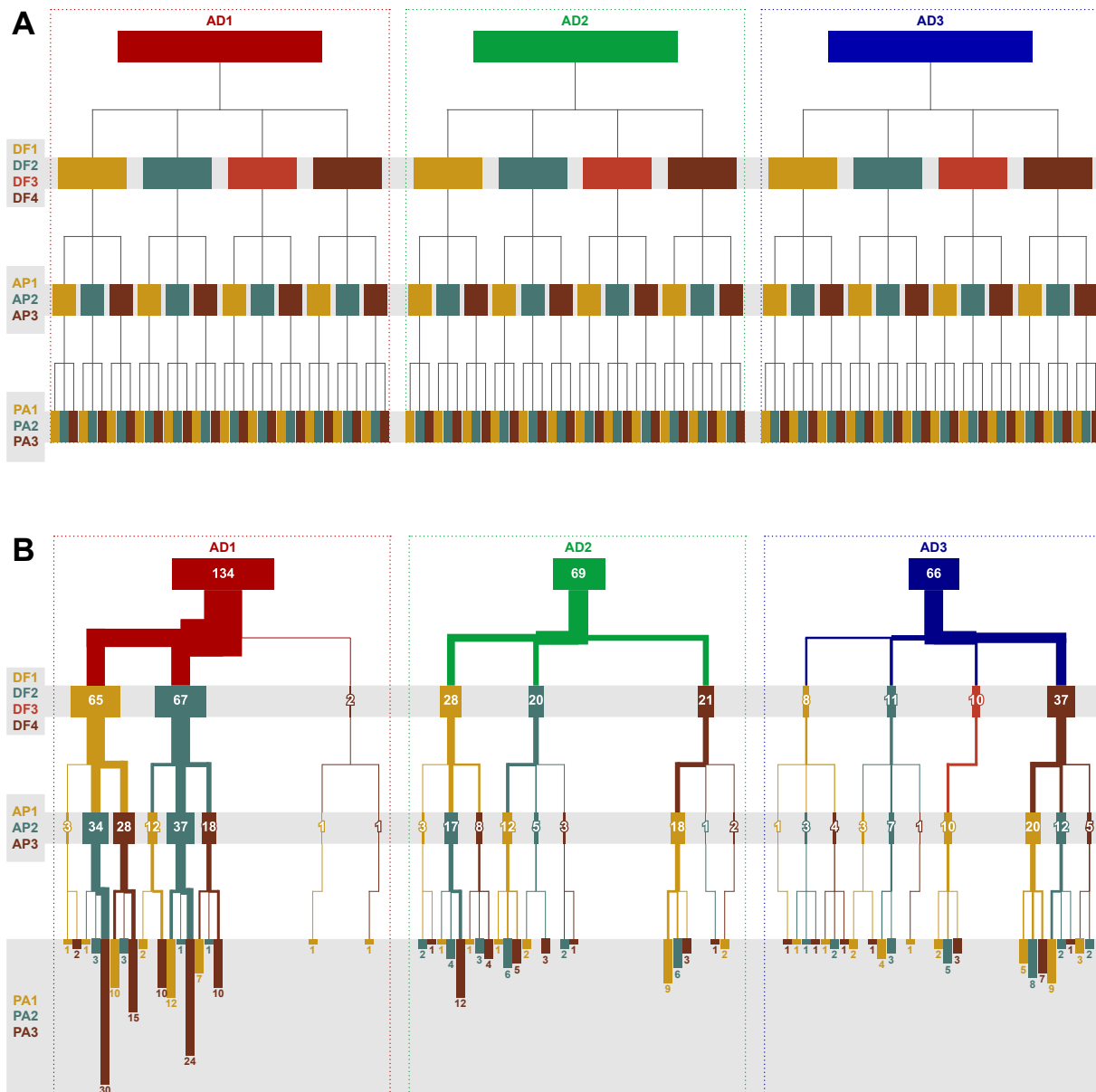
Figure 8 Jellyfish diagram illustrating the electrophysiological heterogeneity of VIP neurons

The four cluster analyses describing firing rate adaptation (AD), dynamic frequency range (DF), AP waveform (AP), and passive properties (PA) of VIP neurons were combined in this figure. AD separated VIP neurons into 3 clusters (AD1 in dark red, AD2 in dark green, and AD3 in dark blue), DF into 4 (DF1 in dark yellow, DF2 in steel blue, DF3 in light red, and DF4 in brown), AP into 3 (AP1 in dark yellow, AP2 in steel blue, and AP3 in brown), and PA into 3 (PA1 in dark yellow, PA2 in steel blue, and PA3 in brown). Hypothetically 108 possibilities of combinations between clusters exist which are visualized in **A**. VIP neurons separate into 61 of 108 possible combinations (**B**). Numbers give the absolute amount of neurons per combination of clusters. Thickness of strokes and width of bars are the relative fraction of neurons. The number of VIP neurons per resulting combinations is shown as inverted bar graphs with the number given beneath these (bottom).

combinations comprising at least 10 neurons. These 46% of all neurons accounted for only 13% of the heterogeneity. 125 neurons were found in combinations of intermediate size (2-9). These 46% of all neurons accounted for 53% of the heterogeneity. 21 of the 61 combinations were shown by individual neurons. These 8% of all 269 neurons formed
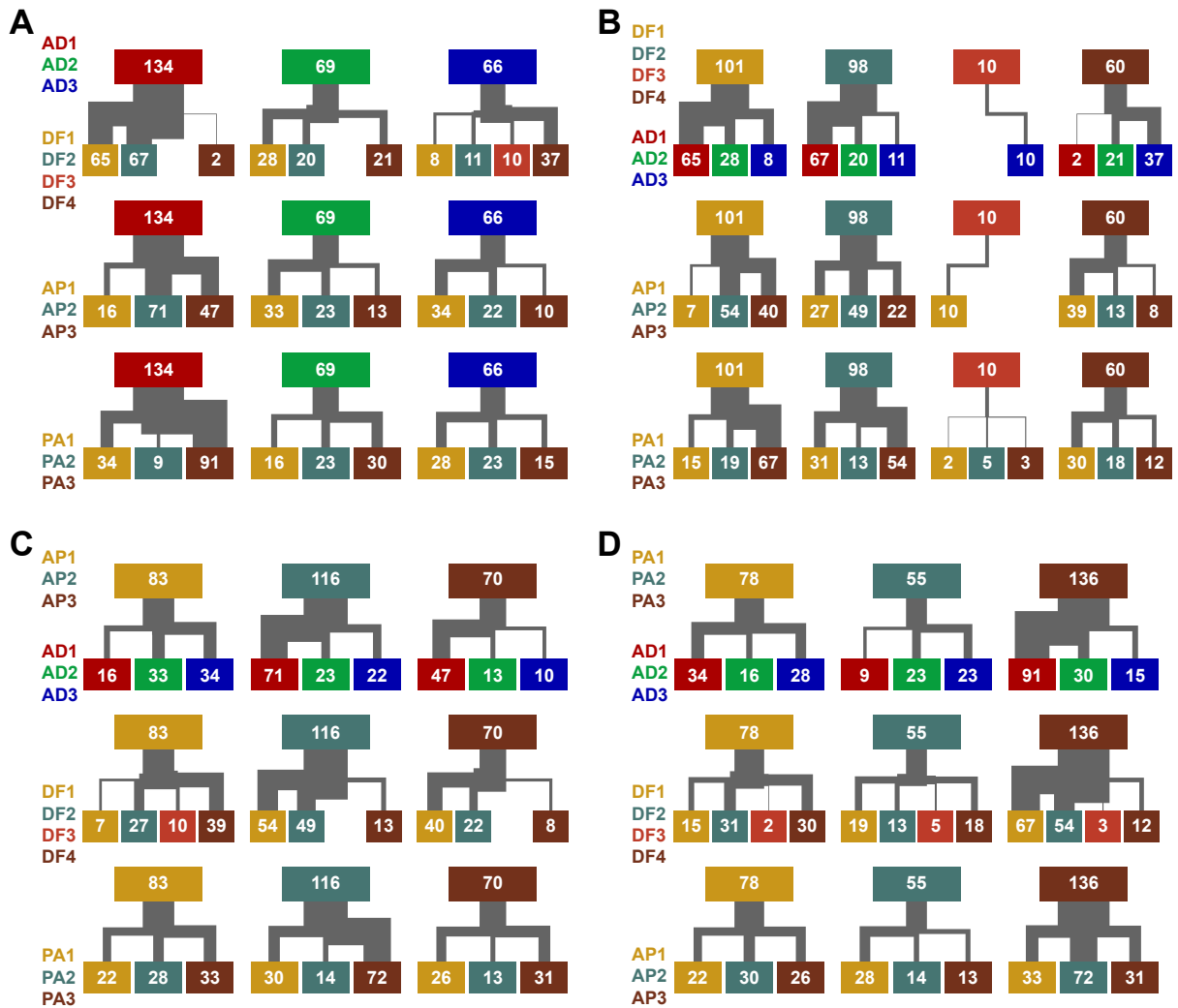
Figure 9 All possible combinations between electrophysiological clusters

AD separated VIP neurons into 3 clusters (AD1 in dark red, AD2 in dark green, and AD3 in dark blue), DF into 4 (DF1 in dark yellow, DF2 in steel blue, DF3 in light red, and DF4 in brown), AP into 3 (AP1 in dark yellow, AP2 in steel blue, and AP3 in brown), and PA into 3 (PA1 in dark yellow, PA2 in steel blue, and PA3 in brown). **A** shows all combinatory possibilities with AD, **B** with DF, **C** with AP, and **D** with PA. Numbers are the absolute number of neurons per cluster or combination, thickness of strokes the fraction of neurons. This illustrates tendencies towards certain combinations.

34% of the heterogeneity. In summary, the population of VIP neurons indeed showed a broad electrophysiological spectrum. But the heterogeneity was not structured in an arbitrary manner because few combinations comprised many neurons. In contrast, a third of the heterogeneity was formed by highly individual neurons.

3.1.8 Identification of 5 major electrophysiological subtypes

The structured manner of the heterogeneity in electrophysiological properties of VIP neurons suggested that there might be electrophysiological subtypes. These
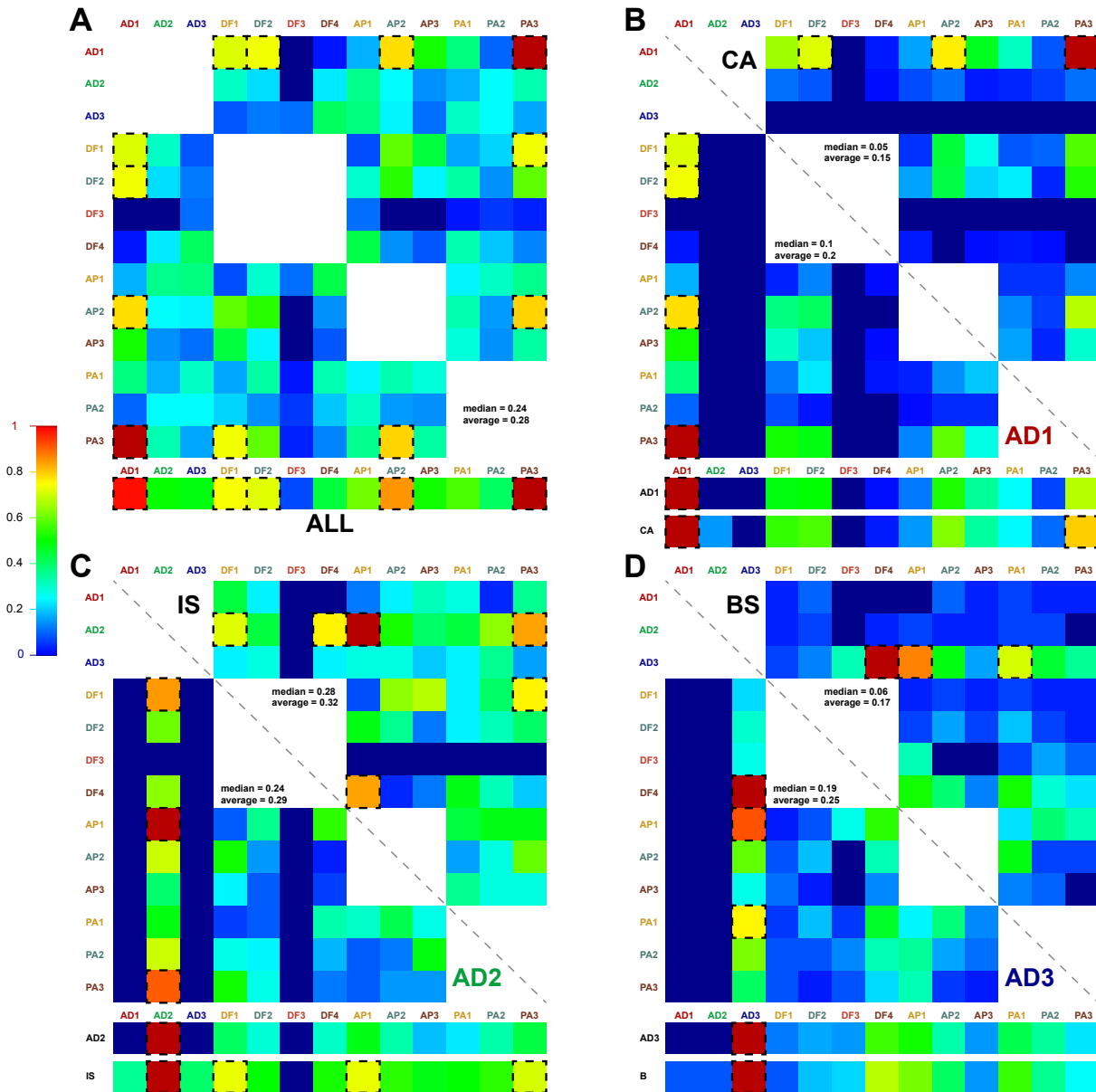
Figure 10 Heat maps illustrating the most common electrophysiological properties of VIP neurons

Relative frequency of occurrence of VIP neurons per cluster (bars beneath each matrix) and combinations of clusters (matrices) is visualized as a heatmap. Each colored square represents the normalized number of neurons counted. Data was normalized to the maximal value (1 in dark red, 0 in dark blue, color key to the middle left). Squares with values above 0.7 are marked by a dashed black outline. These represented that at least 70% of the maximal number of neurons were found in these clusters or combinations of clusters. **A** VIP neurons were most frequently found in clusters AD1, DF1, DF2, AP2, and PA3 (bottom bar) and in the combinations AD1-DF1, -DF2, -AP2, -PA3, DF2-PA3, and AP2-PA3 (matrix). The median of the frequency of occurrence throughout all combinatorial possibilities was 0.24, the average 0.28. **B** VIP neurons classified as CA were sorted most frequently into clusters AD1 and PA3 (bottom bar) and combinations of clusters AD1-DF1, AD1-AP2, and AD1-PA3 (top right of the matrix; median = 0.05, average = 0.15). Neurons of cluster AD1 showed the same preferences except that the relative number of neurons in PA3 did not exceed 0.7 (bottom left and upper bar). The heatmaps describing CA and AD1 VIP neurons are separated by a grey diagonal line. The same visualization was used for VIP neurons classified as IS and AD2 in **C**. IS VIP neurons occurred mostly in clusters AD2, DF2, AP1, PA3, and in the combinations AD2-DF2, AD2-DF4, AD2-AP1, AD2-PA3, DF2-PA3, and DF4-AP1 (median = 0.28, average = 0.32). VIP neurons of cluster AD2 mostly occurred in cluster AD2 and the combinations AD2-DF2, AD2-AP1, and AD2-PA3 (median = 0.24, average = 0.29). In **D** the distribution profile of bursting (BS) and VIP neurons of cluster AD3 are plotted. Bursting neurons were most common in cluster AD3 and the combinations AD3-DF4, AD3-AP1, AD3-PA1. Neurons from cluster AD3 showed the same preferences.
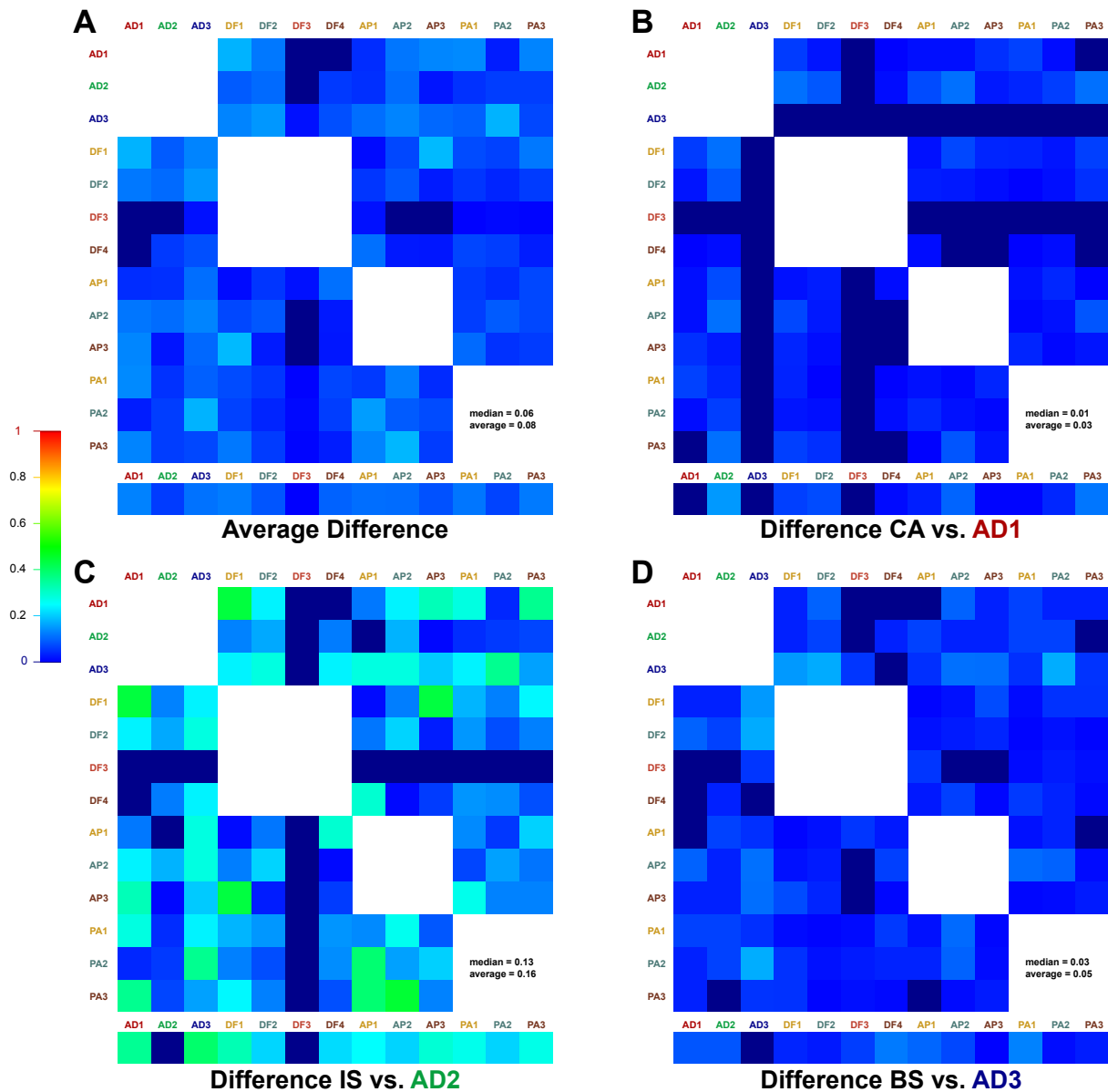
Figure 11 Differences between qualitative and unsupervised classification of VIP neurons

Differences between the categorization of VIP neurons in a qualitative manner (CA, IS, and BS) and results of unsupervised clustering were visualized as heatmaps. Data of Figure 10 was used to calculate the difference in the distribution profile. Resulting values were plotted as squares colored according to their corresponding value (color key to the middle left). CA VIP neurons were compared to AD1 (**B**; median = 0.01, average = 0.03), IS to AD2 (**C**; median = 0.13, average = 0.16), and BS to AD3 (**D**; median = 0.03, average = 0.05). The average difference of these three (median = 0.06, average = 0.08) was plotted in **A**. Note that differences between categorizations IS and AD2 were greater than those between CA and AD1 or BS and AD3.

were described by using an analytical strategy that was based on the frequency of occurrence of neurons throughout the different cluster analyses. In contrast to the analysis of the heterogeneity in chapter 3.1.7 all combinatory possibilites were taken into account (Figure 9). First, the number of neurons was determined for each combination, normalized to the maximal number of neurons and plotted as a heat map
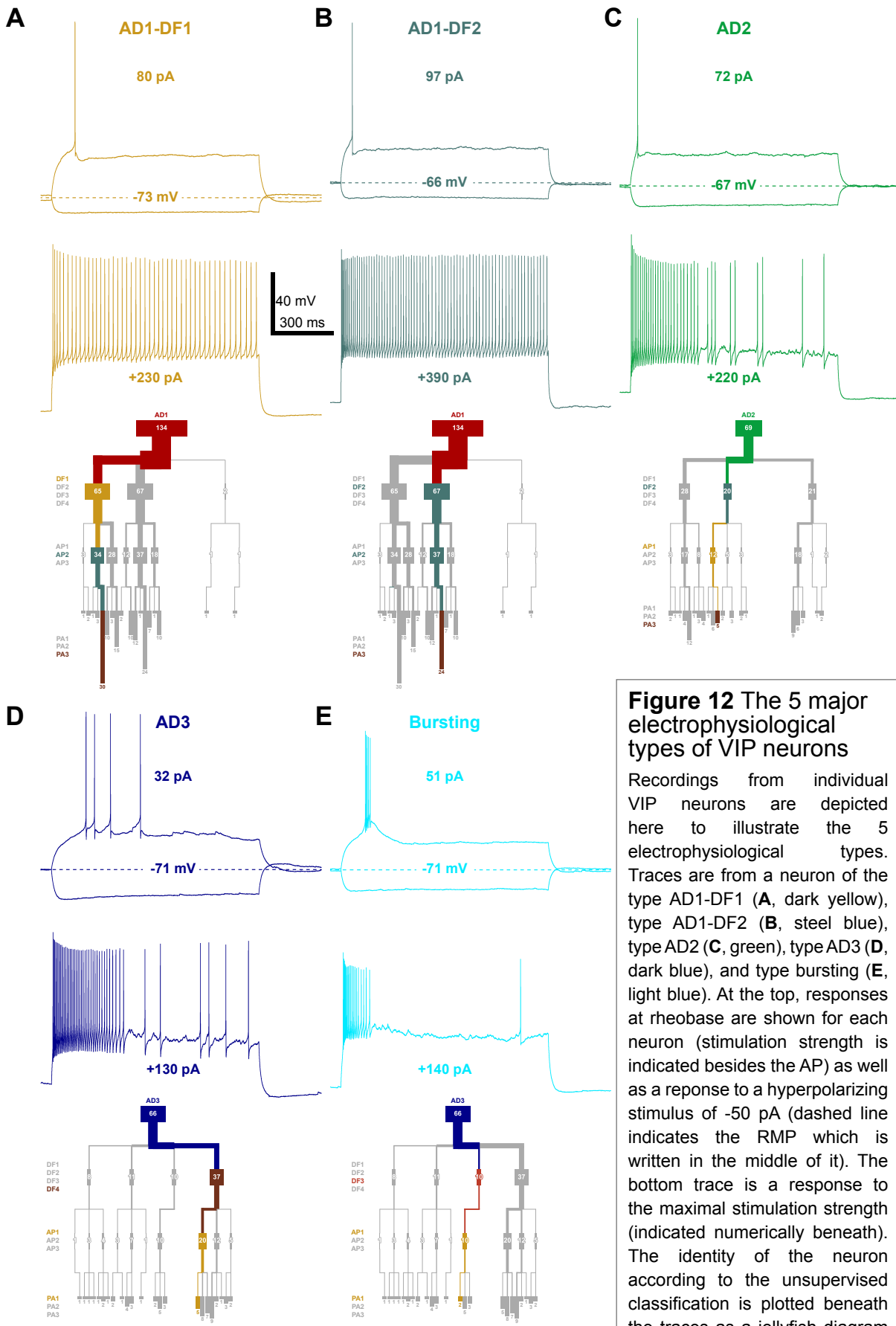
Figure 12 The 5 major electrophysiological types of VIP neurons

Recordings from individual VIP neurons are depicted here to illustrate the 5 electrophysiological types. Traces are from a neuron of the type AD1-DF1 (**A**, dark yellow), type AD1-DF2 (**B**, steel blue), type AD2 (**C**, green), type AD3 (**D**, dark blue), and type bursting (**E**, light blue). At the top, responses at rheobase are shown for each neuron (stimulation strength is indicated besides the AP) as well as a reponse to a hyperpolarizing stimulus of -50 pA (dashed line indicates the RMP which is written in the middle of it). The bottom trace is a response to the maximal stimulation strength (indicated numerically beneath). The identity of the neuron according to the unsupervised classification is plotted beneath the traces as a jellyfish diagram (colored areas are the clusters the neuron was found in).

in Figure 10 A. A comparison of the number of neurons found in specific combinations identified preferences towards certain electrophysiological properties of VIP neurons. Preferences were identified by at least 70% of the maximal number of neurons found in these clusters or combinations. These are indicated by dashed black outlines in Figure 10. When viewed as a population, the greatest fraction of neurons was found in AD1, DF1, DF2, AP2, and PA3 (Figure 10 A, bar beneath the matrix). These preferences were also found in combinations of all clusters. AD1-DF1, AD1-DF2, AD1-AP2, AD1-PA3, DF1-PA3, and AP2-PA3 were most common among VIP neurons. Of all 63 combinations, only 4 never appeared: AD1-DF3, AD2-DF3, DF3-AP2, and DF3-AP3. This reflected that all 10 VIP neurons with a very broad DFR (DF3) had strong firing rate adaptation with a weak current dependency (AD3), and narrow APs with fast fAHPs (AP1). In summary, most of the VIP neurons, when viewed as a population, were slightly adapting with a strong current dependency (AD1), had an either narrow or intermediate DFR (DF1 and DF2), APs of high amplitude (AP2), a RMP of -66.9±3.5 mV and a fast time constant (PA3; Figure 10 A).

The same analytical method was used for subgroups of VIP neurons. These subgroups were identified by their firing rate adaptation (AD1, AD2, and AD3 VIP neurons). Additionally, this method allowed a detailed comparison to the observer-dependent classification which distinguished between 3 major types: CA, IS, and BS VIP neurons (see chapter 3.3 for details) by calculating the differences between electrophysiological preferences (Figure 10 B-D). These differences in relative occurrence throughout all possible combinations were plotted as heat maps (Figure 11). CA VIP neurons matched AD1 neurons best (median of differences = 0.01; 0 = no, 1 = maximal difference), IS VIP neurons resembled those classified as AD2 (median of differences = 0.13), and bursting VIP neurons matched AD3 neurons best (median of differences = 0.03). The information gathered from these analyses was used to describe the following 5 electrophysiological types:

(1) Type **AD1-DF1**

Neurons with firing patterns of type AD1 (n = 134) resembled those identified as CA the most. AD1 VIP neurons were differentiated further by their DFR. The main electrophysiological characteristic of type AD1-DF1 neurons (n = 65) was a slight firing rate adaptation (AD1; 10:1 = 0.6±0.19; 2:1 = 0.32±0.09) with a strong current dependency (min:max = 0.87±0.05; min:half = 0.78±0.08). Their firing rates were low with a narrow DFR (DF1; 10 Hz to 90 Hz with 50% at 40 Hz). Most of these neurons

had APs of high amplitude (AP2; 72.2±5.2 mV), a RMP of -66.9±3.5 mV and a fast time constant (PA3; 12.9±2.9 ms; Figure 12 A).

(2) Type **AD1-DF2**

Neurons of this type (n = 67) were differentiated from AD1-DF1 neurons only because of their DFR. Their firing rates were faster with an intermediate DFR (DF2; 20 Hz to 120 Hz with 50% at 60 Hz). Together with AD1-DF1, AD1-DF2 neurons formed the majority of AD1 (only 2 neurons were AD1-DF3 neurons) and thus the majority of VIP neurons in layer II/III (Figure 12 B).

(3) Type **AD2**

Neurons of this type (n = 69) resembled those classified as IS the most. However, differences to IS neurons were greater than differences between CA and AD1 or bursting and AD3 neurons. This might be due to the literature-established definition of irregular spiking being based on excluding other properties instead of identifying a specific characteristic. Nevertheless, AD2 neurons had a strong firing rate adaptation (10:1 = 0.94±0.05; 2:1 = 0.52±0.12) with a strong current dependency (min:max = 0.88±0.04; min:half = 0.79±0.07). Their DFR could be either narrow (DF1), intermediate (DF2), or broad (DF4). APs of AD2 neurons were preferentially narrow (AP1; width of 0.39±0.05 ms) with a steep incline (slope of 265.5±45 V/s), the most negative fAHP peak (-47.5±3.6 mV) and the fastest fAHPs (time to peak of 0.47±0.12 ms). Their passive property tendency was similar to this of AD1 neurons (PA3; Figure 12 C).

(4) Type **AD3**

Neurons of this type (n = 66) resembled those classified as bursting the most. Their firing rate adaptation was strong (10:1 = 0.96±0.06; 2:1 = 0.68±0.23) with a weak current dependency (min:max = 0.68±0.11; min:half = 0.51±0.13). Their DFR was broad (DF4; 20 Hz to 220 Hz with 50% at 90 Hz). Also, AD3 neurons were the only VIP neurons with an extreme DFR (DF3; 60 Hz to 330 Hz with 50% at 230 Hz). Their APs resembled those of AD2 neurons (AP1). AD3 neurons showed the greatest excitability because most of them had a high input resistance (PA1; 442±91 MΩ) and a low rheobase (35.3±12.6 pA; Figure 12 D).

(5) Type **bursting (BS)**

Bursting VIP neurons were differentiated from all other VIP neurons because of
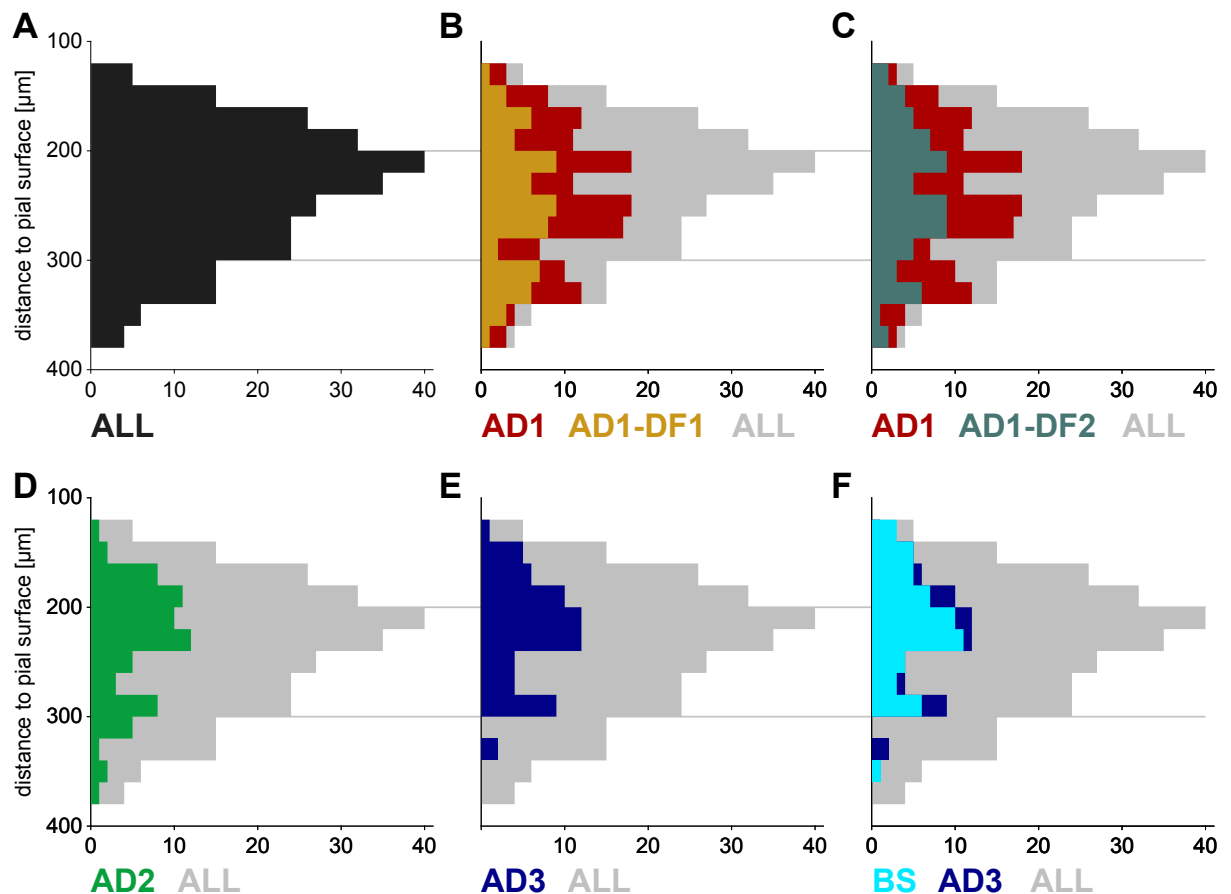
Figure 13 Distribution of the 5 major electrophysiological types of VIP neurons throughout layer II/III

The distance of the somata of recorded neurons to the pial surface is plotted as histograms with a 20 μm bin size. In **A** the distribution of all neurons is plotted (black). **B** depicts the distribution of neurons of the type AD1 (dark red) together with their subset of type AD1-DF1 (dark yellow). In **C** the other subset of AD1 neurons, type AD1-DF2 (steel blue) are plotted. The distribution of AD2 neurons (dark green) is shown in **D**, this of AD3 neurons (dark blue) in **E**, and this of bursting VIP neurons (BS; light blue) together with AD3 neurons in **F**. As a reference, the distribution of all neurons is depicted in grey in **B** to **F**.

their distinct burst firing behavior. This high frequency burst of APs at rheobase was a unique classifier. Consequentially, these neurons were categorized as their own electrophysiological type (Figure 12 E). Furthermore, bursting VIP neurons changed their firing pattern to tonic in a more depolarized state. This will be analyzed further in chapter 3.2. In principle, bursting VIP neurons formed the majority of AD3 neurons (47 of 66). However, not all AD3 neurons were bursting (19 of 66).

3.1.9 Distribution of the 5 electrophysiological subtypes in layer II/III

Somata of the analyzed 269 VIP neurons were located in different depths of layer II/III of the barrel cortex. Their distribution spanned from 126.5 μm to 375.5 μm (distance
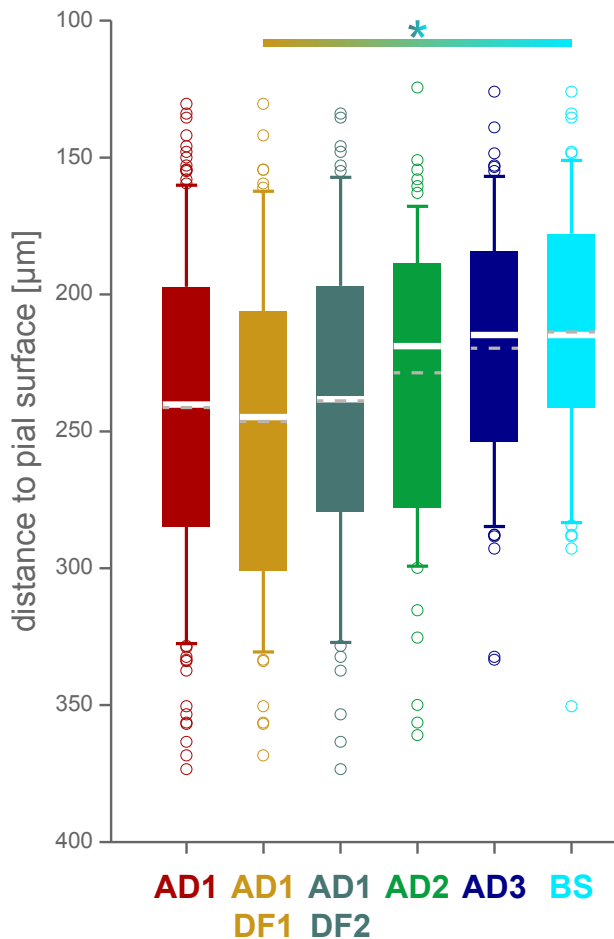
Figure 14 Comparison of the distribution of the 5 major electrophysiological types of VIP neurons in layer II/III

The distribution of somata of VIP neurons of the electrophysiological type AD1 (dark red), AD1-DF1 (dark yellow, a subset of AD1 neurons), AD1-DF2 (steel blue, a subset of AD1 neurons), AD2 (dark green), AD3 (dark blue), and bursting (BS, light blue) is plotted as box plots (median in white, average as dashed grey lines). AD1-DF2 neurons were located significantly deeper in layer II/III than bursting neurons (top bar with asterisk).

of soma center to pial surface). Most of the neurons (40) were located at a depth of ca. 220 µm. This tendency towards upper layer II/III matched the overall distribution profile of VIP neurons (see Introduction for details). But are the 5 electrophysiological subtypes distributed uniformly across layer II/III? Histograms of the distribution of all subtypes showed no obvious differences (Figure 13). However, a significance test revealed that VIP neurons of the type AD1-DF1 were located deeper than bursting VIP neurons (Figure 14; depth of AD1-DF1: 248.6±60.6 µm vs. B: 215.9±47.5 µm, one way ANOVA, H = 15.4, p = 0.009, $post$-hoc Dunn's method). In conclusion, electrophysiological subtypes AD1-DF2, AD2, and AD3 were uniformly distributed throughout layer II/III. VIP neurons of type AD1-DF1 had a tendency towards deeper layer II/III in contrast to bursting VIP neurons which were located more frequently in upper layer II/II.

3.1.10 VIP neurons from layers IV-VI

Before the analysis described above was developed, a paper was published which included a description of VIP neurons from layers IV-VI (Prönneke et al. 2015). In this work, only 34 of these neurons were characterized electrophysiologicaly. This low sample size made a direct comparison to the 269 VIP neurons from layer II/III difficult. Thus, the following chapter can only reveal tendencies, if present.
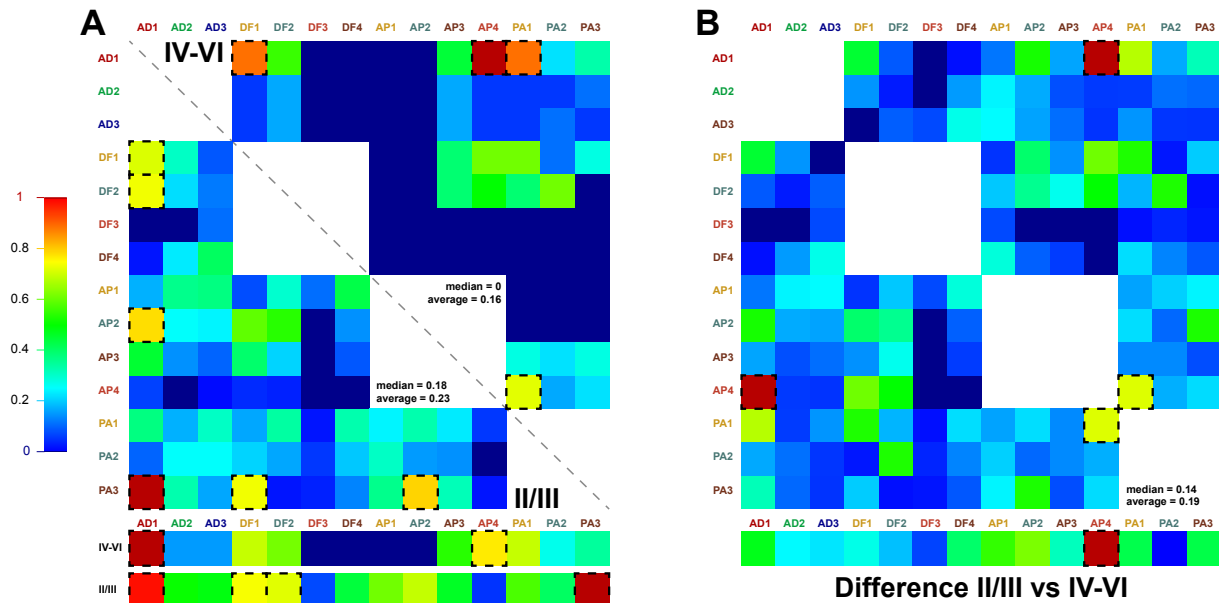
Figure 15 VIP neurons from layers IV-VI were similar but not identical to those from layers II/III

Differences in electrophysiological properties between VIP neurons from layers IV-VI (IV-VI) and VIP neurons from layer II/III (II/III) were visualized as heatmaps. Each colored square represents the normalized number of neurons counted (color key to the middle left). Data was normalized to the maximal value (1 in dark red, 0 in dark blue, color key to the middle left). Squares with values above 0.7 are marked by a dashed blacked outline. These represented that at least 70% of the maximal number of neurons were found in these clusters or combinations of clusters. In **A** the distribution of VIP neurons from layers IV-VI (top right, median = 0, average = 0.16) is plotted in comparison to that of VIP neurons from layer II/III (bottom left, median = 0.18, average = 0.23) separated by a dashed grey line. Data of **A** was used to calculate the difference in the distribution profile. Resulting values were plotted as a heatmap in **B**. The greatest differences were found in the occurrence of APs of type AP4 (bottom bar) as well as in combinations AD1-AP4 and AP4-PA1 (top matrix). The rest of the differences were below 0.7 (median = 0.14, average = 0.19).

In a direct comparison of electrophysiological properties of an equal number of randomly selected VIP neurons from layer II/III to those from layers IV-VI (34 vs. 34) differences were sparse. No significant differences were found in most of the basic properties such as in input resistance (population average of 404.7±212.8 MΩ), sag index (11.2±6.8%), time constant (21.4±7.6 ms), rheobase (51.9±33.9 pA), firing threshold (38.2±3.1 mV), amplitude of action potentials (65.1±9.1 mV), rise time of action potentials (0.75±0.16 ms), half width of action potentials (0.91±0.22 ms), slope of action potentials (118.3±34.5 V/s), or drop of amplitude in the first to the second action potential in a spike train (5.2±4.0 mV).

The two tested populations differed in four parameters: amplitudes of fAHP and mAHP were lower in VIP neurons from layer II/III compared to those of layers IV-VI (fAHP: 8.6±3.1 mV vs. 11.2±3.4 mV; t = 2.930; *p* = 0.005; mAHP: 12.1±2.3 mV vs. 13.5±2.2 mV; U = 229.000; *p* = 0.032). Additionally, VIP neurons from layer II/III had a more depolarized RMP than those found in deeper layers (-66.3±4.8 mV vs. -70.1±5.4 mV;
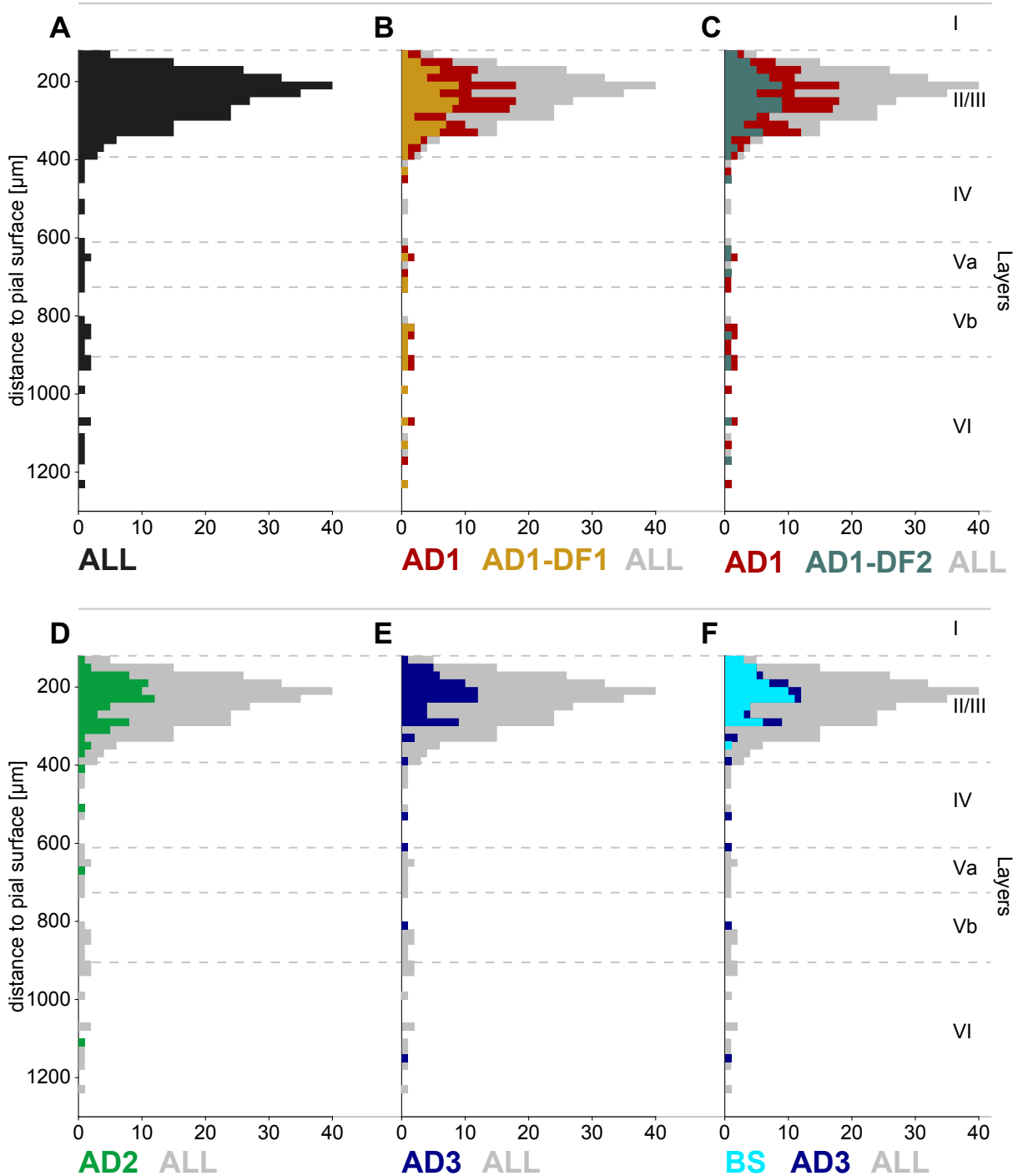
t = 3.207; *p* = 0.001). Furthermore, there was less fast rectification in upper layer VIP neurons (RI of 4.0±3.1% vs. 9.7±5.8%; U = 216.000; *p* < 0.001; Prönneke et al. 2015).

However, the thorough analysis of 269 VIP neurons from layer II/III revealed that these showed a great heterogeneity. When restricting the sample size of a heterogeneous dataset to 34 neurons, significant differences might appear by chance. Thus, the cluster analyses used for the description of the electrophysiological profile of VIP neurons from layer II/III were repeated including the 34 VIP neurons from layers IV-VI.

The firing patterns of this population were different to these of layer II/III in terms of DFR. None of the 34 VIP neurons from layers IV-VI had a broad DFR (30-240 Hz). Either narrow (13 of 34 neurons; 10-100 Hz) or intermediate ranges of AP frequencies (21 of 34 neurons; 30-140 Hz) were found. Also, most of the neurons showed a weak firing rate adaptation with a strong current dependency (AD1: 26, AD2: 4, AD3: 4 of 34 neurons). These differences appeared because no burst firing was observed in deeper layers.

The most prominent difference appeared in the analysis of the AP waveform. Here, 20 of 34 layer IV-VI VIP neurons together with 7 from layer II/III formed a distinct fourth cluster (AP4). The remaining 14 were found in AP3. The novel fourth cluster comprised neurons with even broader APs and flatter inclines than those of cluster 3. Thus, VIP neurons from deeper layers predominantly fired APs that only partially resembled those of neurons from layer II/III since none had properties of AP1 or AP2. Their passive properties, however, showed preference for PA1 (PA1: 18, PA2: 7, PA3: 9 of 34 neurons). The strongest differences in the relative frequency of occurrence between neurons from layers IV-VI and those from layer II/III were found in the combinations AD1-AP4 and AP4-PA1 (Figure 15).

Figure 17 Comparison of the distribution of the 5 major electrophysiological types of VIP neurons from all layers of the barrel cortex

The Distribution of somata of VIP neurons of the electrophysiological type AD1 (dark red), AD1-DF1 (dark yellow, a subset of AD1 neurons), AD1-DF2 (steel blue, a subset of AD1 neurons), AD2 (dark green), AD3 (dark blue), and bursting (BS, light blue) is plotted as box plots (median in white, average as dashed grey lines). AD1 neurons were located significantly deeper in the barrel cortex than AD3 and bursting neurons. AD1-DF1 neurons were located deeper than bursting neurons. AD1-DF2 neurons were located significantly deeper than AD2, AD3, and bursting neurons (top bars with asterisks).

16 of the 34 VIP neurons from layers IV-VI were identified as electrophysiological subtype AD1-DF1, 10 as AD1-DF2, 4 as AD2, and 4 as AD3. None of the neurons

were bursting. How are electrophysiological subtypes distributed across all cortical layers? In conjunction with VIP neurons from layer II/III, the distribution profile showed no obvious preferences for certain layers (Figure 16). However, a statistical analysis revealed that AD1-DF1 and AD1-DF2 neurons were found significantly deeper than bursting neurons (Figure 17). This reflected that bursting VIP neurons were located in layer II/III only. Additionally, AD1-DF1 neurons were deeper than AD2 and AD3 neurons. (depth of AD1-DF1: 365±261.2 µm, median = 265 µm; AD1-DF2: 310.4±208.6 µm, median = 247 µm; AD2: 255.5±131.8 µm, median = 225.5 µm; AD3: 255.6±148.5 µm, median = 221.7 µm; BS: 215.9±47.5 µm, median = 217 µm; one way ANOVA, H = 33.2, $p < 0.001$, *post-hoc* Dunn's method). However, because only 34 neurons from layer IV-VI were analyzed these results have to be interpreted cautiously (see Discussion).

3.2 The Differential Effect of Neuromodulators on VIP Neurons

3.2.1 Bursting VIP neurons

The investigation of firing patterns of VIP neurons unveiled a highly interesting feature. At rheobase 20% (55 of 269) of the analyzed neurons elicited a high frequency burst of APs instead of a single spike. 85% of these bursting VIP neurons were categorized with a strong time but weak current dependent adaptation (46 of 55 in AD3, 4 in AD1, and 4 in AD2). Additionally, 76% of bursting VIP neurons displayed a broad or very broad DFR (31 of 55 in DF4, 10 in DF3, 9 in DF1, and 4 in DF2). APs of bursting VIP neurons were often narrow with fast fAHPs (28 of 54 were classified as AP1, 19 as AP2, and 7 as AP3). Most but not all bursting neurons had a high input resistance and low rheobase (26 of 54 classified as PA1, 17 as PA2, and 11 as PA3). The somata of bursting VIP neurons were exclusively located in layer II/III.

Interestingly, when the membrane potential of bursting VIP neurons was depolarized to -50 mV, these neurons fired a single AP at rheobase and displayed a more tonic firing pattern with stronger stimulation (Figure 18 A). This was observed in all tested bursting neurons (n = 50). In tonic mode, properties of the adaptation of AP trains changed to weaker time but stronger current dependency (Figure 18 B). This resembled firing rate adaptation of AD1 or AD2 neurons. The most prominent change appeared in the DFR since in tonic mode it only spanned from 20 Hz to 140 Hz. All frequency bins from 10 to 360 Hz were significantly different between bursting and tonic mode of the 50 tested VIP neurons (Figure 18 C; $p < 0.05$). The waveform of APs also changed slightly. In tonic mode, APs had lower amplitudes with less steep slopes and slower fAHPs compared to bursting mode (Figure 18 D).

3.2.2 Neuromodulation of VIP neurons by NA, 5HT and ACh

A constant current injection was used to depolarize the aforementioned 50 BS VIP neurons to -50 mV. *In vivo*, some neuromodulators are capable of depolarizing neurons. Here, the effects of 3 neuromodulators were tested on VIP neurons by bath application: noradrenalin (NA), serotonin (5HT), and acetylcholine (ACh; Figure 19). VIP neurons depolarized by 10.3±3.5 mV at the presence of NA (n = 6; 40µM; RMP before: -59.6±6 mV vs. NA: -49.3±4.6 mV; t = 3.335; $p = 0.008$). Due to the low number of tested neurons, NA induced modulation was not analyzed further. 5HT depolarized VIP neurons by
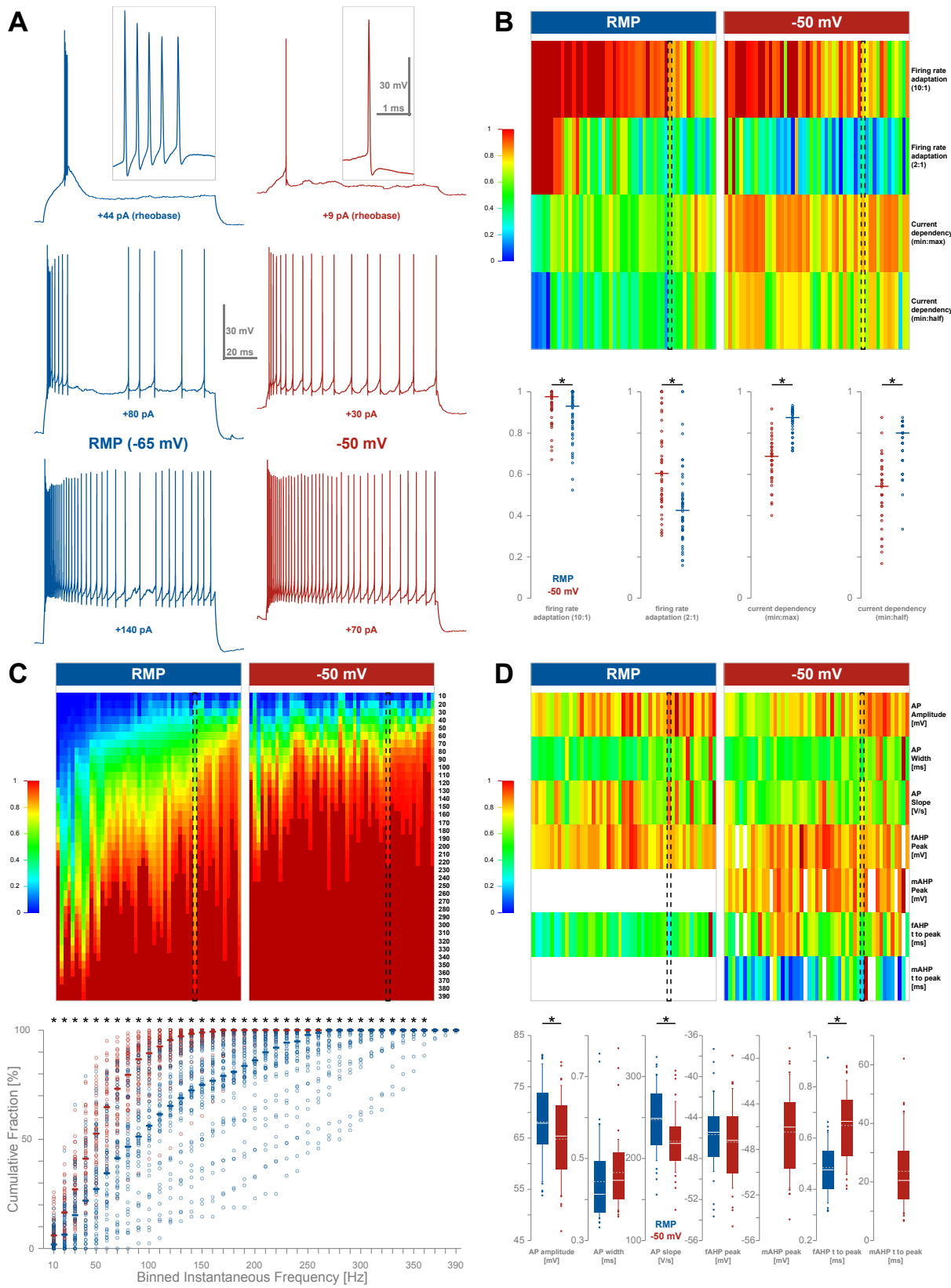
◄**Figure 18** Bursting VIP neurons change their firing behavior from bursting to tonic dependent on membrane potential

50 bursting VIP neurons were analyzed at two different membrane potentials, at RMP (blue) and at -50 mV (red). A single neuron is shown as an example in **A**. Three traces are responses to current stimuli at rheobase (top), half maximal strength (middle), and maximal strength (bottom). The left column shows recordings at RMP, the right at -50 mV. Insets show APs at rheobase with a higher time resolution. Bursting VIP neurons show a prominent burst of APs at RMP which changes into a more tonic firing pattern at -50 mV. Results of a direct comparison of electrophysiological parameters of 50 bursting VIP in the two different states are plotted in **B** to **D**. In **B** firing rate adaptation and current dependency of bursting VIP neurons was compared between bursting and tonic mode. Resulting values are illustrated as heat maps with high values in warm and low values in cold colors (top, color key to the middle left). Each column represents an individual neuron which is found at the same position in both boxes. The left box gives values for bursting neurons at RMP, the right at -50 mV (dashed line marks the neuron shown in **A**). Variables were tested for significant differences between the two states at the bottom. Individual data points are plotted as open circles in their corresponding color. The median is shown as a horizontal bar, significant differences as black bars with asterisks. Firing rate adaptation decreased and current dependency increased in tonic mode. In **C** the DFR of bursting VIP neurons is compared between bursting and tonic mode with the same illustration as in **B** with the cumulative frequency bins from 10 to 390 Hz as variables. The bottom graph plots the cumulative fraction of AP frequencies in 10 Hz bins. Bursting VIP neurons had a significantly broader DFR at RMP than at -50 mV. In **D** the AP waveform of bursting VIP neurons is compared between bursting and tonic mode. The heat maps at top visualize AP waveform variables the same way as in **B** and **C**. Note that at -50 mV bursting neurons showed mAHPs which were not present at RMP. Differences between AP waveform parameters are plotted at the bottom as in **B**. Amplitude and slope of APs slightly decreased in tonic mode, whereas fAHPs peaked later.

7.4±2.8 mV (n = 19; 5 µM; RMP before: -64.6±3.1 mV vs. 5HT: -57.3±4.3 mV; t = 6.136; p < 0.001), whereas ACh depolarized VIP neurons by 8.9±3.9 mV (n = 15; 40 µM; RMP before: -63.9±3.1 mV vs. ACh: -55.1±4.7 mV; t = 6.051; p < 0.001). These depolarizing effects were not restricted to bursting VIP neurons because the tested sample comprised VIP neurons with any kind of firing pattern (Figure 20). To reveal effects of 5HT and ACh besides the change of membrane potential, all determined electrophysiological parameters were tested for significant differences before, during and after neuromodulation (Figure 20 B and D). Neuromodulation by 5HT led to a slight decrease in firing rate adaptation (10:1, before: 0.79±0.21 vs. during: 0.57±0.18, one way ANOVA, p < 0.05, H = 8.5, *post-hoc* Tukey test). Two more differences were found which 5HT was not necessarily responsible for because these were before and after stimulation. The slope of APs decreased (before: 226.9±55.4 V/s vs. after: 173.8±48.9 V/s, one way ANOVA, p = 0.018, *post-hoc* Holm-Sidak method) and time to peak of mAHPs increased (before: 23.6±9.7 ms vs. after: 46.4±21.9 ms, one way ANOVA, p = 0.028, *post-hoc* Holm-Sidak method). These differences might be due to deteriorating effects during long time recordings (Figure 20 B). ACh only induced a change in membrane potential because none of the other electrophysiological parameters were different before and during ACh stimulation. Only 3 were different before and after the application of ACh. Slope (before: 190.3±47.5 V/s vs. after: 148.5±30.8 V/s, one way ANOVA, p = 0.019, *post-hoc* Holm-Sidak method), amplitude of APs (before: 60.9±8
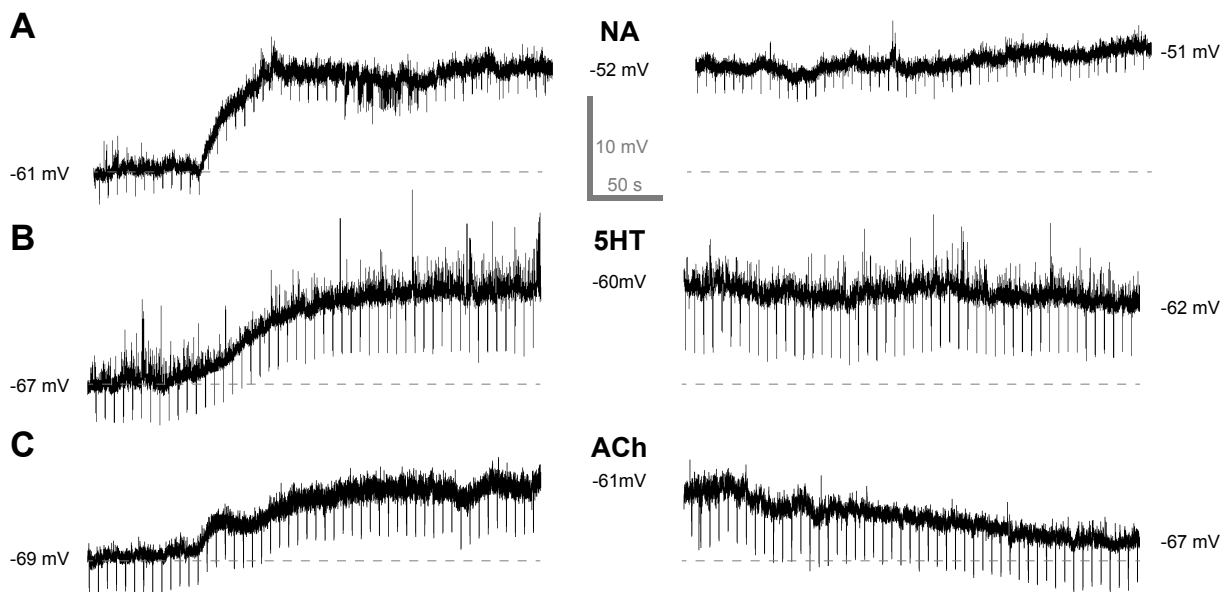
Figure 19 Neuromodulation of VIP neurons

VIP neurons are depolarized by NA (40 µM), 5HT (5 µM), and ACh (40 µM). 3 recordings during bath application of NA (A), 5HT (B), and ACh (C) from individual VIP neurons are shown as examples. During recordings neurons were stimulated with hyperpolarizing currents of -10 pA with 200 ms duration every 6 seconds to monitor the input resistance. RMP is indicated by a dashed line and written as numbers adjacent to the traces. Bath application is shown on the left and recordings after neuromodulation on the right. Note that the membrane potential repolarizes only after modulation by ACh.

mV vs. after: 52.9±8.6 mV, one way ANOVA, p = 0.021, *post-hoc* Holm-Sidak method) as well as sag (before: 11.2±5.9% vs. after: 4.2±3.6%, one way ANOVA, p = 0.008, *post-hoc* Holm-Sidak method) decreased significantly. However, these differences might also reflect deterioration during long lasting recordings (Figure 20 D).

3.2.3 Identification of 5HT and ACh receptors in VIP neurons

The depolarization induced by 5HT and ACh was investigated further by short and local pressure application of these neuromodulators. This technique not only allowed precise control of the timing of the stimulus but also prevented deteriorating effects because the duration of recordings was shorter. Additionally, subtypes of receptors participating in the depolarization could be identified. Responses to short and local pressure application were recorded in voltage clamp without or with the presence of specific antagonists for various receptor subtypes.

A short stimulation of VIP neurons with 5HT (100 ms; n = 24) led to an increase of inward currents with a relatively late onset. These currents were completely blocked when the same neuron was stimulated under the presence of tropisetron which is a specific
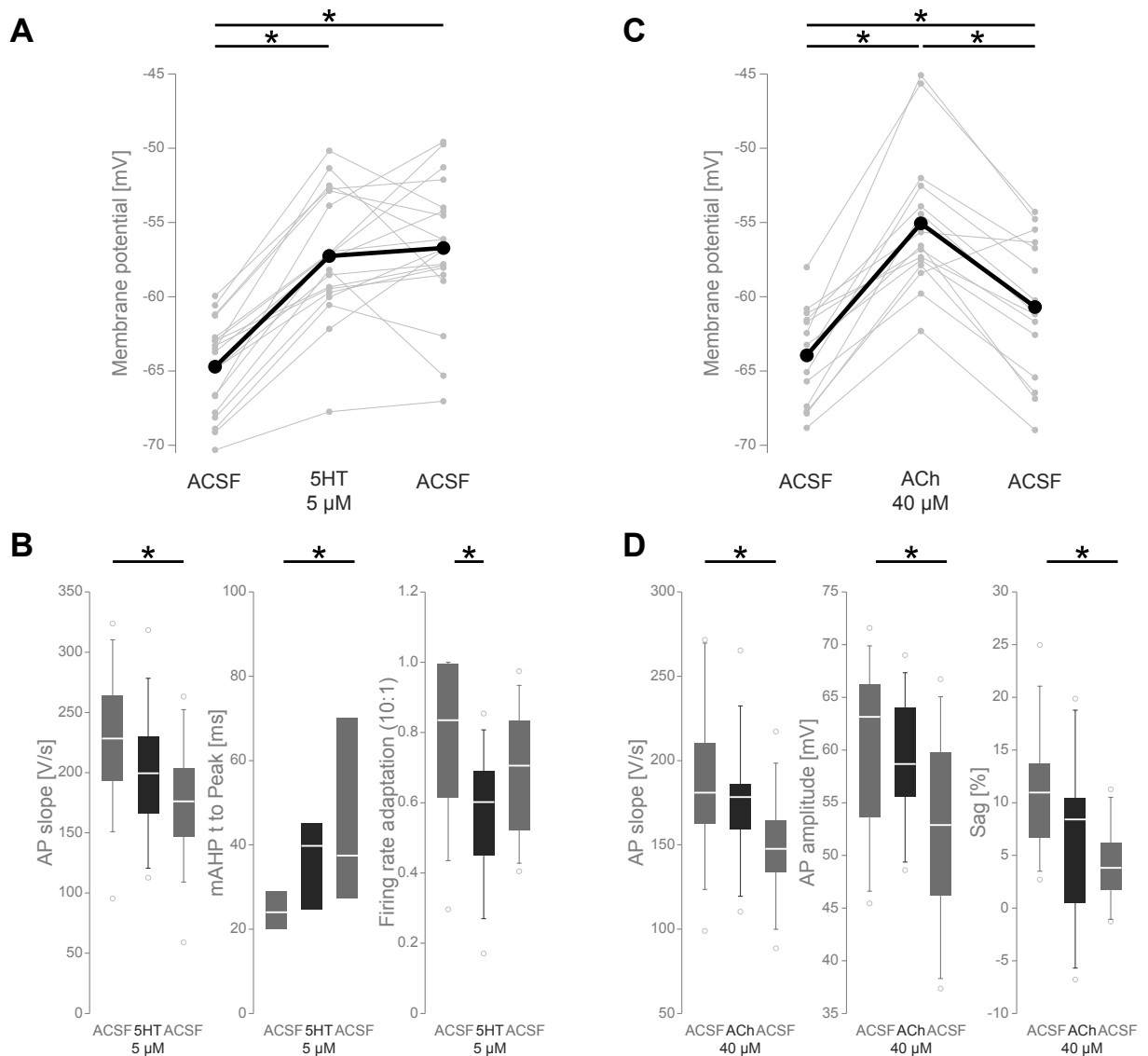
Figure 20 Quantification of the neuromodulation of VIP neurons by 5HT and ACh
5HT (5 µM) and ACh (40 µM) were added to the bath and neurons characterized before, during, and after neuromodulation. 5HT depolarized VIP neurons on average by 7.4±2.8 mV which is plotted as membrane potential vs. state (**A**; n = 19). The membrane potential of individual neurons is shown in grey, the average in black. Differences in membrane potential were significant between before and during as well as before and after the application of 5HT as indicated by black bars with asterisks. In **B** significant differences in electrophysiological properties are shown as box plots. Note that the only difference between before and during the stimulation with 5HT is a decrease in firing rate adaptation. In **C** neuromodulation by ACh is plotted in the same manner as in **A**. ACh depolarized VIP neurons on average by 8.9±3.9 mV (n = 15). The membrane potential differed significantly between all states. 3 electrophysiological parameters differed only before and after the neuromodulation (**D**).

antagonist for the ionotropic $5HT_{3a}R$ (Figure 21 A). Astonishingly, these responses only appeared in ~50% of the tested neurons even though all VIP neurons recorded in current clamp were depolarized by bath-applied 5HT. Bath application exposed VIP neurons to 5HT over several minutes. A stimulation lasting only 100 ms might be too short to activate other 5HT receptors partaking in the depolarization. Thus, stimulation time was increased to 30 seconds. Indeed, a 30 second lasting stimulation with 5HT
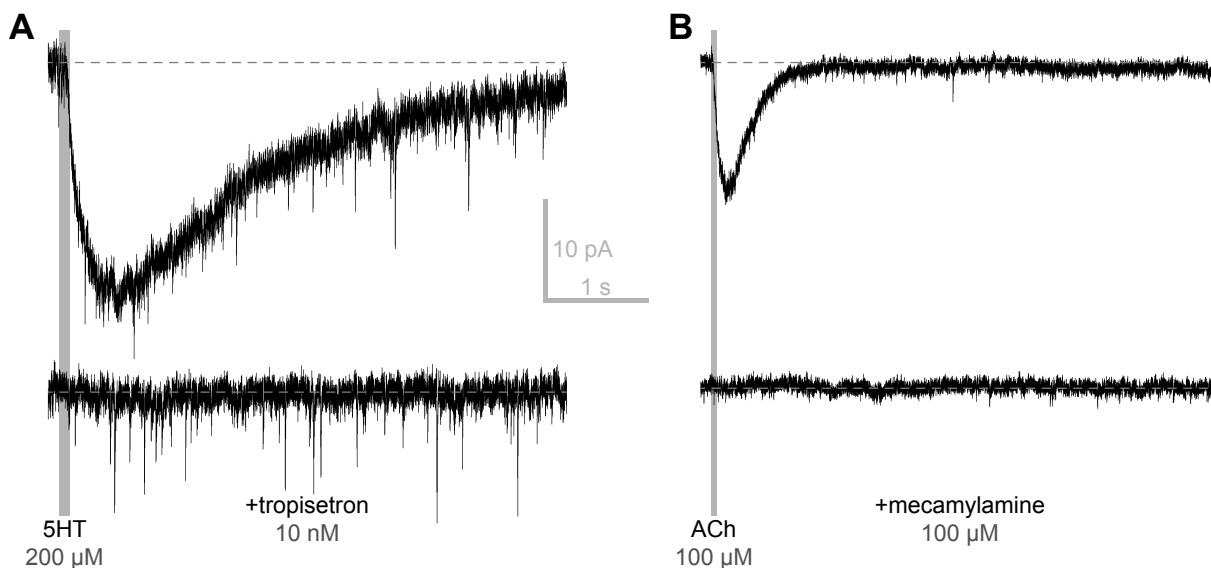
Figure 21 Pressure application of 5HT and ACh

5HT (200 µM; n = 24) and ACh (100 µM; n = 29) were released close to the somata of VIP neurons. Responses were recorded in voltage clamp mode. In **A** the average response of a VIP neuron to 3 stimulations with a 100 ms puff of 5HT is shown natively (top) and under the presence of tropisetron (bottom). In **B** the average response of a VIP neuron to 28 stimulations with a 50 ms puff of ACh is shown natively (top) and under the presence of mecamylamine (average of 14 responses; bottom). Stimulus duration is marked by grey rectangle. Tropisetron abolishes 5HT induced inward currents. Mecamylamine abolishes ACh induced inward currents.

increased inward currents in all tested VIP neurons. However, the time course and strength of these currents was not the same in all neurons but showed two different patterns: fast and strong inward currents that desensitized during the stimulus followed by long lasting but weaker inward currents (Figure 22 B) or long lasting but weak inward currents with a delayed onset (Figure 22 D). VIP neurons displayed either one of these patterns. The bimodality of the first response already hinted towards the presence of at least two different 5HT receptor types. Indeed, when 5HT was applied to neurons with a dual response and tropisetron was present, the first desensitizing component disappeared. However, longer lasting currents with late onset persisted. These could be abolished by a $5HT_2$ receptor antagonist (cinanserin). This antagonist also blocked the currents observed in neurons which showed the second response pattern (Figure 22). The late onset and low amplitude of responses to 5HT mediated by $5HT_2$ receptors suggests that this effect might be mediated by network effects. To exclude network effects, 5HT was applied to the bath while glutamate receptors were blocked by using the AMPA receptor antagonist NBQX and the NMDA receptor antagonist AP5. All tested neurons (n = 9) depolarized as a response to 5HT under these conditions (Figure 23).

Thus, the depolarization induced by 5HT was mediated by postsynaptic $5HT_{3a}$ and $5HT_2$
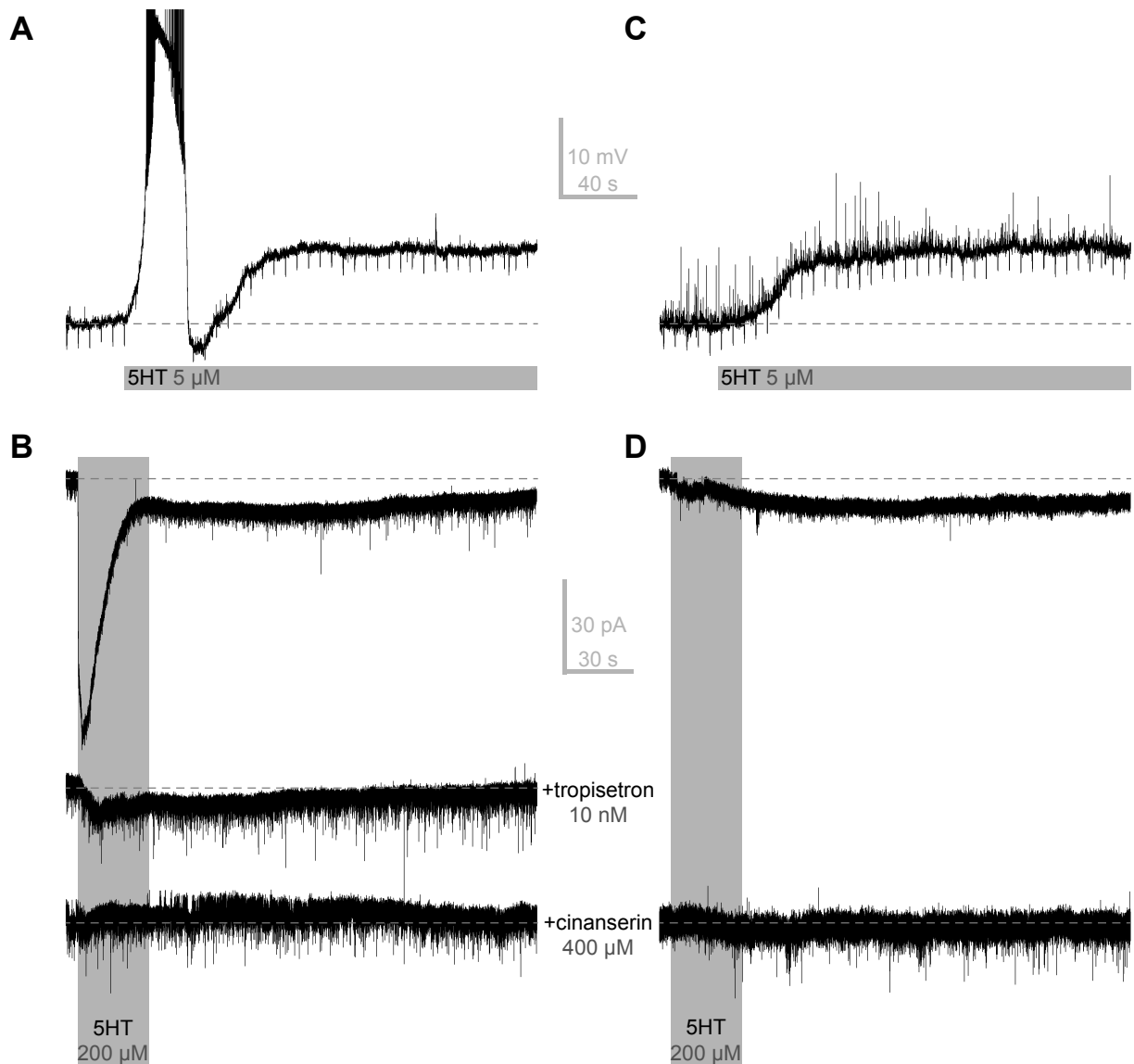
Figure 22 5HT evokes two different response patterns in VIP neurons

VIP neurons recorded in current clamp showed either a bimodal (**A** and **B**) or single response pattern (**C** and **D**) under modulation by 5HT. In **A** a VIP neuron reacted to 5HT (grey rectangle) with a strong desensitizing depolarization followed by a depolarized steady state. The response was recorded in current clamp mode with hyperpolarizing current stimulations of -10 pA with 200 ms duration every 6 seconds to monitor the input resistance. Voltage clamp recordings show that these two components can be blocked by two different 5HT receptor antagonists (**B**). The average of 3 responses of a VIP neuron to a 30 second lasting stimulation of 5HT (200 µM, grey rectangle) show an initial fast increase of inward currents that desensitize while 5HT is present. The initial response is followed by long lasting but weak inward currents (top trace). The initial response is absent under the presence of the 5HT$_{3a}$R antagonist tropisetron. However, the weak and long lasting currents persist (middle trace, average of 2 responses of the same neuron). The 5HT$_2$ receptor antagonist cinanserin abolishes these currents (bottom trace, average of 2 reponses of the same neuron, baseline is indicated by a dashed line). **C** shows the voltage clamp recording of a VIP neuron without the initial fast depolarization (illustration as in **A**). In these neurons cinanserin blocks all evoked currents (**D**, average of 3 responses).

receptors. In only 46% of all tested VIP neurons (36 of 75) a 5HT$_{3a}$ receptor mediated response was present but all of them showed 5HT$_2$ receptor mediated responses. Somata of VIP neurons with a functional 5HT$_{3a}$R were distributed throughout layer II/III in the same manner as VIP neurons with only 5HT$_2$ receptors (Figure 24 A). But

A

10 mV

30 s

-66 mV

5HT 5 µM +AP5 (50 µM) +NBQX (10 µM)

B

-70 mV

5HT 5 µM +AP5 (50 µM) +NBQX (10 µM)

Figure 23 5HT responses are mediated by postsynaptic 5HT receptors

5HT depolarizes VIP neurons when glutamatergic input is antagonized by AP5 (NMDA receptor antagonist, 50 µM) and NBQX (AMPA receptor antagonist, 10 µM) in both (n = 9), VIP neurons with a bimodal (**A**) or a single response (**B**). A response of an individual VIP neuron to 5HT (grey rectangle, RMP indicated by ddashed line) recorded in current clamp mode with hyperpolarizing current stimulations of -10 pA with 200 ms duration every 6 seconds to monitor the input resistance is shown in **A**. This neuron had a bimodal response pattern. The neuron in **B** had a single response. This demonstrates that $5HT_{3a}$ and $5HT_2$ receptor mediated depolarizations are independent of glutamatergic presynaptic activity.

the two populations differed in their electrophysiological profile. VIP neurons of types AD1-DF2 and AD2 did not show preferences towards a certain 5HTR expression. Only 2 non-bursting AD3 VIP neurons were tested with 5HT. Preferences were found for 2 electrophysiological types: 70% of the bursting VIP neurons (16 of 23) had a functional $5HT_{3a}R$. In contrast, 75% of the AD1-DF1 VIP neurons (12 of 16) were depolarized via $5HT_2R$ exclusively (Figure 24 B).

A

B
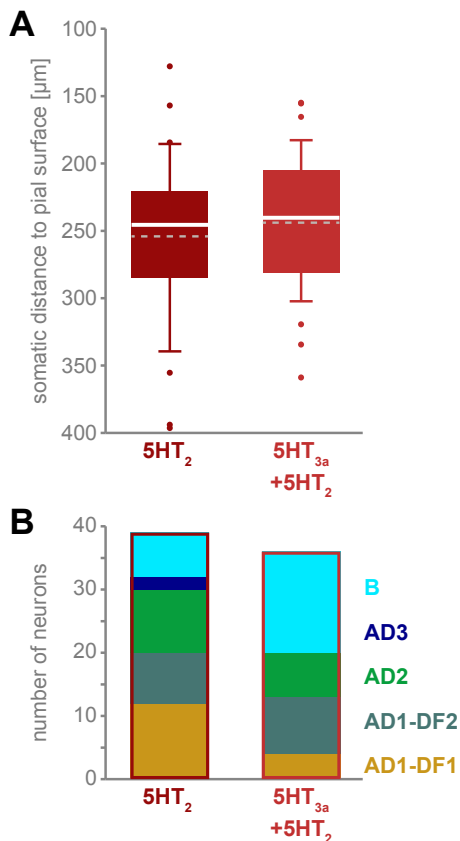
ACh induced depolarization was less complex. Inward currents as responses to short stimuli (50 ms) were immediate and lasted as long as ACh was present (n = 48). An antagonist for nicotinic non-α7 ACh receptors (mecamylamine) fully inhibited these currents. Thus, the depolarization

Figure 24 Comparison of VIP neurons with $5HT_{3a}R$ mediated responses to those without

VIP neurons with functional $5HT_{3a}R$ were distributed in the same manner throughout layer II/III as those without which is shown as box plots (**A**, average as a dashed line). 36 of 75 tested VIP neurons had functional $5HT_{3a}R$. Bursting VIP neurons preferentially express $5HT_{3a}R$. In contrast, AD1-DF1 VIP neurons preferentially showed $5HT_2$ receptor mediated responses only (**B**).

A

5 mV
40 s

ACh 40 µM

B

30 pA
30 s

ACh
100 µM

+mecamylamine
100 µM
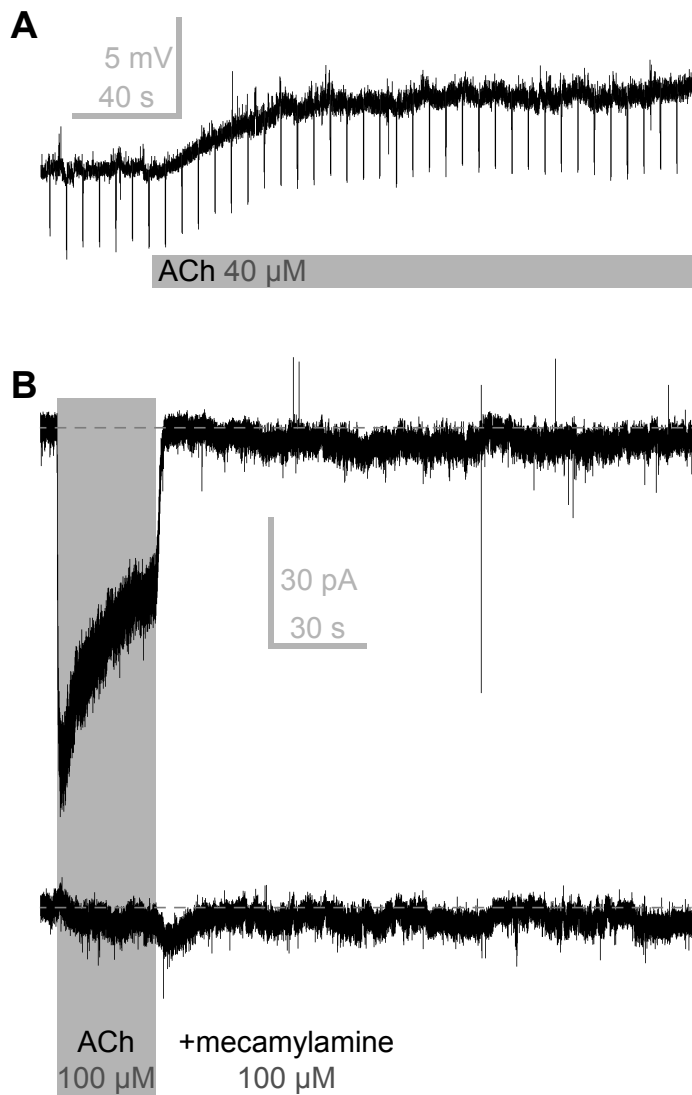
Figure 25 ACh induced depolarizations are mediated by nicotinic non-α7 receptors

VIP neurons recorded in current clamp were depolarized by ACh. In **A** a response was recorded in current clamp mode with hyperpolarizing current stimulations of -10 pA with 200 ms duration every 6 seconds to monitor the input resistance. Voltage clamp recordings show that this depolarization can be blocked by a non-α7 nicotinic receptor antagonist (**B**). The average of 3 responses of a VIP neuron to a 30 second lasting stimulation of ACh (100 µM, grey rectangle) show an immediate increase of inward currents that desensitizes slightly while ACh is present. These currents last exactly as long as the stimulus (top trace). Inward currents are blocked by Mecamylamine, a non-a7 receptor antagonist (bottom trace, average of 3 responses).

induced by ACh was mediated by non-α7 ACh receptors. No long lasting currents appeared when VIP neurons were stimulated with ACh for 30 seconds (Figure 25). Somata of tested VIP neurons were distributed ubiquitously throughout layer II/III.

3.2.4 Neuromodulation of bursting VIP neurons

Indeed, 5HT and ACh depolarized VIP neurons. But is this depolarization sufficient to trigger the switch of firing mode in bursting VIP neurons? To test this, the DFR of bursting VIP neurons was analyzed before and during the application of 5HT (n = 8) and ACh (n = 5), respectively. The DFR was chosen because it showed the most prominent change due to the differences in firing behavior between bursting and tonic mode. All tested bursting VIP neurons changed their firing pattern from bursting to tonic signified by a shift of DFR towards lower frequencies during neuromodulation. This change in DFR was significant in various bins because high

frequencies from bursts did not occure in tonic mode (Figure 26 A and B; rank sum tests, $p < 0.05$). However, other effects of the neuromodulator besides the change in membrane potential could be responsible for switching firing modes in bursting VIP
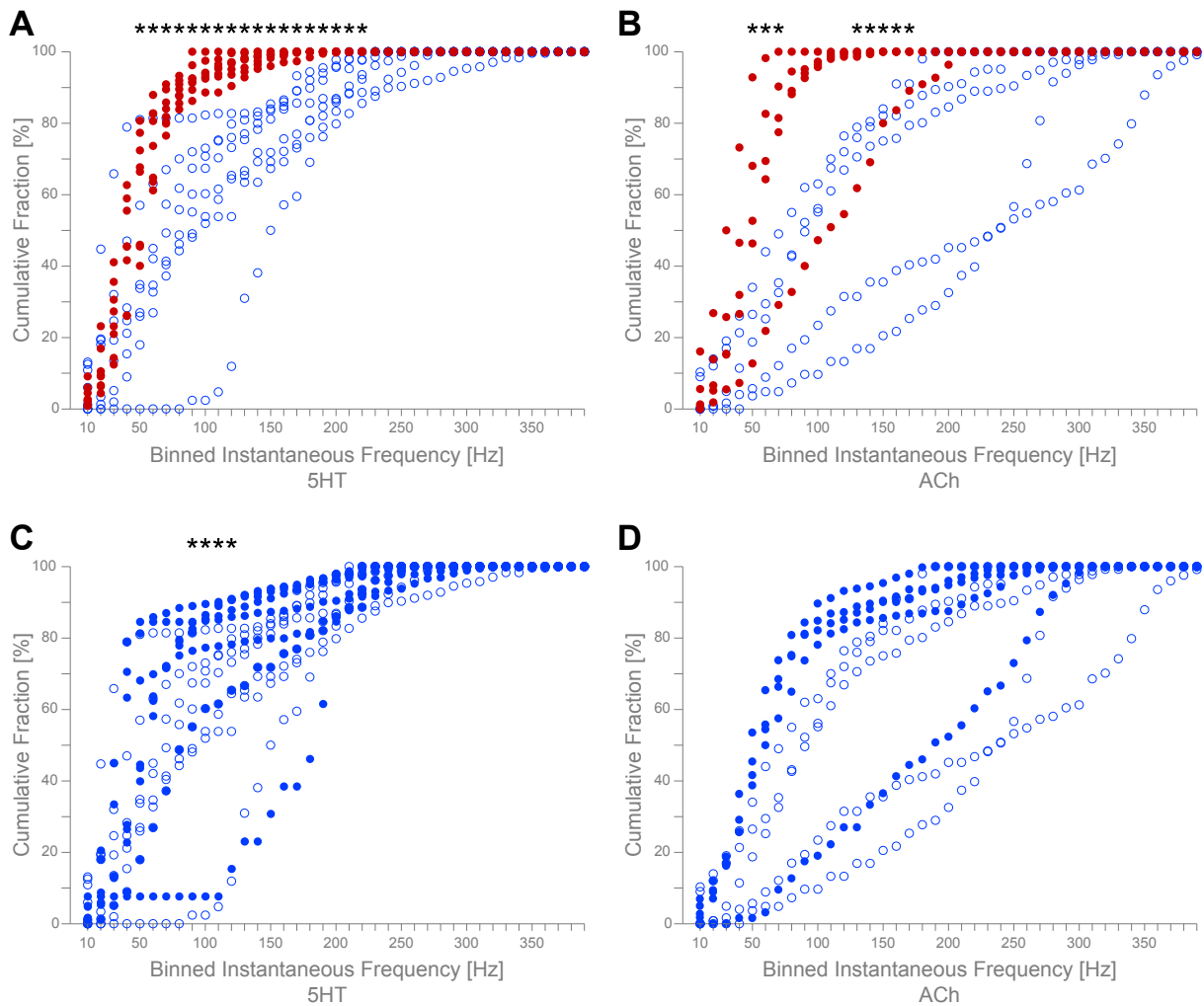
Figure 26 Depolarization induced by 5HT and ACh suffices to trigger the switch of firing modes in bursting VIP neurons

The DFR of bursting VIP neurons was analyzed before and during the modulation by 5HT (**A** and **C**) and ACh (**B** and **D**). The 8 bursting neurons tested with 5HT showed a broad DFR before neuromodulation (**A**; blue open circles). Under the presence of 5HT their DFR narrowed significantly (red circles, significant different bins marked by asterisks above). The 5 bursting neurons tested with ACh also changed their firing pattern to tonic (**B**). However, the neuromodulator instead of the depolarization induced by it could be responsible for the change in firing modes. Thus, the DFR of bursting VIP neurons was also analyzed when the neuromodulator was present but repolarized to their RMP. Under these conditions their DFR was similar to before (**C** and **D**, blue open circles before, blue filled circles repolarized to RMP under the presence of 5HT (**C**) and ACh (**D**)). Note that the frequency bins from 90 Hz to 120 Hz are significantly different between before and during stimulation with 5HT and repolarized to RMP (**C**).

neurons. Thus, tested neurons were hyperpolarized by a constant current injection to their original RMP during neuromodulation. Under these conditions, all neurons fired a high frequency burst at rheobase. The DFR of VIP neurons which were repolarized to their original RMP during cholinergic modulation did not differ from the DFR before cholinergic modulation (Figure 26 D). Also the the DFR of bursting neurons modulated by 5HT shifted towards higher frequencies despite some differences from 90 Hz to 120 Hz (Figure 26 C; rank sum tests, $p < 0.05$). As mentioned above, 5HT had an effect on firing rate adaptation. The decrease in firing rate adaptation translates into more

continuous firing of APs. Bursting VIP neurons seemed to be affected by this, hence the differences in DFR. In summary, neuromodulation mediated a depolarization which was responsible for the switch from bursting to tonic mode in bursting VIP neurons. Long exposure to 5HT seemed to have a subtle effect on the firing rate of VIP neurons as well.

These results demonstrated that VIP neurons in layer II/III of the barrel cortex were depolarized by NA, 5HT, and ACh. Depolarizations by 5HT were induced by metabotropic $5HT_2$ receptors in all VIP neurons. In only 46% of all tested VIP neurons a response to 5HT was mediated by ionotropic $5HT_{3a}$ receptors. All cholinergic responses were induced by ionotropic non-α7 ACh receptors. 20% of VIP neurons in layer II/III responded with a change in firing mode from bursting to tonic to depolarizations induced by neuromodulation.

3.3 Morphological Characterization of VIP Neurons

The morphology of 43 VIP neurons from all layers of the barrel cortex was recovered, reconstructed and quantified. For a comparison of general properties, all sufficiently reconstructed neurons were analyzed as a population. To precisely describe spatial relationships of neurons within the barrel cortex, the following analyses were based on a specific orientation of the reconstructed neurons. The pial surface was always at the top and the white matter at the bottom. Based on this orientation, the term *horizontal* is defined as parallel and *vertical* as perpendicular to the pial surface. The quantification of dendritic trees was based on their length because their thickness was highly variable. Distributions of axonal trees were quantified on the basis of their boutons since these were previously described as being presynaptic specializations (Staiger et al. 2004). Additionally, the distribution of boutons was highly correlated with the axonal length (0.99, spearman test). Somata of the 43 reconstructed VIP neurons were distributed across the layers of the barrel cortex as follows: 1 in layer I, 34 in layer II/III, 2 in layer IV, 2 in layer Va, 3 in layer Vb, and 1 in layer VI.

3.3.1 Somatodendritic and axonal properties

Somata of VIP neurons were oriented perpendicular to the pial surface because of their elliptic appearance with a larger vertical than horizontal diameter (roundness = 0.62±0.12; vertical diameter of 16.5±2.7 µm vs. horizontal diameter of 10.8±2.2 µm).

Dendrites. Somatodendritic configurations were determined following the nomenclature of Bayraktar et al. (2000) and Ascoli et al. (2008) and included 16 bipolar, 8 modified bipolar (tripolar), 12 tufted, 4 multipolar, and 3 undefined VIP neurons. Differences in somatodendritic configurations were based on the number of primary dendrites emanating from the soma which indeed varied: two (n = 16 VIP neurons), three (n = 19), four (n = 5), five (n = 2), and six (n = 1) primary dendrites of VIP neurons were observed. Dendritic trees had an average length of 2903±845 µm with 16 to 55 endings (median = 30) suggesting a complex ramification pattern. For a detailed description of this dendritic ramification pattern of VIP neurons, reconstructed cells were aligned at their somata and analyzed in 10 µm wide bins (Figure 27). 95% of all dendrites spread 150 µm in the horizontal and 470 µm in the vertical direction. In total, dendritic trees of VIP neurons were ~3 times longer than wide with a perpendicular orientation to the
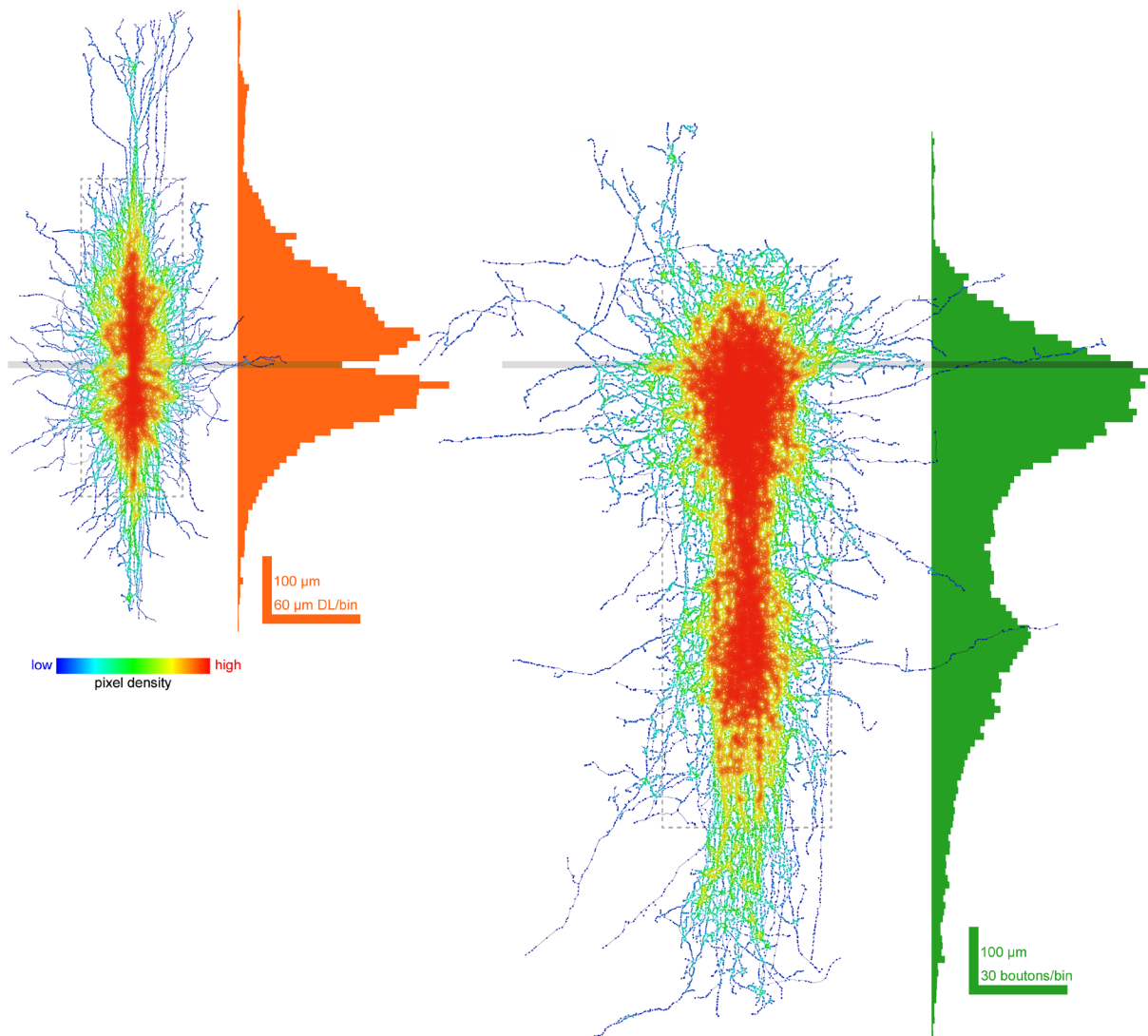
Figure 27 Superimposition of dendritic and axonal trees of 43 VIP neurons

Individual reconstructions were aligned at their somata and superimposed to illustrate the blueprint of VIP neurons. Dendritic trees (left) are shown separately from axonal trees (right). The position of the somata is indicated by a grey rectangle. Density of structures is visualized using a color look up table ranging from cold colors (low pixel density) to warm colors (high pixel density, color key beneath dendritic trees). Horizontal bar graphs depict results of the bin size analysis of individual reconstructions. The orange graph is the average dendritic length (DL) per 10 µm wide bin, the green graph the average number of axonal boutons per 10 µm wide bin. Error bars are not shown, because data was not distributed normally. Dashed grey rectangles behind superimposed reconstructions indicate the area in which 95% of either dendrites or axon is found.

pial surface. Interestingly, the vertical distribution pattern of dendrites was bimodal with one peak of density at 40 µm above the somata (111.5±83.3 µm dendritic length per bin) and a second peak at 30 µm beneath the somata (129.4±110.8 µm dendritic length per bin). The distribution of these dendrites was slightly asymmetric with more dendritic ramifications above than beneath the soma (above: 1560±573 µm vs. beneath: 1279±707, t = 2.019, p = 0.023). This bimodality resulted in an overall bitufted ramification pattern of dendritic trees of VIP neurons (Figure 27).

Figure 28 VIP neurons aligned at the pial surface and to the center of their home barrel

Dendritic trees (left) are shown separately from axonal trees (right). Visualization technique is the same as in Figure 27 but with a different alignment of individual reconstructions. Vertical alignment at the pial surface and horizontal alignment at the center of the home barrel reveals the density profile of neurites throughout the barrel cortex. Horizontal bar graphs illustrate the vertical distribution profile. Vertical bar graphs at the bottom show the horizontal distribution profile. Bars corresponding to bins covering the home barrel are indicated by a darker shade. The original shape of the home barrels is shown in the superimpositions as an overlay of transparency (the darker the more are overlaid). Layer thickness was determined after Prönneke et al. 2015. Roman numerals indicate layers, dashed lines layer borders (wm = white matter).

Axons. The axon of the majority of VIP neurons originated at a first, second, or third order dendrite directed towards the white matter (35 of 43). In only 8 of 43 neurons the axon emanated from the soma. Axonal trees showed varying degrees of complexity with 26 to 271 bifurcations (median = 95). Their long branches (7647±2752 µm) were studded with boutons (2314±1104 boutons; 29.7±5.7 boutons per 100 µm axonal length). 95% of these axonal boutons were found within a cortical area spanning 250 µm horizontally and 830 µm vertically. Thus, proportions of axonal ramifications of VIP neurons were also ~3 times longer than wide (Figure 27).
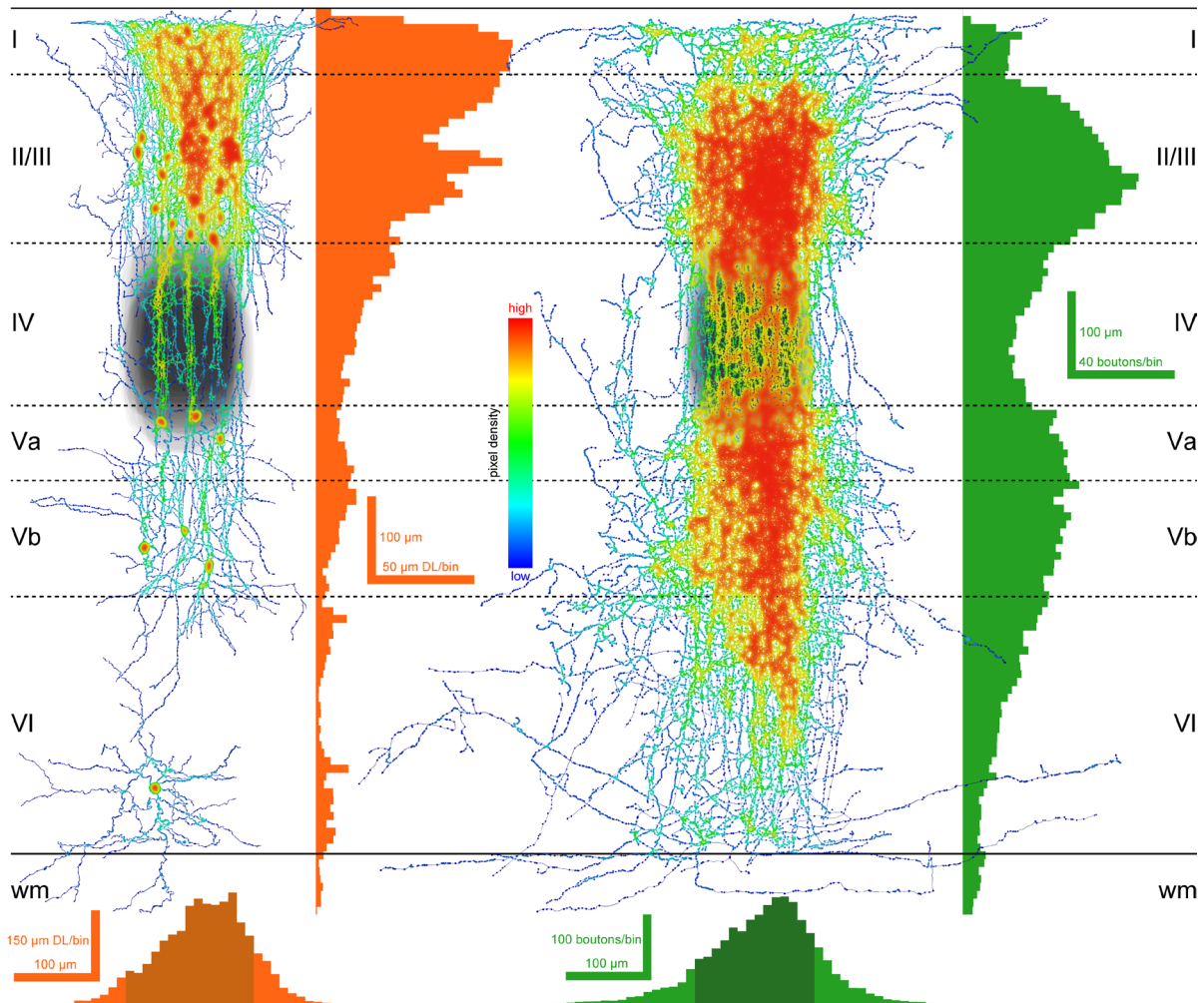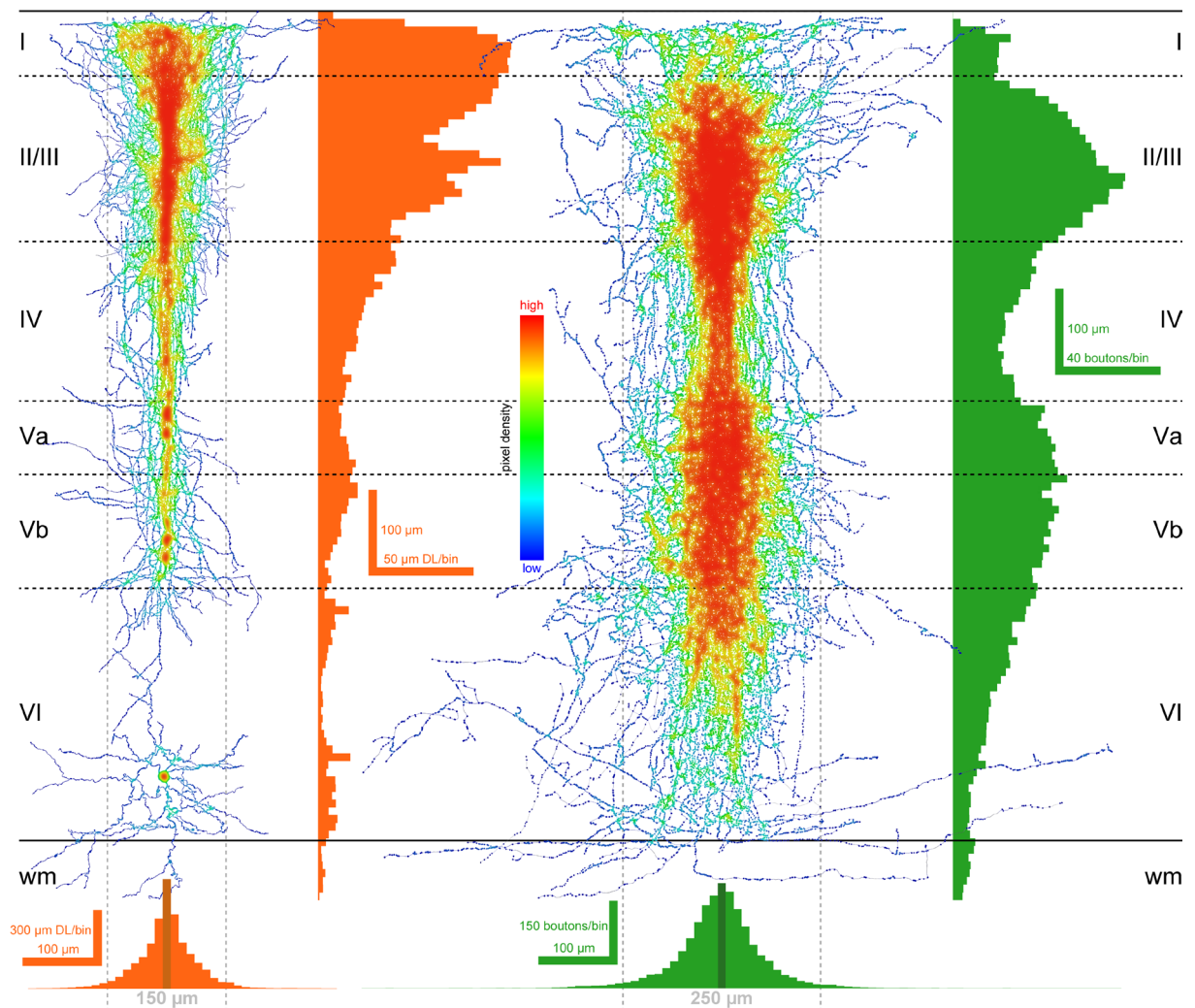
Figure 29 VIP neurons aligned at the pial surface and to the center of their somata
Dendritic trees (left) are shown separately from axonal trees (right). Visualization technique is the same as in Figures 27 and 28 but with somata being aligned at the same horizontal position. This reveals that the horizontal distribution profile of neurites is distributed normally (vertical bar graphs at the bottom). Bars corresponding to bins including somata are indicated by a darker shade. Numbers beneath graphs and dashed grey rectangles give the horizontal spread in which 95% of the neurites are found. Layer thickness was determined after Prönneke et al. 2015. Roman numerals indicate layers, dashed lines layer borders (wm = white matter).

The highest density of axonal boutons was observed 10 to 80 µm beneath the soma (> 60 boutons per bin). In total, axonal trees were highly asymmetric with axonal boutons found at a distance of 340 µm above their somata compared to a distance of 1040 µm beneath them. Additionally, the number of boutons above VIP neuron somata was significantly lower than beneath them (above: 385±404 boutons vs. beneath: 1868±859, U = 52, $p < 0.001$). Thus, VIP neurons preferentially extended their axonal trees towards the white matter.

In conclusion, the blueprint for the morphology of a VIP neuron followed certain recurring themes. Individual VIP neurons appeared to be slender because soma, dendritic and axonal trees were longer than wide with a perpendicular orientation relative to the

pial surface. Dendrites were predominantly organized in a bipolar or tufted manner, which was also reflected in their overall ramification pattern. Since in most cases the axon emanated from a dendrite beneath the soma, axonal trees were densest beneath the soma and preferentially extended towards the white matter (Figure 27). This organizational principle was determined by analyzing VIP neurons from all layers of the barrel cortex. But the somata of these neurons were located in different depths of the cortex which is why it is unlikely that neurons in all layers share the same morphology.

3.3.2 Distribution of neurites of VIP neurons throughout the barrel cortex

One prominent feature of the barrel cortex is its barrels in layer IV. Barrels are shaped by excitatory neurons which receive thalamic input. Hypothetically, the morphology of a VIP neuron could be dictated by the location relative to the barrel which might indicate that these neurons participate in processing somatosensory information entering the barrel cortex. To test for a dependency of the morphology of VIP neurons with respect to their localization to a barrel, all reconstruced neurons were horizontally aligned to the center of their home-barrel, superimposed and quantified in 10 µm wide bins (Figure 28). Both, the distribution of dendrites and axonal boutons, peaked along ca. 60 µm. However, these peaks were shifted to one side of the barrel. In contrast, when VIP neurons were aligned at the center of their somata, the horizontal distribution profile of dendrites and axon peaked in the bin containing the soma and rapidly declined in a symmetrical manner to both sides of the soma (Figure 29). This clearly demonstrates that not the barrel but the soma is the point of reference for the horizontal distribution of neurites of VIP neurons. The vertical distribution of neurites was more complex. In conjunction with barrel containing layer IV, no obvious peak of density of dendrites or axon was observed in this compartment. Thus, neither dendrites nor axon of VIP neurons preferentially extended into the barrels of layer IV suggesting a barrel-independency for the morphology of VIP neurons.

To answer the question of which areas of the barrel cortex are preferred by dendritic and axonal trees, individual reconstructed VIP neurons were aligned at the vertical position of the pial surface as a point of reference and the distribution of their neurites quantified in a layer-dependent and -independent manner (Figures 28 and 29).

Dendrites of VIP neurons were distributed across all layers of the barrel cortex in varying proportions. From the pial surface downwards, the first peak of density of dendrites

was observed at a distance of 50 µm (89.8±85 µm dendritic length per bin). This was situated within layer I (79 µm wide in the vertical direction) with 21.7% of all dendrites. Dendritic density increased 200 µm away from the pial surface to 87.9±93.5 µm per bin which corresponded to layer II/III (spanning from 79 to 282 µm). This layer contained the greatest fraction of all dendrites (49.7%). Further towards the white matter, fewer dendrites were found with no obvious peaks: 11.9% in layer IV, 5% in layer Va, 6.2% in layer Vb, 5% in layer VI, and 0.6% in the white matter. Thus, dendrites of VIP neurons were most dense in layers I and II/III.

Axon of VIP neurons was also found in all layers of the barrel cortex. The distribution profile of axonal boutons, however, was different to that of dendritic trees. Layer I only contained 3.2% of all axonal boutons. The number of boutons increased to its peak of 49±50 boutons per bin in a distance of 220 µm to the pial surface within layer II/III with 37.7% of all axonal boutons. From this peak downwards, the density of axonal boutons decreased because only 13.7% were found within layer IV. In layer Va an increment to 14.9% was observed. A secondary peak of 32±31 axonal boutons followed at a depth of 610 µm which corresponded to upper layer Vb (spanning from 567 to 707 µm depth) where 18% of all axonal boutons were located. From here on downwards, the density continuously decreased with 11.9% of all axonal boutons in layer VI and 0.5% within the white matter.

Even though dendrites and axon of VIP neurons spread throughout all layers of the barrel cortex, the analysis of their distribution profile revealed a distinct pattern: Dendrites were densest in layers I and II/III, whereas most axonal boutons where located in layers II/III and V. However, this sample was biased towards VIP neurons from layer II/III (34 of 43 neurons).

3.3.3 Identification of morphological subclasses

The description of the morphology in previous chapters was based on all 43 reconstructed VIP neurons. However, when comparing a similar amount of VIP neurons with their somata in layer II/III to those located in layers IV-VI (8 vs. 8), differences in their dendritic and axonal organization became apparent: dendrites of VIP neurons from layer II/III were vertically more restricted than those of layers IV-VI (vertical spread of 296.7±38.3 µm vs. 519.3±180.7 µm; U = 9.000; p = 0.029). Furthermore, a smaller fraction of dendrites of layer II/III VIP neurons were found outside their home layer
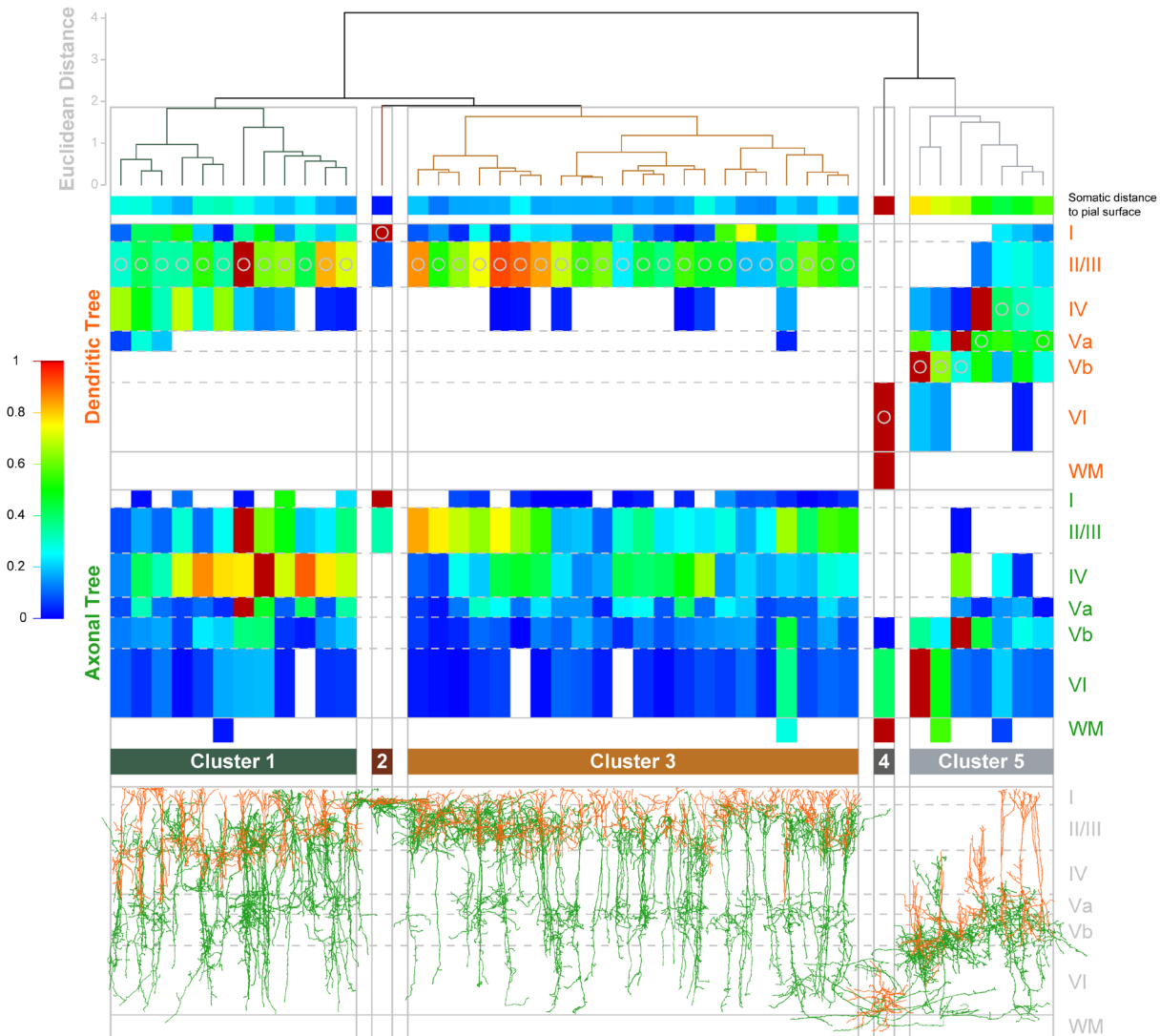
Figure 30 Unsupervised clustering of VIP neurons from all layers of the barrel cortex

Results of the cluster analysis of 43 VIP neurons were plotted as a dendrogram (top). Leaves of the dendrogram represent individual neurons. Horizontal bars connecting individual neurons are the average euclidean distance between neurons based on 15 variables. These variables are shown as a heat map with highest values in warm colors and lowest in cold colors (color key to the left, grey open circles mark the layer the somata were positioned in). The 15 variables were (from top to bottom) distance of the soma to the pial surface, dendritic length in layers I, II/III, IV, Va, Vb, VI, and the white matter (orange Roman numerals on the right, WM = white matter), number of axonal boutons in layers I to VI and the white matter (green Roman numerals on the right, layer thickness was adjusted according to Prönneke te al. 2015). 5 clusters were identified by using the euclidean distance of the outliers of layer I (cluster 2) and layer VI (cluster 4) as a separation criterion. At the bottom the original reconstructed VIP neurons are shown with somatodendritic structures in orange and axonal trees in green.

(location of soma) in comparison to VIP neurons from deeper layers (23.8±12.8% vs. 62.3±22.2%; t = 3.765; *p* = 0.001). Also the axon of VIP neurons from layer II/III had a greater vertical spread than this of neurons from layers IV-VI (961.9±100.9 µm vs. 495.5±90 µm; t = 9.487; *p* < 0.001). In summary, VIP neurons from layer II/III displayed this spatial relationship within the barrel cortex: their dendritic trees were restricted to layers I-IV with a strong focus on layer II/III whereas their axon spread throughout
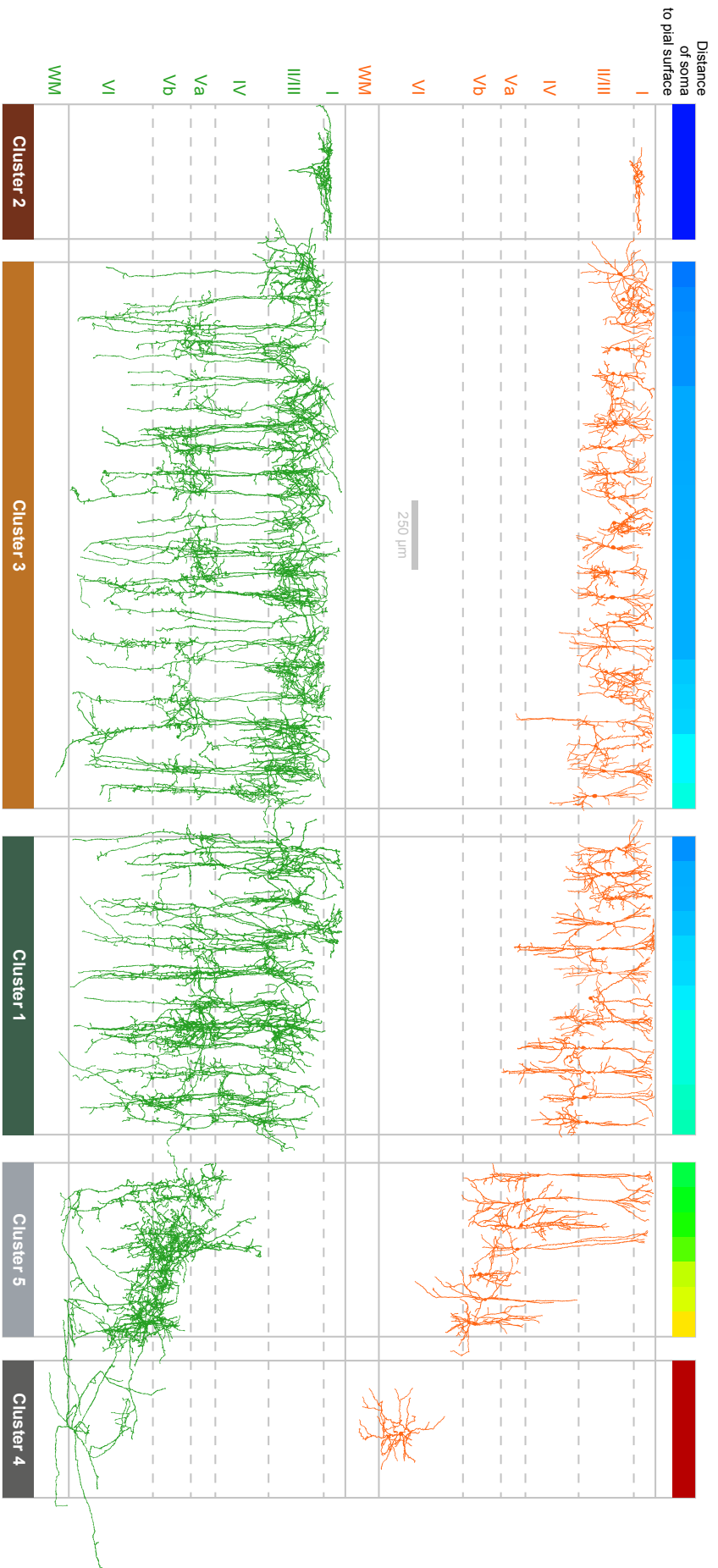
Figure 31 VIP neurons sorted by clusters and location in the barrel cortex

Somatodendritic structures are shown at the top (orange), axonal trees at the bottom (green). Clusters were determined by unsupervised clustering Figure 30) and neurons sorted by the distance of their somata to the pial surface (illustrated as a heat map from blue as close to the pial surface to red as far from the pial surface, top row). Note that the morphology of these neurons seems to change gradually. Roman numerals indicate layers, dashed lines layer borders (WM = white matter).

the whole barrel cortex with the highest density in layers II/III and Va. In contrast, VIP neurons from layers IV-VI had a more extensive dendritic tree, partially reaching into layer I, and a locally more restricted axon which focused on layers Vb and VI (Prönneke et al. 2015). These results suggest that the layer targeting of dendritic and axonal trees of VIP neurons is dependent on the location of their somata within the barrel cortex.

However, these findings were based on a more or less arbitrary subdivision of the dataset into VIP neurons from layer II/III and those found in layers IV-VI. If differences in the morphology are really dependent on the location of the somata of VIP neurons, these should become apparent in an analysis that is not operating under a pre-analytical subdivision into groups. Ward's clustering algorithm provides hierarchical agglomeration and was used to sort the 43 reconstructed neurons in an unsupervised manner. This clustering algorithm was applied to all variables that were derived from spatial relationships of these neurons. These were dendritic length and number of axonal boutons in each layer of the barrel cortex including the white matter as well as the distance of the soma to the pial surface for each neuron. Objectively obtained relationships between individual VIP neurons were complex (Figure 30). Two major groups were separated from each other. Interestingly, the first group comprised all 34 VIP neurons from layer II/III and the single neuron from layer I. The second group included all 8 neurons from layers IV-VI. The dendrogram was further subdivided by using the euclidean distance of the outliers from layers I and VI as a reference. This revealed that the group of VIP neurons from layers I and II/III subdivided into 3 clusters: 12 neurons from layer II/III, the individual VIP neurons from layer I and another 22 neurons from layer II/III. The neurons from layers IV-VI subdivided into 2 clusters: the individual cell from layer VI and 7 neurons from layers IV-Vb.

The resulting dendrogram could also be interpreted as a relationship diagram. Following this, VIP neurons from layer II/III were more similar to each other than to VIP neurons from layers IV-VI. The individual layer I VIP neuron was more similar to layer II/III VIP neurons whereas the individual layer VI VIP neuron was more related to VIP neurons from layers IV-Vb. Thus, unsupervised clustering reflected the same differences in morphology as the observer-dependent quantification. In summary, VIP neurons from layer II/III indeed differed in their domains of input and output in comparison to those from deeper layers of the barrel cortex.

Another feature became apparent when VIP neurons were sorted by the distance of their somata to the pial surface with respect to their clusters (Figure 31). Dendritic and

axonal morphology seemed to change continuously throughout the depth of the cortex. These changes were already visible in the 34 VIP neurons from layer II/III. Thus, VIP neurons from layer II/III were analyzed separately for a deeper understanding of their morphological properties and potential subdivision into types (Figure 32).

Unsupervised clustering was based on 5 variables describing the distribution of dendrites (fraction of dendrites in layer II/III and dendritic length in layers I-IV), 5 variables describing the distribution of boutons (for layers I-Vb), as well as the distance of the soma to the pial surface. Two major subgroups emerged. 6 neurons (cluster 1) were separated from a larger group with 28 neurons. These 28 neurons further subdivided into 4 clusters containing 2 (cluster 2), 8 (cluster 3), 7 (cluster 4), and 11 neurons (cluster 5).

Cluster 1: Somata of these 6 neurons were significantly deeper in layer II/III than those of clusters 3, 4, and 5 (somatic distance to pial surface of cluster 1: 253±57 µm vs. 3: 171±37, 4: 170±37, 5: 177±38 µm, respectively; one way ANOVA, $p = 0.003$, *post-hoc* Holm-Sidak analysis ($p < 0.05$)). These neurons also had more dendritic tree in layer IV than those of clusters 3, 4, and 5 (median of dendritic length of cluster 1: 1336 µm vs. 3: 0, 4: 0, 5: 20 µm, respectively; one way ANOVA, H = 21.7, $p < 0.001$, *post-hoc* Dunn's analysis ($p < 0.05$)).

Cluster 2: These 2 VIP neurons were exceptionable in some regards. They had the longest axon (13863 and 18182 µm), most axonal bifurcations (215 and 271), and the highest number of boutons (4865 and 6816) of all reconstructed VIP neurons. However, their axonal distribution profile resembled this of neurons from clusters 3, 4, and 5 thus forming the cluster of outliers related to these.

Cluster 3: Of all VIP neurons from clusters 2-5 these 8 neurons had the least dense dendritic tree in layer II/III (dendritic length cluster 3: 1199±505 µm vs. 2: 2523±850, 4: 2424±466, 5: 1796±437 µm, respectively; one way ANOVA, $p < 0.001$, *post-hoc* Holm-Sidak analysis ($p < 0.05$)). The greater number of axonal boutons in layer II/III differentiated these VIP neurons from cluster 1 cells (cluster 3: 1066±471 vs. 1: 455±242; one way ANOVA, $p = 0.014$, *post-hoc* Holm-Sidak analysis ($p < 0.05$)).

Cluster 4: These 7 VIP neurons had more dense dendritic trees in layer II/III than those of clusters 1, 3, and 5 (dendritic length cluster 4: 2424±466 µm vs. 1: 1185±277, 3: 1199±505, 5: 1796±437 µm, respectively; one way ANOVA, $p < 0.001$, *post-hoc* Holm-Sidak analysis ($p < 0.05$)). Additionally, the number of axonal boutons was higher in
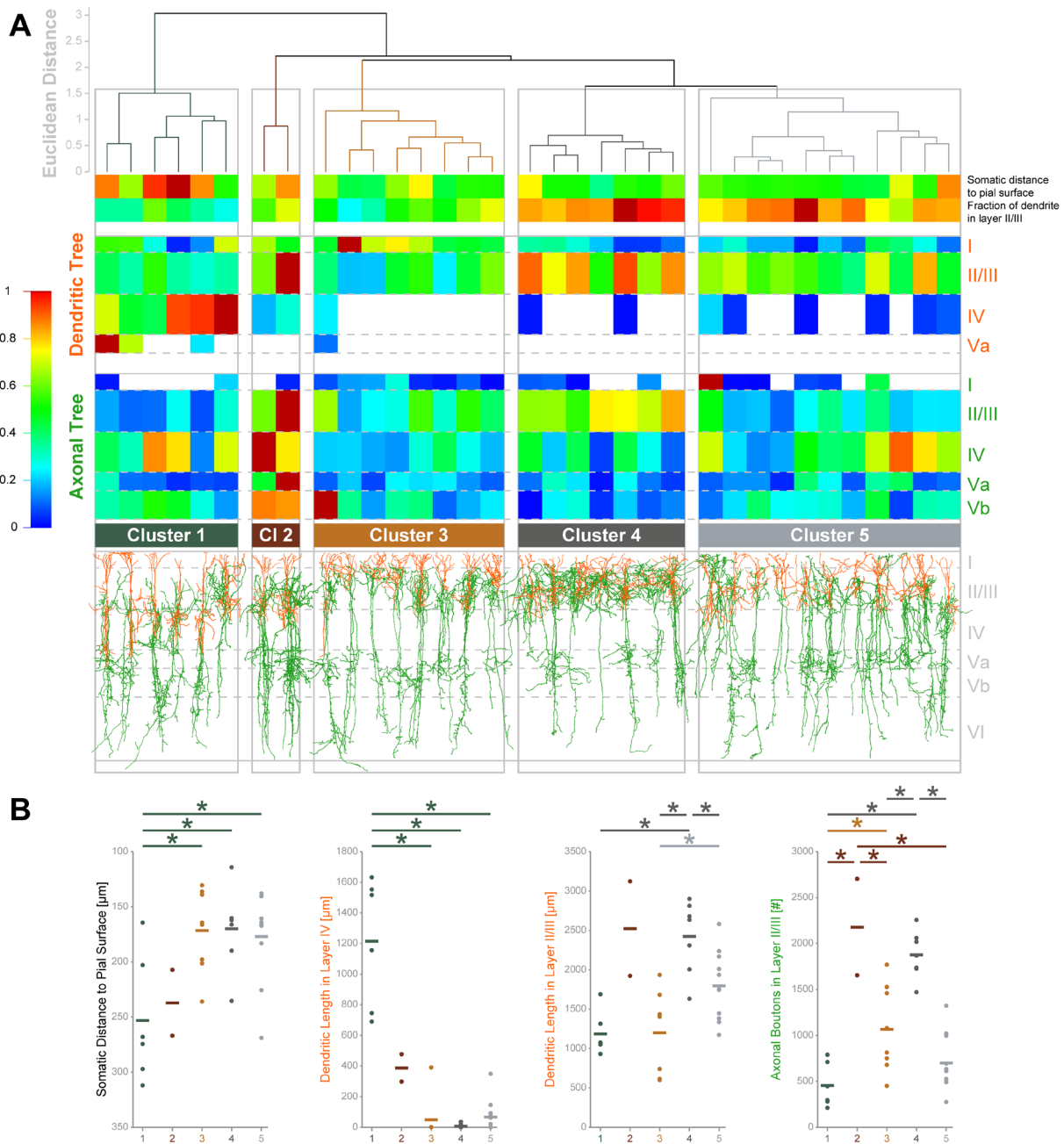
Figure 32 Unsupervised clustering of VIP neurons from layer II/III

Results of the cluster analysis of 34 layer II/III VIP neurons were plotted as a dendrogram (**A**; top). Leaves of the dendrogram represent individual neurons. Horizontal bars connecting individual neurons are the average euclidean distance between neurons based on 11 variables. These variables are shown as a heat map with highest values in warm colors and lowest in cold colors (color key to the left. The 15 variables were (from top to bottom) distance of the soma to the pial surface, fraction of dendritic tree in layer II/III, dendritic length in layers I, II/III, IV, and Va (orange roman numerals on the right), as well as the number of axonal boutons in layers I to Vb (Roman numerals on the right). 5 clusters were identified. At the bottom the original reconstructed VIP neurons are shown with somatodendritic structures in orange and axonal trees in green. In **B** distinguishing features between clusters are plotted as individual data points with the median as a horizontal bar. Significant differences are indicated by bars with asterisks.

layer II/III compared to neurons from clusters 1, 3, and 5 (cluster 4: 1877±260 vs. 1: 455±242, 3: 1066±471, 5: 700±297, respectively; one way ANOVA, $p < 0.001$, *post-hoc* Holm-Sidak analysis ($p < 0.05$)).
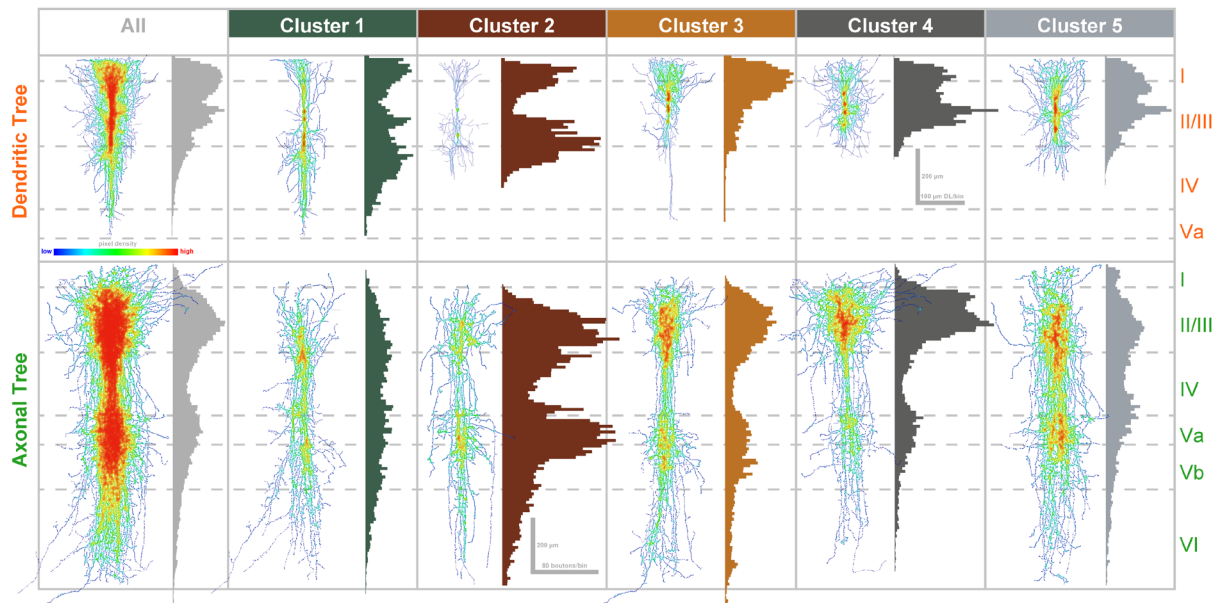
Figure 33 VIP neurons of the 5 clusters visualized as superimpositions and density plots

Dendritic (top) and axonal trees (bottom) are shown separately. Visualization technique as in Figures 26 to 28. Horizontal bar graphs show the average dendritic length per 10 µm wide bin (DL, top) or the average number of axonal boutons per bin (bottom) of all neurons assigned a cluster. Error bars are not shown because data was not distributed normally. This illustrates differences in dendritic and axonal domains between clusters. Roman numerals indicate layers, dashed lines layer borders.

Cluster 5: These 11 VIP neurons had a dendritic distribution profile with less dense trees in layer II/III compared to those in cluster 4 but more dense compared to those in cluster 3 (dendritic length cluster 5: 1796±437 µm vs. 4: 2424±466, 3: 1199±505, respectively; one way ANOVA, $p < 0.001$, *post-hoc* Holm-Sidak analysis ($p < 0.05$)). A smaller number of their axonal boutons were found in layer II/III than those of clusters 2 and 4 (cluster 5: 700±297 vs. 2: 2179±742, 4: 1877±260, respectively; one way ANOVA, $p < 0.001$, *post-hoc* Holm-Sidak analysis ($p < 0.05$)).

Overall, the distribution of neurites (i.e. domains of input and output) of VIP neurons from layer II/III of the barrel cortex of mice was heterogeneous. However, cluster analysis revealed that there are recurring motifs (Figure 33). In upper layer II/III 3 types of VIP neurons were distinguished by their domains of input and output within layer II/III: (i) neurons that focused their domains of input and output on layer II/III (cluster 4), (ii) neurons with a smaller domain of input and an intermediately sized domain of output in layer II/III, and (iii) neurons with an intermediately sized domain of input and a smaller domain of output in layer II/III. In lower layer II/III a 4th type of VIP neurons appeared (cluster 1). Their distinguishing feature was a large domain of input in layer IV and an axon that was not distributed in a bimodal manner as all other types of VIP
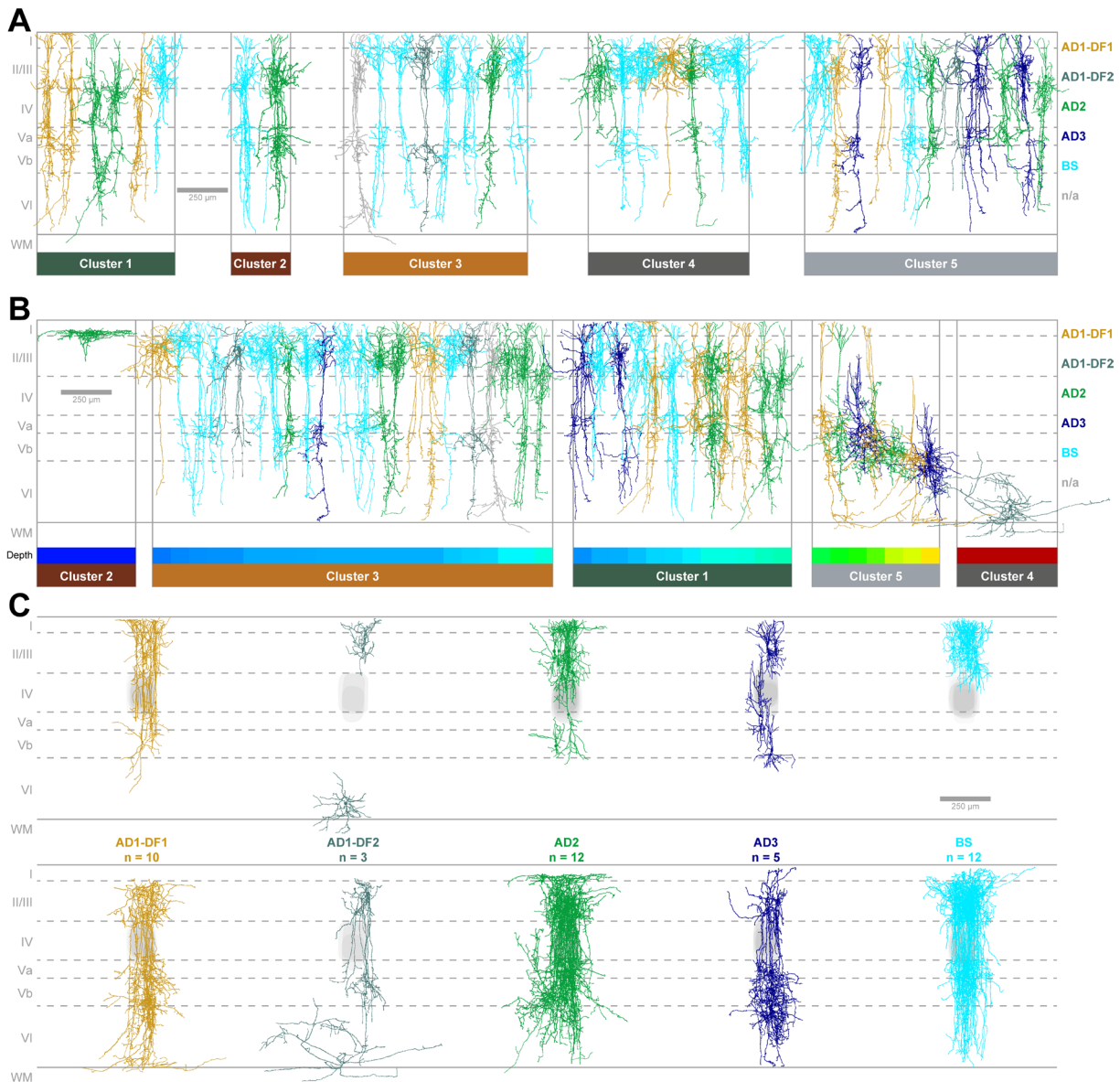
Figure 34 The morphology of VIP neurons does not correlate with electrophysiological types

Individual neurons are colored according their electrophysiological type (AD1-DF1 in dark yellow, AD1-DF2 in steel blue, AD2 in green, AD3 in dark blue, bursting (BS) in light blue, and not identifiable (n/a) in grey). In **A** VIP neurons are sorted into the clusters identified in layer II/III. In **B** VIP neurons are sorted by the clusters identified in all layers and the distance of their somata to the pial surface (depth; pictured as a heat map at the bottom with cold colors close and warm colors further away from the pial surface; WM = white matter). Note that all electrophysiological types were present in all clusters. Bursting neurons were predominantly closer to the pial surface. Additionally, electrophysiological types were arbitrarily distributed in relation to the home barrel (**C**). Neither dendrites (top) nor axonal trees (bottom) showed a preference for a horizontal position in the barrel cortex. Home barrels of individual neurons in light grey, dendritic and axonal trees superimposed and colored according to their electrophysiological type.

neurons in layer II/III. The 5th cluster (cluster 2) consisted of only 2 VIP neurons. The structure of their domain of input was a transitional form between deeper and upper layer II/III VIP neurons. However, their domain of output was organized similar to those from upper layer II/III. This indicated that the change in morphology of VIP neurons

throughout the depth of layer II/III was continuous. Thus, a definition of distinct types or morphological subgroups might be ambiguous.

The analysis of the electrophysiologcial profile of VIP neurons also hinted towards a tendency in the distribution of electrophysiological types throughout the barrel cortex. Thus the morphology of VIP neurons might correlate with the electrophysiological type. However, after identifying the electrophysiological type of the reconstructed neurons it became apparent that all types were present in this dataset. No preference for a cluster or certain depth was apparent in the morphological clusters identified in layer II/III (Figure 34 A) or when VIP neurons were sorted by depth. Only bursting neurons were found predominantly closer to the pial surface (Figure 34 B). Also the horizontal position of electrophysiological types seemed to be arbitrary. When reconstructed neurons were aligned at the center of their home barrel and sorted by electrophysiological type, all positions were found by any electrophysiological type (Figure 34 C).

4 Discussion

The description of electrophysiological and morphological properties of VIP neurons was based on a variety of experiments and analyses. For a clear interpretation of the results, the methodology is discussed first.

Quantification of firing patterns. Firing patterns were analyzed by evaluating AP trains as responses to incremental current stimulations. The current dependency of firing patterns was determined by comparing responses at maximal current stimulation to those at just above threshold. This analysis requires a clear definition of *maximal* current stimulation. Because VIP neurons show great differences in excitability, using identical stimulation protocols for each neuron was impossible. Thus, for each neuron, the lowest and the strongest current strength to elicit APs were determined individually. The lowest was set after determining the rheobase. The strongest stimulation strength was determined when AP amplitudes fluctuated extensively. This was done to prevent injection of too strong currents which might damage the neuron. The problem is that this current strength might not be the *maximal* current strength because theoretically a neuron could be stimulated with even stronger currents. However, using abundant AP amplitude fluctuations as a threshold to stop stimulation in all neurons makes these comparable. Thus, for this study, *maximal* current strength is not defined as absolute but as relative. Additionally, the second ratio describing current dependency depended on comparing the number of APs at minimal to half-maximal stimulation strength. For this dataset, it correlated strongly with the ratio depending on maximal stimulation strength (0.95; spearman test). This indicates that the current dependency of firing patterns is describable already at half of the current strength needed to evoke fluctuations of AP amplitudes.

Recovery of morphology. VIP neurons were recorded and filled with biocytin in 300 μm thick slices. This restricted the recovery of morphology to these 300 μm. Every reconstruction had at least one neurite which terminated at either the top or the bottom of each brain section. Thus, the morphology of VIP neurons was never fully reconstructed. The only way to recover the complete morphology of neurons is to label them *in vivo*. However, several measures were taken to ensure recovery of as much morphological information as possible *in vitro*. After histological processing, the labelling of neurons was carefully examined. Neurons were only reconstructed if their labelling fulfilled the following requirements: (i) sufficient signal-to-noise ratio to clearly identify neurites; (ii)

dendrites and axon are labeled and distinguishable (identified as described in Materials and Methods); (iii) no truncation of neurites close to the soma; (iv) no obvious gaps in the labelling that break the continuity of branches; (v) no structures that were labeled unspecific and interfere with the morphology of the recorded neuron. Neurons were only reconstructed if their labeling fulfilled all of these requirements. These rather strict rules explain the low recovery rate of the morphology of VIP neurons of only 10%. Because of the incompleteness of the recovered morphology, the analysis in this study was always based on several neurons. In this manner, the impact of missing branches in individual neurons on the overall appearance is minimized.

Cluster analysis. The challenging feature within this dataset is the diversity of properties. To identify recurring motifs, a statistical method was employed that sorts variables by their similarity: cluster analysis. For this study Ward's clustering algorithm was chosen because it sorts variables in a hierarchical manner and illustrates the relationship between neurons described by their variables. Also, it was used successfully to distinguish between neuronal populations previously (Krimer et al. 2005; Karagiannis et al. 2009). The main difference between previous studies and this work lies within the neuronal populations described. Pyramidal neurons, for example, are very different from PV neurons in their electrophysiological properties. These populations were included in the aforementioned studies and Ward's clustering performed well in distinguishing between these groups. VIP neurons are, despite of their variability, more similar to each other than to PV neurons (Karagiannis et al. 2009). If VIP neurons are analyzed in an isolated manner, differences between neurons are expected to be less drastic. For a thorough understanding of small differences, electrophysiological parameters describing firing rate adaptation, DFR, AP waveform, and passive properties were clustered independently of each other. In this manner, differences within these electrophysiological realms became describable. This strategy also generated insight into the structure of the heterogeneity of VIP neurons.

4.1 Potential classifications of VIP neurons

Inhibitory interneurons that express VIP in the barrel cortex of mice are a heterogeneous subgroup in their electrophysiological, morphological, and neuromodulatory characteristics. They show a variety of firing patterns, differ in their responses to 5HT, and their morphology is dependent on the vertical position of their somata within the cortex.

What unifies these interneurons is the responsiveness to ACh and NA, the vertical orientation to the pial surface in conjunction with a lateral restriction of neurites, and the release of GABA and VIP. Results of this work allow multiple classification schemes which depend on the perspective chosen: (i) from the perspective of firing patterns, the population of VIP neurons can be subdivided into 5 types.
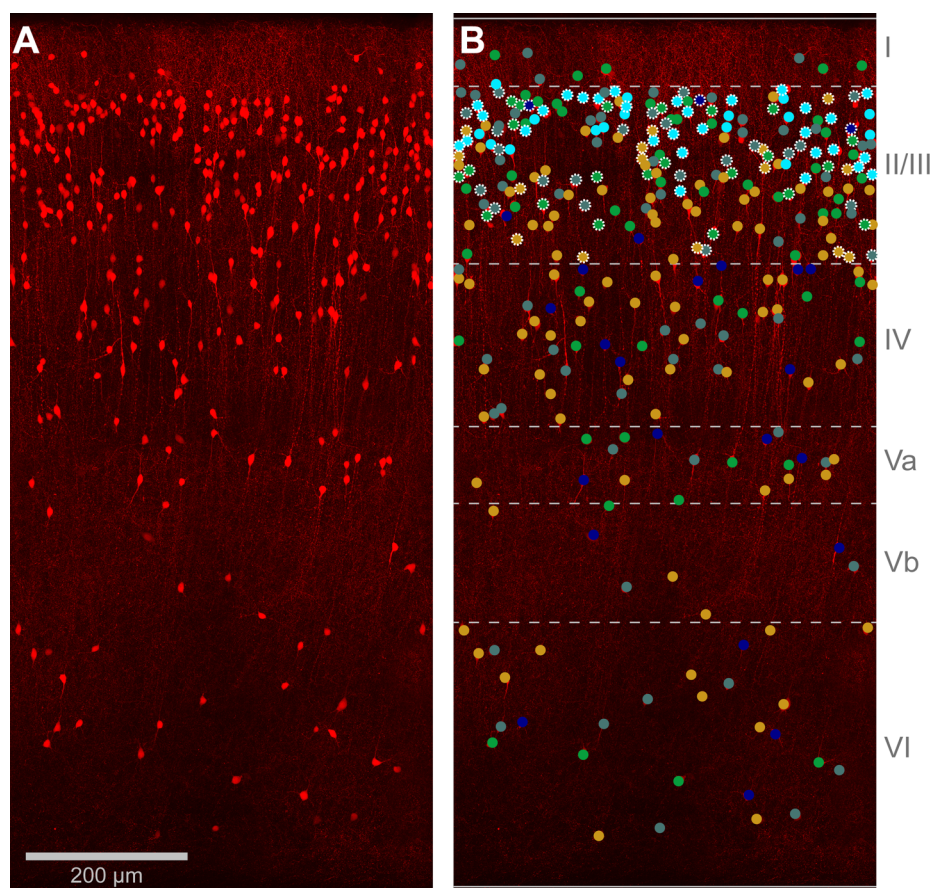
Figure 35 Electrophysiological types of VIP neurons in the barrel cortex

(A) Projection view of an image stack visualizing the native fluorescence in a 300 µm thick coronal section through the barrel cortex of a VIPcre/tdTomato mouse. In (B) all VIP neuron somata are assigned a hypothetical electrophysiological type following the distribution pattern identified in chapter 3 (AD1-DF1 in dark yellow, AD1-DF2 in steel blue, AD2 in green, AD3 in dark blue, and bursting in light blue). White stippled outlines mark neurons with functional $5HT_{3a}$ receptors, roman numerals indicate layers.

This classification is based on adaptation rates, current dependency, and frequency ranges of APs elicited by strong stimulation. (ii) The morphological perspective is more ambiguous and almost independent of the classification by firing patterns because the morphology of a VIP neuron does not predict its firing pattern. Morphological subgroups could be formed by the preferred target layers of axonal and dendritic trees, describing the spatial relationship of their domains of input and output. This criterion unraveled that VIP neurons from deeper layers are different to those in layer II/III. Additionally, VIP neurons in layer II/III show depth-dependent differences in their morphology. (iii) Neuromodulation of VIP neurons is a third classifier which is also independent of electrophysiological and morphological properties. Even though all VIP neurons are innervated by ACh and NA in a similar manner, they may be classified by response

patterns to 5HT. 46% respond to 5HT with $5HT_{3a}R$ and $5HT_2R$ mediated currents whereas all others only express $5HT_2$ receptors. This subdivision does not correlate with the electrophysiological or morphological classification because VIP neurons with a functional $5HT_{3a}R$ can show any firing pattern or morphology. Conclusively, VIP neurons eluded a clear definition of subtypes which integrates their electrophysiology, morphology, and sensitivity to neuromodulation. The morphology of an individual VIP neuron does not predict its firing behavior and response pattern to 5HT or vice versa. This feature of VIP neurons increases the level of their heterogeneity because they are not only variable within properties but also in any combination of these. This prevents a simplified classification scheme.

However, this heterogeneity might not be arbitrary because a recurring trend is observable throughout the aforementioned classifications of VIP neurons. Interestingly, it is based on the location of the somata of individual VIP neurons. In upper layer II/III, populated by VIP neurons the most (Lee et al. 2010; Taniguchi et al. 2011; Prönneke et al. 2015), more bursting VIP neurons are found than in lower layer II/III. Additionally, bursting VIP neurons are never located outside of layer II/III. The morphology of layer II/III VIP neurons differs between upper and lower layer II/III. Whereas dendritic trees of VIP neurons in upper layer II/III are confined to layers I and II/III, those of neurons in lower layer II/III sometimes reach into layer IV and Va. Thus, the domain of input to bursting VIP neurons is biased towards layers I and II/III. Furthermore, the majority of bursting neurons (70%) expresses functional $5HT_{3a}R$. The subpopulation contrasting bursting VIP neurons are neurons classified by their CA-like firing pattern of low frequency (AD1-DF1). These neurons preferentially populate lower layer II/III and deeper areas of the barrel cortex. Their dendritic trees can span from layer I to Va and 75% of these do not express $5HT_{3a}R$. This suggests that bursting VIP neurons might integrate input in a different manner than AD1-DF1 neurons. More distinctions can be made when VIP neurons from layer II/III are compared directly to VIP neurons from layers IV-VI. These groups differ in their morphology because dendritic trees of layer II/III VIP neurons are restricted to layer I to IV while their axonal trees innervate all layers. In contrast, VIP neurons from deeper layers IV-VI extend their dendrites throughout all layers and restrict their axon to layers V and VI. They also differ in their electrophysiological profile because bursting neurons never appear in deeper layers where VIP neurons might have a different AP waveform. Thus, VIP neurons in deeper areas of the cortex could be involved in other cortical circuits than those in layer II/III (Figures 35 and 36).
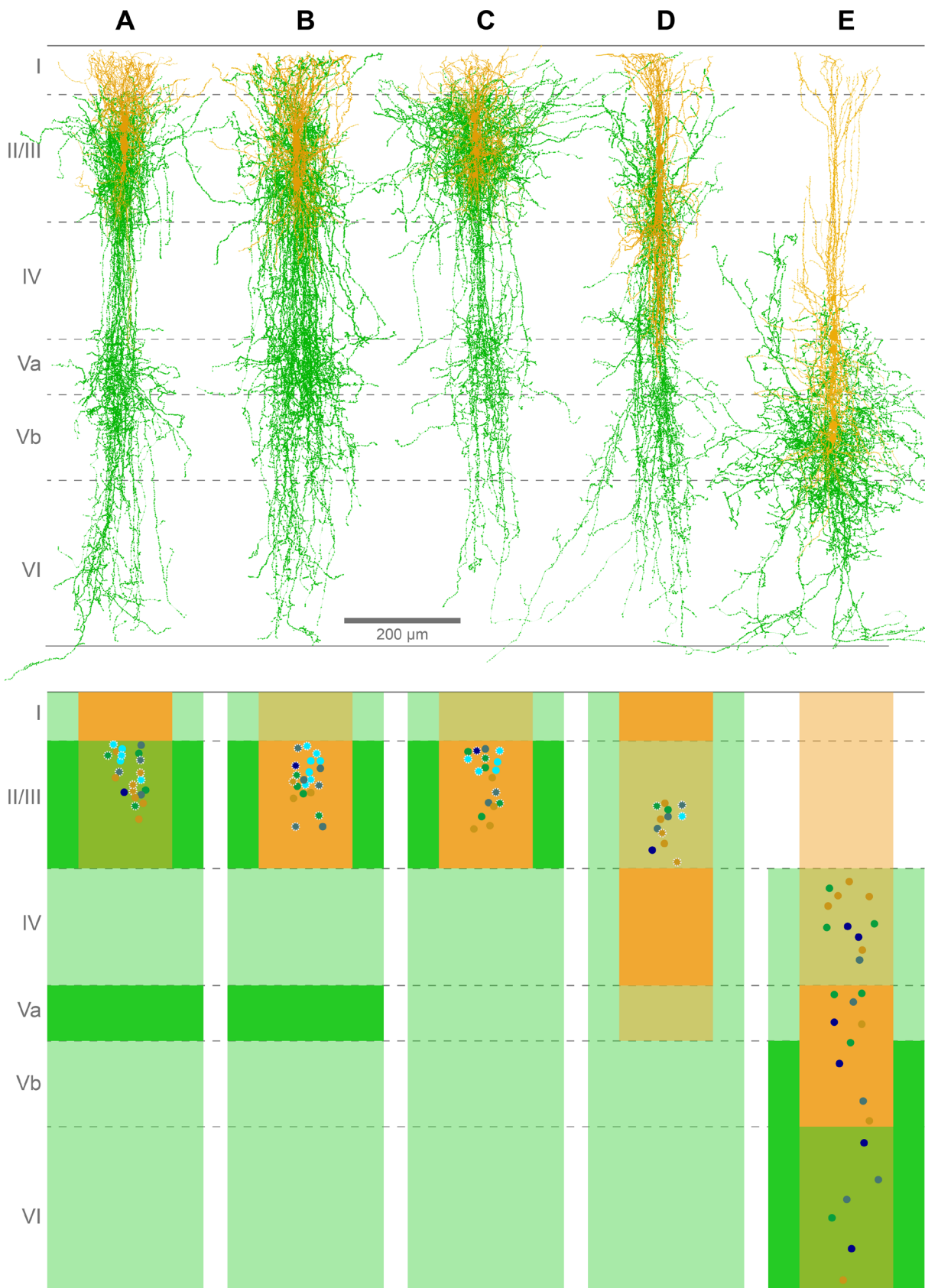
Figure 36 Morphology of VIP neurons in the barrel cortex

The different morphological types (A-E) of VIP neurons in the barrel cortex are visualized superimposed in the top panel (dendrites in orange, axon in green). Morphological features as described in chapter 5 are schematized in the bottom panel. The extent of neurites is shown as transparent rectangles with preferred layers being opaque (dendrites in orange, axon in green). Additionally, location of somata and electrophysiol256cial type are shown as in Figure 35. Roman numerals indicate layers, dashed lines layer borders.

One of the major reasons why differences in the population of VIP neurons became apparent is that firing patterns were analyzed thoroughly in this work. In previous studies, firing patterns of VIP neurons were distinguished mainly on the basis of their adaptation as CA, IS, and bursting VIP neurons. (Porter et al. 1998; Karagiannis et al. 2009). These firing pattern types were also found in this work and distinguished in an unsupervised manner. More importantly, the frequency spectrum of APs of VIP neurons was included as an essential component of firing patterns. Interestingly, the unsupervised analysis of the CA firing pattern in VIP neurons shows that these are not a homogeneous group. Instead, some CA VIP neurons are capable of firing APs in higher frequencies than others (AD1-DF1 vs. AD1-DF2). Bursting VIP neurons fire the fastest among VIP neurons whereas IS VIP neurons can show any frequency spectrum. These differences in AP frequencies are decisive in neuronal communication. The frequency in which APs arrive at a synapse impacts synaptic plasticity. If a neuron is only capable of low frequency discharges of APs it will affect synaptic plasticity less than a neuron with high frequency bursts of APs. Additionally, these data provides a basis for experimentalists to properly configure stimulation protocols in multi-neuron recordings.

4.2 Possible firing behavior of VIP neurons in awake and behaving animals

Before discussing possible roles of VIP neurons in cortical circuits it must be noted that the characterization in this work was performed in acute brain slices. Experiments *in vitro* are highly useful for a detailed characterization of intrinsic properties of neurons. However, there are crucial differences to living animals. Sensory stimulation, long range input, and neuromodulation is absent in cortical slices. Thus, recorded neurons may behave differently under these conditions. There is evidence, also within this work, that VIP neurons are less heterogeneous in awake and behaving animals than the *in vitro* data suggests. Bursting VIP neurons show an intriguing firing behavior because their firing pattern switches from bursting to tonic when the membrane potential is in a more depolarized state. This phenomenon has never been described for cortical inhibitory interneurons before. But it is well understood in excitatory thalamic relay neurons (Llinas and Jahnsen 1982). However, there are several differences to bursting VIP neurons. Thalamic relay neurons are excitatory and innervate the cortex. In contrast, bursting VIP neurons are inhibitory and located in the cortex. Also, there is evidence for physiological differences. The burst in thalamic relay neurons is mediated by T-type

calcium channels which can be identified electrophysiologically by longer lasting depolarizations after strong hyperpolarizing pulses. These rebound depolarizations were never observed in bursting VIP neurons which is why the burst of APs in VIP neurons should be dependent on a different mechanism. The switch in firing pattern can be induced by ACh and 5HT. These neuromodulators are present abundantly in the cortex of awake and behaving animals. Under these conditions bursting neurons fire in a tonic mode that resembles the firing pattern of CA VIP neurons. Even though it was not elucidated further in this work, a previous study has shown that IS VIP neurons are also capable of changing their firing pattern to a more tonic mode. Blockage of delayed K^+-currents (I_D) results in a more CA-like firing pattern in IS VIP neurons (Porter et al. 1998). I_D-like currents are voltage-dependent, fast activating, and inactivate after hundreds of milliseconds (Storm 1988). Their recovery from inactivation lasts several seconds and they also contribute to irregular AP discharges in pyramidal neurons (Locke and Nerbonne 1997; Saviane et al. 2003). Further evidence shows that I_D-like currents are downregulated by Ca^{2+} (Saviane et al. 2003). This could imply that persistent firing in IS VIP neurons which increases intracellular Ca^{2+} concentrations changes their firing behavior to more CA-like because I_D-like currents are subdued. Thus, similar to bursting neurons, IS VIP neurons could also fire more continuously. Together, these lines of evidence might predict that AP discharges of VIP neurons are more homogeneous in awake and behaving animals. If this hypothesis is valid, then why are VIP neurons so heterogeneous in their electrophysiological profile? The simple answer is that subgroups of VIP neurons are specialized to integrate and process information in a specific manner. For a more sophisticated answer, the role of VIP neurons in cortical information processing is discussed next.

4.3 VIP neurons in cortical circuits

VIP neurons modulate the inhibitory tone of various cortical areas. More specifically, activation of VIP neurons results in an increase of excitation throughout cortical areas (Lee et al. 2013; Pi et al. 2013; Fu et al. 2014; Zhang et al. 2014). This is achieved by a variety of means. VIP neurons release VIP upon stimulation (Cauli et al. 2004). VIP not only dilates blood vessels in the brain (Chedotal et al. 1994; Cauli et al. 2004) but also modulates glutamatergic synapses on excitatory neurons by increasing their efficacy (Pellegri et al. 1998). Apart from this, VIP also induces glycogenolysis in astrocytes thus indirectly stabilizing the energy household of surrounding cells (Magistretti et

al. 1981). By increasing cortical blood flow, the energy household of astrocytes, and efficacy of glutamatergic synapses, the protein VIP seems to serve two purposes in the cortex: firstly, to counteract deteriorating effects of cellular activity by increasing the availability of oxygen and glucose, and secondly, to increase excitation. It is not clear, which neuronal compartment releases VIP upon stimulation. But during reconstructions of the morphology of VIP neurons for this work, dendrites and axon were frequently observed in close proximity to blood vessels in any cortical location (data not shown). This suggests that VIP neurons control cortical blood flow and astrocytic metabolism not only in superficial layers where most of the dendrites are found but in all cortical layers because of their extensive axonal trees.

The primary neurotransmitter of VIP neurons is GABA. Interestingly, VIP neurons preferentially target other subgroups of inhibitory interneurons. These subgroups are mainly PV (David et al. 2007; Hioki et al. 2013; Pfeffer et al. 2013; Jiang et al. 2015) and SOM neurons (Staiger et al. 2004; Lee et al. 2013; Pfeffer et al. 2013; Pi et al. 2013; Fu et al. 2014; Zhang et al. 2014; Karnani et al. 2016a; Walker et al. 2016). PV and SOM neurons inhibit excitatory neurons. Thus, VIP neurons are capable of decreasing the inhibitory input to excitatory neurons. The morphology of VIP neurons predicts that the activity of PV and SOM neurons is controlled in all layers of the barrel cortex more or less simultaneously. Axonal trees of layer II/III VIP neurons span all layers of the barrel cortex with preferences towards layers II/III and V. The distribution of the axon of VIP neurons is very similar to the relative distribution profile of PV and SOM neurons (Gonchar et al. 2007). Additionally, the connection probability between individual VIP neurons and SOM neurons is highest in a lateral distance of ca. 150 µm (Karnani et al. 2016a), a measurement that fits the lateral extent of 250 µm for axonal trees determined in this work. Releasing excitatory neurons of inhibition must be controlled tightly which raises the question of how VIP neurons are innervated. Tracing experiments identified a large group of local presynaptic neurons, thalamic neurons, and various sources of long-range input (Fu et al. 2014; Karnani et al. 2016b; Wall et al. 2016). Little is known about the activation of VIP neurons by local cortical circuits. VIP neurons are innervated by local pyramidal cells in a depressing manner (Porter et al. 1998; Caputi et al. 2009). These excitatory neurons might be preferentially located in lower layer II/III (Karnani et al. 2016b) and do not seem to be ubiquitously distributed across all layers of the cortex. Conclusively, local activation of VIP neurons might be mediated by a subpopulation of excitatory neurons. VIP neurons seem to receive more input from non-local sources than PV or SOM neurons (Wall et al. 2016) suggesting that VIP neuron mediated

disinhibition could be activated under various and distinct conditions. Previous studies have shown that VIP neurons receive thalamic input from the ventral posteriomedial nucleus (Staiger et al. 1996), the motor cortex (Lee et al. 2013), the prefrontal cortex (Zhang et al. 2014), and the basal forebrain (Fu et al. 2014). These sources of input partially translate into the role of VIP neurons during behavior. Innervation of VIP neurons in the barrel cortex by fibers from the motor cortex is induced during active whisking (Gentet et al. 2012; Lee et al. 2013). Locomotion shifts the gain of excitation in the visual cortex which is mediated by cholinergic input from the basal forebrain to VIP neurons (Fu et al. 2014). Also, visual discrimination is enhanced by activation of projections from the cingulate cortex to VIP neurons in the visual cortex (Zhang et al. 2014). In the auditory cortex, VIP neurons are most active during the reinforcement period while learning a task (Pi et al. 2013). This enhancement of excitation during learning has also been described for the barrel cortex (Sachidhanandam et al. 2016). The recurring theme of these studies is that they explain the cortical circuitry underlying tasks of higher cognitive order on the basis of their key neuronal element: VIP neurons. Apparently, VIP neurons are capable of integrating a plethora of local, top-down, and bottom-up input and tune inhibition in cortical areas to the needed level. This would require specializations in VIP neurons to discriminate between the various sources of input. One of these structural specializations might be that in the majority of VIP neurons the axon originated not directly at the soma but at a dendrite extending toward the white matter. In previous studies this morphological feature was investigated under functional aspects (Hausser et al. 1995; Thome et al. 2014). Postsynaptic currents evoked in axon-carrying dendrites have a greater impact on spike generation than those which have to pass through the somatic current sink. Axon-carrying dendrites are primarily oriented towards the white matter in VIP neurons. Consequentially, input to dendritic trees below somata of VIP neurons might be integrated in a preferential manner. Despite little knowledge about the precise location of synapses on dendritic trees of VIP neurons, an assumption based on the laminar distribution of input can be made. Axonal fibers from the motor cortex are considered to innervate layer I. Dendrites of most VIP neurons in this layer do not carry an axon. Thus, input from the motor cortex might not drive VIP neuron activity as strongly as yet unidentified input to axon-carrying dendrites.

More evidence from this work hints towards further specializations of VIP neurons. VIP neurons are also integrating brain states because they are depolarized by NA, ACh, and 5HT. Of these neuromodulators, 5HT has the most differential effect on VIP neurons.

All VIP neurons are depolarized by 5HT if it is presented long enough. However, 46% of the tested neurons also show a fast and strong desensitizing depolarizing component which is mediated by $5HT_{3a}$ receptors. This is surprising given the fact that all VIP neurons are classified as $5HT_{3a}R$ expressing interneurons but only half of them seem to express functional $5HT_{3a}$ receptors. This does not necessarily mean that the classification as $5HT_{3a}R$ expressing interneurons is false. Instead, this categorization was done on the basis of mRNA expression and transgenic animals (Rudy et al. 2011; Taniguchi et al. 2011). Thus, it is possible that $5HT_{3a}$ receptors are functional during certain developmental periods or at least once during the lifetime of a VIP neuron. But, in adult mice, only half of all VIP neurons respond to short applications of 5HT. Long exposure to 5HT, however, leads to depolarizations in all VIP neurons. This is mediated by $5HT_2$ receptors which was not described for VIP neurons as of yet. This was shown in this study by the antagonizing effect of cinanserin which is unspecific for $5HT_{2a}$ and $5HT_{2c}$ receptors. From these experiments it is unclear whether VIP neurons express $5HT_{2a}$, $5HT_{2c}$, or both receptors. However, there is evidence for the expression of mRNA coding for $5HT_{2c}$ receptors (Tasic et al. 2016) but none for $5HT_{2a}$ receptors. Interestingly, according to the data from Tasic et al. (2016), VIP neurons and a novel type of interneurons (*Sncg*) are the only cells in the visual cortex which express mRNA for $5HT_{2c}$ receptors.

Serotonergic fibers innervating the cortex originate in the dorsal raphe. These dorsal raphe neurons are active during movement, feeding, and grooming, and are suppressed when postural muscle tone is absent (Veasey et al. 1997). Activity of a single dorsal raphe neuron is sufficient to activate a VIP neuron (Ferezou et al. 2002). In cortical circuitry, short serotonergic modulation could increase excitation for a small period of time to a lower degree than cholinergic modulation because only half of all VIP neurons are activated. Prolonged serotonergic modulation, however, could increase the level of disinhibition because all VIP neurons are recruited. Intriguingly, the increase of excitability is not the only effect any depolarizing neuromodulator has on VIP neurons because 20% of the VIP neurons in layer II/III also change their firing behavior from bursting to tonic firing. Consequentially, under neuromodulation, the population of VIP neurons fires more homogeneously. In contrast, when neuromodulators are present less abundantly (for example during sleep), some VIP neurons display burst firing. In conjunction with the greater excitability of these bursting neurons, less input is needed to elicit a burst of APs and subsequent disinhibition. This mechanism could encode a wake-up signal by a short serotonergic impulse that activates some VIP neurons. It

could also keep cortical areas more active during sleep when most sensory input is absent. There is more evidence supporting this hypothesis. As mentioned above, $5HT_{2c}$ receptors are almost exclusively expressed by VIP neurons. Studies on specific $5HT_{2c}R$ agonists found that rats treated with these agonists had more quiet-waking and less REM phases during sleep (Martin et al. 1998). Furthermore, amplified $5HT_{2c}R$ activity also reduced appetite, symptoms of obsessive compulsive disorder, and depression, functions associated with the activity of serotonergic dorsal raphe neurons (Veasey et al. 1997). In contrast, the absence of $5HT_{2c}$ receptors induces overeating and epileptic seizures which indicates a disturbance of the inhibitory system controlling excitation (Tecott et al. 1995). Even though the neuronal circuitry underlying these behavioral phenotypes is not known, it could be speculated that VIP neurons are involved.

Cholinergic innervation of VIP neurons is immediate, strong and lasts as long as ACh is present. Evoked currents are abolished by mecamylamine. This antagonist for nicotinic non-a7 ACh receptors was also used in a previous functional study in the visual cortex (Fu et al. 2014). Here, it subdued VIP neuron activity during locomotion demonstrating that VIP neurons are activated by cholinergic neurons from the basal forebrain via non-α7 ACh receptors. Results of previous studies confirm that the innervation of VIP neurons by ACh is mediated by nicotinic non-α-7 receptors (Porter et al. 1999; Arroyo et al. 2012; Bennett et al. 2012). The cortex is innervated by basal forebrain neurons ubiquitously (Mesulam et al. 1983). The organization of basal forebrain neuron projections and their spatiotemporal precision, however, is still under debate (for a review see: Munoz and Rudy (2014)). Impairment of the functionality of cortical nicotinic receptors results in deficits in attention and learning (King et al. 2003; Guillem et al. 2011) and might also play a role in Alzheimer's disease (Wilson et al. 1991). Interestingly, $5HT_{3a}R$ expressing interneurons seem to be the only cortical interneurons which express nicotinic ACh receptors. This suggests that VIP neurons are involved in cortical tasks of higher order since they are the largest group of $5HT_{3a}R$ expressing interneurons (Lee et al. 2010).

The depolarization induced by NA was not investigated further in this work but it is in line with the results of an anatomical study (Paspalas and Papadopoulos 1999). In the study of Tasic et al. (2016) mRNA for the adrenergic receptors α1A and α1B was detected in VIP neurons. The metabotropic nature of these receptors fit the observation that VIP neurons barely repolarize after long exposures to NA. However, little is known about the role of NA in cortical circuits.

4.4 Conclusion and outlook

VIP neurons are a heterogeneous subclass of cortical inhibitory interneurons. Their heterogeneity allows multiple classification schemes that depend on the context in which VIP neurons are viewed. One of their primary functions seems to be the modulation of inhibition in cortical areas. This control of the gain of excitation is involved in the computation of tasks the cortex is typically associated with. For a proper integration of information encoding different brain states, the neurons integrating this information into local cortical circuitry should be capable of differentiating between inputs and modulate local inhibition accordingly. A plethora of evidence supports the hypothesis that VIP neurons are such integrators. In this context, the heterogeneity of VIP neurons could be viewed as specializations which enable these neurons to locally tune inhibition to its needed level in a sub-layer specific manner. The detailed description of the electrophysiology, morphology, and neuromodulation of VIP neurons presented in the present thesis serves as a foundation for further investigations. Apart from providing a resource to identify VIP neurons, several properties were discovered that expand the knowledge about the capabilities of these neurons. Some of these could be used to unravel in which circumstances VIP neurons act synchronously and when the specializations described in this work become relevant. This necessitates a complete picture of all inputs to VIP neurons and their target neurons. For example the connectivity between local excitatory neurons and VIP neurons exists but nothing is known about whether the local drive of VIP neurons and their direct inhibition of local excitatory neurons can be more impactful than the disinhibitory circuit motif. Only a holistic approach that considers the differences in sensitivity to neuromodulation, response patterns, and morphology in conjunction with the circuitry VIP neurons are involved in will provide meaningful insight into cortical functions. This line of work might be the basis to understand the intricate workings of cognition.

Summary

VIP expressing interneurons are an essential component of cortical circuitry. This distinct subgroup of inhibitory interneurons was always described as the most heterogeneous subgroup of inhibitory interneurons. However, little is known about the precise structure of this heterogeneity and whether these neurons nevertheless form distinct subgroups on the basis of their characteristic properties. This question was addressed in this work by targeting genetically-labeled VIP neurons in acute thalamo-cortical section of the barrel cortex in mice. Based on whole cell patch-clamp experiments, the electrophysiological profile of VIP neurons was characterized. Their morphology was reconstructed and quantified subsequently if neurons were labeled sufficiently. Additionally, responses to NA, ACh, and 5HT were recorded to access information about the sensitivity of VIP neurons to neuromodulation. Receptors mediating the responses to ACh and 5HT were identified in pressure application experiments in conjunction with antagonists for certain receptor subtypes. The analysis of the electrophysiological profile of VIP neurons confirmed the previously observed heterogeneity. To describe this heterogeneity in detail, firing patterns were quantified using a novel method that included not only their adaptation rates but also the current dependency and frequency spectrum. These important features allowed an observer-independent description of the firing behavior of VIP neurons and also generated insight into AP waveforms and passive properties of these neurons. Based on these data, VIP neurons could be subdivided into 5 electrophysiological types. The distribution profile of these types throughout the barrel cortex unveiled that bursting VIP neurons were exclusively found in layer II/III with a tendency towards upper layer II/III. In contrast, CA VIP neurons of low frequency (one of the 5 electrophysiological types) were found predominantly in lower layer II/III and layers IV-VI. The three remaining types were found intermingled throughout all layers of the barrel cortex. The location preference of bursting VIP neurons was partially reflected in the morphology of VIP neurons. Although a clear definition of subtypes was ambiguous due to the low number of recovered neurons, differences in the organization of dendritic trees became apparent in lower layer II/III. Here, VIP neurons spread their dendrites towards layer Va, whereas in upper layer II/III VIP neurons restricted their dendrites to layers I and II/III. In conjunction with the distribution profile of electrophysiological types, bursting VIP neurons seem to have a different laminar input domain than low frequency CA VIP neurons. Furthermore, the morphology of the few reconstructed neurons from layers

IV-VI indicates that their domains of input and output greatly differ in comparison to VIP neurons from layer II/III: in deeper layers of the cortex, the dendrites of VIP neurons are found in all layers, whereas their axon is virtually restricted to layers V and VI. In contrast, VIP neurons from layer II/III restrict their dendrites to superficial layers I-IV and spread their axon into all layers of the barrel cortex. These morphological differences suggest a differential involvement into cortical circuitry. In layer II/III, VIP neurons are depolarized by NA, ACh, and 5HT confirming earlier studies. The depolarization induced by ACh is mediated by nicotinic non-α7 ACh receptors in all tested VIP neurons. Interestingly, responses to 5HT are mediated by $5HT_2R$ in all VIP neurons but $5HT_{3a}R$ mediated currents were only observed in 46% of all tested VIP neurons identifiable by a biphasic response pattern. The depolarization induced by ACh and 5HT was sufficient to trigger a switch in the firing behavior of 20% of all VIP neurons: bursting VIP neurons. Their firing pattern switches from bursting to a more tonic CA-like when their membrane potential is depolarized. This firing behavior was never described for VIP neurons before and suggests an additional specialization to integrate brain states. In conclusion, VIP neurons eluded a precise classification which integrates all aspects of their electrophysiology, morphology, and neuromodulation. However, the description of VIP neurons provided in this work serves as a foundation to integrate observations from past and future studies.

References

Arroyo S, Bennett C, Aziz D, Brown SP, Hestrin S. 2012. Prolonged disynaptic inhibition in the cortex mediated by slow, non-alpha7 nicotinic excitation of a specific subset of cortical interneurons. J Neurosci. 32: 3859-3864.

Ascoli GA, Alonso-Nanclares L, Anderson SA, Barrionuevo G, Benavides-Piccione R, Burkhalter A, Buzsaki G, Cauli B, Defelipe J, Fairen A, Feldmeyer D, Fishell G, Fregnac Y, Freund TF, Gardner D, Gardner EP, Goldberg JH, Helmstaedter M, Hestrin S, Karube F, Kisvarday ZF, Lambolez B, Lewis DA, Marin O, Markram H, Munoz A, Packer A, Petersen CC, Rockland KS, Rossier J, Rudy B, Somogyi P, Staiger JF, Tamas G, Thomson AM, Toledo-Rodriguez M, Wang Y, West DC, Yuste R. 2008. Petilla terminology: nomenclature of features of GABAergic interneurons of the cerebral cortex. Nat Rev Neurosci. 9: 557-568.

Bayraktar T, Welker E, Freund TF, Zilles K, Staiger JF. 2000. Neurons immunoreactive for vasoactive intestinal polypeptide in the rat primary somatosensory cortex: morphology and spatial relationship to barrel-related columns. J Comp Neurol. 420: 291-304.

Bennett C, Arroyo S, Berns D, Hestrin S. 2012. Mechanisms generating dual-component nicotinic EPSCs in cortical interneurons. J Neurosci. 32: 17287-17296.

Buzsaki G, Wang XJ. 2012. Mechanisms of gamma oscillations. Annu Rev Neurosci. 35: 203-225.

Caputi A, Rozov A, Blatow M, Monyer H. 2009. Two calretinin-positive GABAergic cell types in layer 2/3 of the mouse neocortex provide different forms of inhibition. Cereb Cortex. 19: 1345-1359.

Cauli B, Tong XK, Rancillac A, Serluca N, Lambolez B, Rossier J, Hamel E. 2004. Cortical GABA interneurons in neurovascular coupling: relays for subcortical vasoactive pathways. J Neurosci. 24: 8940-8949.

Chedotal A, Umbriaco D, Descarries L, Hartman BK, Hamel E. 1994. Light and electron microscopic immunocytochemical analysis of the neurovascular relationships of choline acetyltransferase and vasoactive intestinal polypeptide nerve terminals in the rat cerebral cortex. J Comp Neurol. 343: 57-71.

Chen SX, Kim AN, Peters AJ, Komiyama T. 2015. Subtype-specific plasticity of inhibitory circuits in motor cortex during motor learning. Nat Neurosci. 18: 1109-1115.

David C, Schleicher A, Zuschratter W, Staiger JF. 2007. The innervation of parvalbumin-containing interneurons by VIP-immunopositive interneurons in the primary somatosensory cortex of the adult rat. Eur J Neurosci. 25: 2329-2340.

Donato F, Rompani SB, Caroni P. 2013. Parvalbumin-expressing basket-cell network plasticity induced by experience regulates adult learning. Nature. 504: 272-276.

Ferezou I, Cauli B, Hill EL, Rossier J, Hamel E, Lambolez B. 2002. 5-HT3 receptors mediate serotonergic fast synaptic excitation of neocortical vasoactive intestinal peptide/cholecystokinin interneurons. J Neurosci. 22: 7389-7397.

Freund TF, Martin KA, Smith AD, Somogyi P. 1983. Glutamate decarboxylase-immunoreactive terminals of Golgi-impregnated axoaxonic cells and of presumed basket cells in synaptic contact with pyramidal neurons of the cat's visual cortex. J Comp Neurol. 221: 263-278.

Fu Y, Tucciarone JM, Espinosa JS, Sheng N, Darcy DP, Nicoll RA, Huang ZJ, Stryker MP. 2014. A cortical circuit for gain control by behavioral state. Cell. 156: 1139-1152.

Gentet LJ, Kremer Y, Taniguchi H, Huang ZJ, Staiger JF, Petersen CC. 2012. Unique functional properties of somatostatin-expressing GABAergic neurons in mouse barrel cortex. Nat Neurosci. 15: 607-612.

Gonchar Y, Wang Q, Burkhalter A. 2007. Multiple distinct subtypes of GABAergic neurons in mouse visual cortex identified by triple immunostaining. Front Neuroanat. 1: 3.

Guillem K, Bloem B, Poorthuis RB, Loos M, Smit AB, Maskos U, Spijker S, Mansvelder HD. 2011. Nicotinic acetylcholine receptor beta2 subunits in the medial prefrontal cortex control attention. Science. 333: 888-891.

Hausser M, Stuart G, Racca C, Sakmann B. 1995. Axonal initiation and active dendritic propagation of action potentials in substantia nigra neurons. Neuron. 15: 637-647.

Hioki H, Okamoto S, Konno M, Kameda H, Sohn J, Kuramoto E, Fujiyama F, Kaneko T. 2013. Cell type-specific inhibitory inputs to dendritic and somatic compartments of parvalbumin-expressing neocortical interneuron. J Neurosci. 33: 544-555.

Jiang X, Shen S, Cadwell CR, Berens P, Sinz F, Ecker AS, Patel S, Tolias AS. 2015. Principles of connectivity among morphologically defined cell types in adult neocortex. Science. 350: aac9462.

Karagiannis A, Gallopin T, David C, Battaglia D, Geoffroy H, Rossier J, Hillman EM, Staiger JF, Cauli B. 2009. Classification of NPY-expressing neocortical interneurons. J Neurosci. 29: 3642-3659.

Karnani MM, Jackson J, Ayzenshtat I, Hamzehei Sichani A, Manoocheri K, Kim S, Yuste R. 2016a. Opening Holes in the Blanket of Inhibition: Localized Lateral Disinhibition by VIP Interneurons. J Neurosci. 36: 3471-3480.

Karnani MM, Jackson J, Ayzenshtat I, Tucciarone J, Manoocheri K, Snider WG, Yuste R. 2016b. Cooperative Subnetworks of Molecularly Similar Interneurons in Mouse Neocortex. Neuron. 90: 86-100.

King SL, Marks MJ, Grady SR, Caldarone BJ, Koren AO, Mukhin AG, Collins AC, Picciotto MR. 2003. Conditional expression in corticothalamic efferents reveals a developmental role for nicotinic acetylcholine receptors in modulation of passive avoidance behavior. J Neurosci. 23: 3837-3843.

Krimer LS, Zaitsev AV, Czanner G, Kroner S, Gonzalez-Burgos G, Povysheva NV, Iyengar S, Barrionuevo G, Lewis DA. 2005. Cluster analysis-based physiological classification and morphological properties of inhibitory neurons in layers 2-3 of monkey dorsolateral prefrontal cortex. J Neurophysiol. 94: 3009-3022.

Lee S, Hjerling-Leffler J, Zagha E, Fishell G, Rudy B. 2010. The largest group of superficial neocortical GABAergic interneurons expresses ionotropic serotonin receptors. J Neurosci. 30: 16796-16808.

Lee S, Kruglikov I, Huang ZJ, Fishell G, Rudy B. 2013. A disinhibitory circuit mediates motor integration in the somatosensory cortex. Nat Neurosci. 16: 1662-1670.

Llinas R, Jahnsen H. 1982. Electrophysiology of Mammalian Thalamic Neurons Invitro. Nature. 297: 406-408.

Locke RE, Nerbonne JM. 1997. Role of voltage-gated K+ currents in mediating the regular-spiking phenotype of callosal-projecting rat visual cortical neurons. J Neurophysiol. 78: 2321-2335.

Madisen L, Zwingman TA, Sunkin SM, Oh SW, Zariwala HA, Gu H, Ng LL, Palmiter RD, Hawrylycz MJ, Jones AR, Lein ES, Zeng H. 2010. A robust and high-throughput Cre reporting and characterization system for the whole mouse brain. Nat Neurosci. 13: 133-140.

Magistretti PJ, Cardinaux JR, Martin JL. 1998. VIP and PACAP in the CNS: regulators of glial energy metabolism and modulators of glutamatergic signaling. Ann N Y Acad Sci. 865: 213-225.

Magistretti PJ, Morrison JH, Shoemaker WJ, Sapin V, Bloom FE. 1981. Vasoactive intestinal polypeptide induces glycogenolysis in mouse cortical slices: a possible regulatory mechanism for the local control of energy metabolism. Proc Natl Acad Sci U S A. 78: 6535-6539.

Martin JR, Bos M, Jenck F, Moreau J, Mutel V, Sleight AJ, Wichmann J, Andrews JS, Berendsen HH, Broekkamp CL, Ruigt GS, Kohler C, Delft AM. 1998. 5-HT2C receptor agonists: pharmacological characteristics and therapeutic potential. J Pharmacol Exp Ther. 286: 913-924.

Mesulam MM, Mufson EJ, Wainer BH, Levey AI. 1983. Central cholinergic pathways in the rat: an overview based on an alternative nomenclature (Ch1-Ch6). Neuroscience. 10: 1185-1201.

Meyer HS, Schwarz D, Wimmer VC, Schmitt AC, Kerr JN, Sakmann B, Helmstaedter M. 2011. Inhibitory interneurons in a cortical column form hot zones of inhibition in layers 2 and 5A. Proc Natl Acad Sci U S A. 108: 16807-16812.

Miyoshi G, Hjerling-Leffler J, Karayannis T, Sousa VH, Butt SJ, Battiste J, Johnson JE, Machold RP, Fishell G. 2010. Genetic fate mapping reveals that the caudal ganglionic eminence produces a large and diverse population of superficial cortical interneurons. J Neurosci. 30: 1582-1594.

Morrison JH, Magistretti PJ, Benoit R, Bloom FE. 1984. The distribution and morphological characteristics of the intracortical VIP-positive cell: an immunohistochemical analysis. Brain Res. 292: 269-282.

Munoz W, Rudy B. 2014. Spatiotemporal specificity in cholinergic control of neocortical function. Curr Opin Neurobiol. 26: 149-160.

Paspalas CD, Papadopoulos GC. 1999. Noradrenergic innervation of peptidergic interneurons in the rat visual cortex. Cereb Cortex. 9: 844-853.

Pellegri G, Magistretti PJ, Martin JL. 1998. VIP and PACAP potentiate the action of glutamate on BDNF expression in mouse cortical neurones. Eur J Neurosci. 10: 272-280.

Pfeffer CK, Xue M, He M, Huang ZJ, Scanziani M. 2013. Inhibition of inhibition in visual cortex: the logic of connections between molecularly distinct interneurons. Nat Neurosci. 16: 1068-1076.

Pi HJ, Hangya B, Kvitsiani D, Sanders JI, Huang ZJ, Kepecs A. 2013. Cortical interneurons that specialize in disinhibitory control. Nature. 503: 521-524.

Porter JT, Cauli B, Staiger JF, Lambolez B, Rossier J, Audinat E. 1998. Properties of bipolar VIPergic interneurons and their excitation by pyramidal neurons in the rat neocortex. Eur J Neurosci. 10: 3617-3628.

Porter JT, Cauli B, Tsuzuki K, Lambolez B, Rossier J, Audinat E. 1999. Selective excitation of subtypes of neocortical interneurons by nicotinic receptors. J Neurosci. 19: 5228-5235.

Porter JT, Johnson CK, Agmon A. 2001. Diverse types of interneurons generate thalamus-evoked feedforward inhibition in the mouse barrel cortex. J Neurosci. 21: 2699-2710.

Prönneke A, Scheuer B, Wagener RJ, Mock M, Witte M, Staiger JF. 2015. Characterizing VIP Neurons in the Barrel Cortex of VIPcre/tdTomato Mice Reveals Layer-Specific Differences. Cereb Cortex. 25: 4854-4868.

Rudy B, Fishell G, Lee S, Hjerling-Leffler J. 2011. Three groups of interneurons account for nearly 100% of neocortical GABAergic neurons. Dev Neurobiol. 71: 45-61.

Sachidhanandam S, Sermet BS, Petersen CC. 2016. Parvalbumin-Expressing GABAergic Neurons in Mouse Barrel Cortex Contribute to Gating a Goal-Directed Sensorimotor Transformation. Cell Rep.

Saviane C, Mohajerani MH, Cherubini E. 2003. An ID-like current that is downregulated by Ca2+ modulates information coding at CA3-CA3 synapses in the rat hippocampus. J Physiol. 552: 513-524.

Silberberg G, Markram H. 2007. Disynaptic inhibition between neocortical pyramidal cells mediated by Martinotti cells. Neuron. 53: 735-746.

Somogyi P, Kisvarday ZF, Martin KA, Whitteridge D. 1983. Synaptic connections of morphologically identified and physiologically characterized large basket cells in the striate cortex of cat. Neuroscience. 10: 261-294.

Staiger JF, Masanneck C, Schleicher A, Zuschratter W. 2004. Calbindin-containing interneurons are a target for VIP-immunoreactive synapses in rat primary somatosensory cortex. J Comp Neurol. 468: 179-189.

Staiger JF, Zilles K, Freund TF. 1996. Innervation of VIP-immunoreactive neurons by the ventroposteromedial thalamic nucleus in the barrel cortex of the rat. J Comp Neurol. 367: 194-204.

Storm JF. 1988. Temporal integration by a slowly inactivating K+ current in hippocampal neurons. Nature. 336: 379-381.

Taniguchi H, He M, Wu P, Kim S, Paik R, Sugino K, Kvitsiani D, Fu Y, Lu J, Lin Y, Miyoshi G, Shima Y, Fishell G, Nelson SB, Huang ZJ. 2011. A resource of Cre driver lines for genetic targeting of GABAergic neurons in cerebral cortex. Neuron. 71: 995-1013.

Tasic B, Menon V, Nguyen TN, Kim TK, Jarsky T, Yao Z, Levi B, Gray LT, Sorensen SA, Dolbeare T, Bertagnolli D, Goldy J, Shapovalova N, Parry S, Lee C, Smith K, Bernard A, Madisen L, Sunkin SM, Hawrylycz M, Koch C, Zeng H. 2016. Adult mouse cortical cell taxonomy revealed by single cell transcriptomics. Nat Neurosci. 19: 335-346.

Tecott LH, Sun LM, Akana SF, Strack AM, Lowenstein DH, Dallman MF, Julius D. 1995. Eating disorder and epilepsy in mice lacking 5-HT2c serotonin receptors. Nature. 374: 542-546.

Thome C, Kelly T, Yanez A, Schultz C, Engelhardt M, Cambridge SB, Both M, Draguhn A, Beck H, Egorov AV. 2014. Axon-carrying dendrites convey privileged synaptic input in hippocampal neurons. Neuron. 83: 1418-1430.

Veasey SC, Fornal CA, Metzler CW, Jacobs BL. 1997. Single-unit responses of serotonergic dorsal raphe neurons to specific motor challenges in freely moving cats. Neuroscience. 79: 161-169.

Von Engelhardt J, Eliava M, Meyer AH, Rozov A, Monyer H. 2007. Functional characterization of intrinsic cholinergic interneurons in the cortex. J Neurosci. 27: 5633-5642.

Wall NR, De La Parra M, Sorokin JM, Taniguchi H, Huang ZJ, Callaway EM. 2016. Brain-Wide Maps of Synaptic Input to Cortical Interneurons. J Neurosci. 36: 4000-4009.

Walker F, Möck M, Feyerabend M, Guy J, Wagener RJ, Schubert D, Staiger JF, Witte M. 2016. PV- and VIP-expressing neocortical interneurons impose differential inhibition on Martinotti cells. Nat Commun. *In revision*.

Ward JH. 1963. Hierarchical Grouping to Optimize an Objective Function. J Am Stat Assoc. 58: 236-&.

Wilson K, Bowen D, Francis P, Tyrrell P. 1991. Effect of central cholinergic stimulation on regional cerebral blood flow in Alzheimer's disease. Br J Psychiatry. 158: 558-562.

Zeisel A, Munoz-Manchado AB, Codeluppi S, Lonnerberg P, La Manno G, Jureus A, Marques S, Munguba H, He L, Betsholtz C, Rolny C, Castelo-Branco G, Hjerling-Leffler J, Linnarsson S. 2015. Brain structure. Cell types in the mouse cortex and hippocampus revealed by single-cell RNA-seq. Science. 347: 1138-1142.

Zhang S, Xu M, Kamigaki T, Hoang Do JP, Chang WC, Jenvay S, Miyamichi K, Luo L, Dan Y. 2014. Selective attention. Long-range and local circuits for top-down modulation of visual cortex processing. Science. 345: 660-665.

Acknowledgements

This work would have not come into existence without the contribution of many others. The past years in this work group have not only been exciting on a scientific level but also on a personal note.

I feel sincerely grateful for the unrelenting support and supervision of Jochen Staiger. He infected me with his passion for VIP neurons by trusting me with this project. His patience, advice, and wealth of knowledge inspired me to complete this journey. As a group leader he created the thriving lab I had the pleasure of working in for the past years.

I was lucky that I could learn the intricacies of electrophysiology from Martin Möck. His keen eye for any detail related to experiments and analysis always directed me towards the best outcome. Thankfully, he also provided me with ingenious scripts without which I would have never been able to cope with this dataset. It was a true mind-expanding experience to work with him. I owe him my deepest gratitude.

My thesis committee helped me to refine and greatly improve my work. I am grateful for the effort of Camin Dean and Swen Hülsmann. I thank Mirko Witte for providing me with a constant supply of animals, plenty of helpful advice, and constructive criticism when needed most. I always enjoyed his talent in maintaining the great spirit of this group by organizing awesome extracurricular events. Robin Wagener helped me with imaging, discussions about graphic design, and a bike for which I am thankful.

The efforts of Patricia Sprysch were the sole reason why the neurons in this work became visible. Her mastery of histological techniques provided me the access to the morphology for which I cannot thank her enough.

Annette Mertens, Adrian Villalobos, and Megha Patwa dedicated parts of their time to reconstruct some of the neurons for which I am grateful. I also want to thank Julien Guy and Florian Walker for many fruitful discussions and the great time we had together. This of course goes for everyone else in the lab, too.

Last but definitely not least, I want to express the bliss of being unconditionally loved and supported in all my endeavors by Nicole, my family, and friends.

Thank you!

Curriculum Vitae

Alvar Prönneke

Walkemühlenweg 9

37083 Göttingen

Born on the 16.06.1984 in Engelskirchen, Germany

Education

2013 – present	**Doctorate** in Neuroscience
	GGNB, sensory and motor neuroscience program
	Georg-August University, Göttingen, Germany
	Supervisor: Prof. Dr. Jochen Staiger
2005 – 2011	**Diplom** in Biologie (Master)
	Free University, Berlin, Germany
	Supervisor: Prof. Dr. Randolf Menzel
	Title of thesis: Physiological and Morphological Characterization of A3 Neurons in *Apis melifera*
1994 – 2004	**Allgemeine Hochschulreife** (Abitur)
	Gymnasium Andreanum, Hildesheim, Germany

Professional experience

2012 – present	**Research assistant**
	Institute for Neuroanatomy, Göttingen, Germany
2008 – 2009	**Tutor** for the basic course in neurobiology
	Free University, Berlin, Germany
2007 – 2008	**Student research assistant**
	Free University, Berlin, Germany

Publications

Prönneke A, Scheuer B, Wagener RJ, Mock M, Witte M, Staiger JF. 2015. Characterizing VIP Neurons in the Barrel Cortex of VIPcre/tdTomato Mice Reveals Layer-Specific Differences. Cereb Cortex. 25: 4854-4868.

Staiger JF, Möck M, Prönneke A, Witte M. 2015. What types of neocortical GABAergic neurons do really exist? e-Neuroforum, 6(2), 49-56.

Poster

Prönneke A, Möck M, Staiger JF. Morphological and Electrophysiological Characterization of VIP Expressing Interneurons in Mouse Barrel Cortex. 2013. NWG, Göttingen.

Prönneke A, Möck M, Staiger JF. Diversity of VIP Expressing Interneurons in Mouse Barrel Cortex. 2014. Barrels Conference, Göttingen.

Prönneke A, Scheuer B, Witte M, Möck M, Staiger JF. VIP Expressing Interneurons in Supragranular Layers of Mouse Barrel Cortex. 2014. FENS, Milano.

Prönneke A, Scheuer B, Witte M, Möck M, Staiger JF. VIP Expressing Interneurons in Layer II/III of the Barrel Cortex. 2015. NWG, Göttingen.

Prönneke A, Scheuer B, Witte M, Möck M, Staiger JF. VIP Expressing Interneurons in the Barrel Cortex of VIPcre/tdTomato mice. 2015. SfN, Chicago.

Awards

Barrels Conference, Göttingen, 2014. Best poster.

SFB retreat, Dresden, 2014. 2nd best speaker.

Paper of the year 2016 of the Anatomische Gesellschaft (anatomical society)

Additional information

German native speaker. Fluent in English.

Solid knowledge of Illustrator, Photoshop, InDesign, ImageJ, and Neurolucida. Basic knowledge of R.